Active Management of Voltage Control Devices in PV-Rich Distribution Systems

Seyyed Mahdi Noori Rahim Abadi
January 2023

A thesis submitted for the degree of
Doctor of Philosophy of
The Australian National University

Declaration

Except where otherwise indicated, this thesis is my own original work.

Seyyed Mahdi Noori Rahim Abadi
January 2023

Acknowledgments

I would like to express my sincere gratitude to my supervisor Prof. Sylvie Thiébaux who has helped me throughout my PhD. This thesis could not have been completed without her trust, guidance and continuous support. I would also like to thank my associate supervisor Dr Paul Scott who has helped me at every step along the way, and was and is a true teacher for me. Moreover, I wish to show my appreciation to my associate supervisor Prof. Lachlan Blackhall for his help in different stages of my PhD.

I wish to extend my special thanks to my colleague, partner, and love of my life Masoume Mahmoodi without whom I would not even dream of doing a PhD.

I would like to thank Dr Dan Gordon, Dr José Iria, Dr Behzad Naderi and Prof. Hemanshu Pota for their technical help and discussions. In addition, I would like to thank my colleagues and friends, particularly my colleague Ahmad Attarha for all his technical discussions and wild extravaganza, and Rabbia Saleem, Mark Burgess, Wilhiam de Carvalho and James Russell for their friendship that made doing a PhD a pleasant journey.

Finally, I thank my parents who taught me to follow my dreams and stay strong.

List of Publications

1. S. Mahdi Noori R.A., M. Mahmoodi, P. Scott, L. Blackhall and S. Thiébaux, "Active management of LV residential networks under high PV penetration," *IEEE Milan PowerTech*, 2019.
2. S. Mahdi Noori R.A., A. Attarha, P. Scott and S. Thiébaux, "Affinely Adjustable Robust Volt/Var Control for Distribution Systems with High PV penetration," *IEEE Transactions on Power Systems*, 2020.
3. S. Mahdi Noori R.A., P. Scott and S. Thiébaux, "A Combined Central-Local Volt/Var Approach in Distribution Systems with High PV Uptake," *International Conference on Smart Grids and Energy Systems (SGES), IEEE*, 2020.
4. S. Mahdi Noori R.A., P. Scott, M. Mahmoodi and A. Attarha, "Data-Driven Adjustable Robust Solution to Voltage-Regulation Problem in PV-Rich Distribution Systems," *International Journal of Electrical Power & Energy Systems*, 2022.
5. S. Mahdi Noori R.A., M. Burgess, M. Mahmoodi, A. Attarha and P. Scott, "An Adjustable Scenario Optimisation Approach in Operating PV-Rich Distribution Systems," *IEEE Transactions on Power Systems*, 2022.

Other Publications

1. A. Attarha, S.Mahdi Noori R.A., P. Scott and and S. Thiébaux, "Network-Secure Envelopes Enabling Reliable DER Bidding in Energy and Reserve Markets," *IEEE Transactions on Smart Grids*, 2021.
2. M. Mahmoodi, A. Attarha, S. Mahdi Noori R.A., P. Scott and L. Blackhall, "Adjustable Robust Approach to Increase DG Hosting Capacity in Active Distribution Systems," *Electric Power Systems Research*, 2022.

3. M. Mahmoodi, S. Mahdi Noori R.A., A. Attarha, L. Blackhall and J. Hendriks, "Impact Assessment of Active Network Management Schemes on DG Capacity of Distribution Systems," *IEEE International Conference on Power Systems Technology (POWERCON)*, 2022.

Abstract

In the last decade, environmental concerns and technological advancement have led to a transition from centralised fossil fuel-based generation towards distributed energy resources (DER), such as rooftop photovoltaic (PV) systems. This transition, however, has resulted in new technical challenges, such as the over-voltage problem. Traditionally, the distribution system operators (DSOs / DNSPs) periodically manage slow-acting regulating devices such as on-load tap changers or suggest a grid reinforcement plan to keep the networks secure. However, such approaches may no longer be reliable, as they are either too costly or were designed to control fluctuations caused by slow changes in demand. Fortunately, the utilisation of PV smart inverters presents an alternative solution to the voltage rise problem.

An important question arises: how to coordinate voltage control devices in PV-rich distribution systems to guarantee a safe and economical operation for both the networks and consumers? This thesis explores innovative technical solutions to answer this question. The first step towards finding a solution is to establish whether the DSOs can rely on existing communication-less control devices, or there is an urgent need to invest in building a communication infrastructure in the PV-rich distribution systems. Our analysis of various available standards and innovative control schemes confirms the inadequacy of existing communication-less schemes to deal with the voltage rise problem. Hence, with the uptake of PV systems in the distribution systems, it is highly suggested that the DSOs invest in a communication infrastructure to coordinate the inverters with other existing voltage control devices.

Assuming that communication infrastructure exists in distribution systems, we study how to realise a control algorithm that coordinates thousands of residential inverters. We propose two approaches based on the application of affinely adjustable robust counterpart (AARC) methodology that respond to changes in local real power (AARBP) and voltage magnitude (AARBV), respectively. Through numerical simulations, we show that our proposed approaches can keep the voltages inside the accepted limits for a wider range of scenarios compared

to alternative approaches in the literature while significantly decreasing the reactive power usage, real power loss, and line congestion.

Next, we build upon our approach and extend its modelling in three main ways. Firstly, we extend the modelling to three-phase unbalanced distribution systems. Secondly, we allow the full control of both real and reactive power output of the PV inverters. Finally, we incorporate the probability distribution function of uncertain parameters to improve the performance of our approach in scenarios away from the worst-case realisation of the uncertainty. Our simulations confirm that our approach is robust against parameter uncertainty while decreasing the real power curtailment up to 60% compared to the conventional AARC approach.

Finally, we further extend our approach to incorporate soft constraints. We propose an adjustable scenario optimisation-based solution approach that maximises the usage of DER generation within the operation horizon while providing the required level of network security. Our modelling i) guarantees hard constraints satisfaction, ii) allows fast-acting devices, e.g., inverters, to adjust in response to live realisations, and iii) enables the operators to maintain the soft constraints with a pre-determined probability using a joint chance-constrained (JCC) program. We show that our approach outperforms the conventional scenario optimisation and adjustable robust approaches, respectively, by 88% and 86% in our experiments.

Contents

Chapter 1

Introduction

1.1 Introduction

With the growing concern about climate change in the last decades, more attention is given to the importance of urgent action in response to excessive carbon emissions. The International Renewable Energy Agency, in its 2019 report [1] states that accelerated deployment of renewables can achieve over 90% of the energy-related carbon dioxide emission reductions needed to set the world on an energy pathway towards meeting the Paris climate targets. Among low-carbon technology options, solar Photovoltaic (PV) technology solely accounts for 21% of the total emission reduction in the energy sector [1]. Government incentive policies and rapid decline in the price of PV panels in the past decade have led to the massive installation of this technology in power systems worldwide. Figures 1.1 and 1.2 show the global growth in PV power generation and the reduction in the cost of PV installation in different countries over the past decade. With these trends, it is estimated that solar power will be capable of generating more than 25% of total electricity needs in 2050 [1].

Over one-third of new solar PV capacity installations worldwide are rooftop attachments [3]. The high share of rooftop solar indicates that the incentive policies and technological advances have indeed been successful in presenting rooftop PV as an economically viable alternative to the more traditional fossil fuel-based energy generating units. However, this transition from large centralised generation towards small-scale distributed renewable energy generation opens a new paradigm for the electricity distribution system operators (DSOs)[1].

[1] We use the term DSO broadly to capture the entity that manages the distribution network. This entity in Australia is known as the Distribution Network Service Provider (DNSP). Throughout this thesis, we use these two terms interchangeably.

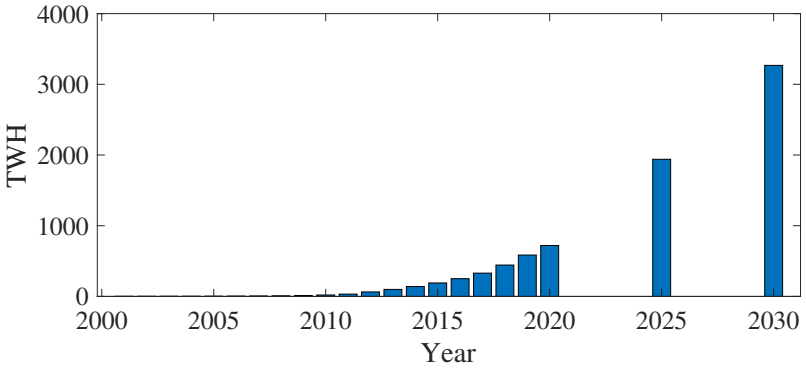

Figure 1.1: Annual solar PV generation worldwide [2]

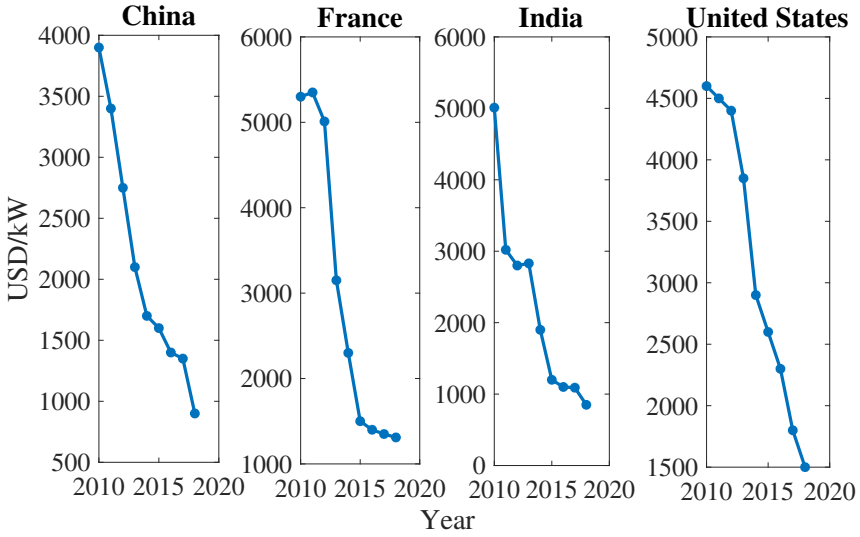

Figure 1.2: Installation cost of solar PV systems [1]

Prior to the uptake of rooftop PVs, distribution networks typically experienced one-way energy flows and relatively smooth aggregate fluctuations in consumers' demand due to low load factor[2]. Hence, the DSOs could run the system using a fit-and-forget approach [5], which was sufficient to ensure the safe operation of the system. They set the settings of the legacy voltage regulating devices such as on-load tap changers (OLTC), voltage regulators and capacitor banks and were confident that these devices could keep the distribution system volt-

[2]Load factor is defined as the ratio of the average demand of any individual customer or a group of customers over a period to the maximum demand over the same period [4]. In distribution systems, the load factor is often less than 0.4.

ages within the standards [6]. However, studies have shown that the coincidence of peak PV generation and low residential consumption, commonly found during weekdays, will cause reverse power flows [7]. Moreover, unlike the demand, the rapid fluctuations in PV generation are often synchronised, making their fluctuations change the system operating point significantly in a short amount of time. Indeed, studies have reported new technical challenges in PV-rich distribution systems such as over-voltage [8], overloading [9], power quality [10], protection [11], stability [12] issues. Among those issues, the steady-state over-voltage is considered as the most critical one [13] and is the focus of this thesis.

To alleviate the voltage rise problem, traditional approaches suggest grid reinforcement or the use of slow-acting legacy voltage regulating devices [14]. However, such approaches are either costly or were designed to control voltage fluctuations caused by slow changes in demand, and are not adequate to respond to the fast and often synchronised variations of PV systems. Fortunately, the utilisation of PV smart inverters present an alternative solution to the voltage rise problem [15]. These resources are already available in LV systems, which significantly reduces the investment cost for the DSO relative to the grid reinforcement option. Moreover, the real power curtailment and reactive power compensation capabilities of these inverters can adjust the output of the inverters promptly, which makes them a suitable option to manage the fast changes in rooftop PV generation [16]. However, a challenge is that although the real power curtailment reduces the PV real power injection to the network [6] and hence reduces the voltage rise problem, it effectively throws away surplus renewable generation, reducing the value to PV owners [17]. On the other hand, reactive power consumption can decrease the required real power curtailment at the expense of increasing network losses [18]. Hence, these resources should not be used without careful consideration.

This thesis explores innovative technical solutions to efficiently and safely operate the available resources in PV-rich distribution systems. It addresses the question:

How to coordinate voltage-control devices in PV-rich distribution systems to guarantee safe and economic operation for both the network operators and consumers?

In what follows, we look at the available solutions to the above question in the literature and categorise them based on their assumption on the existence of communication infrastructure in distribution systems.

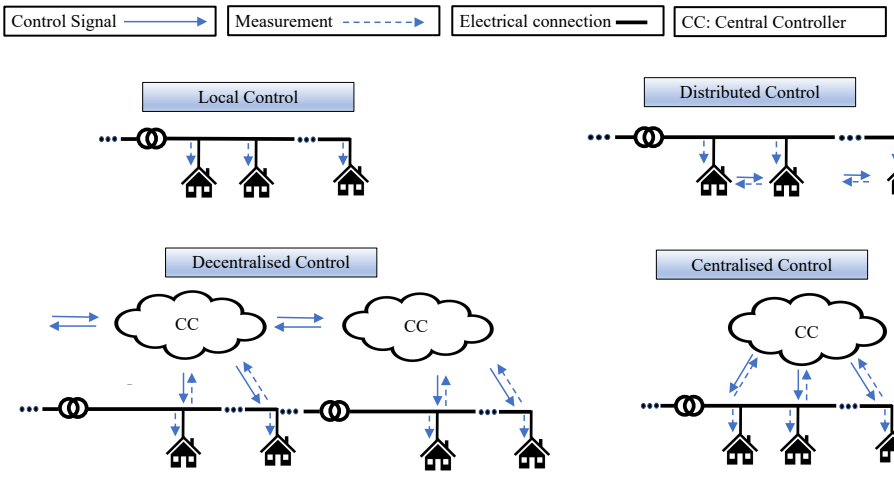

Figure 1.3: Different Control Architectures based on their communication requirements

1.1.1 Operation of Existing Communication-Less Distribution Networks

Installed residential PV inverters need to be coordinated to get an effective and flexible response at the network-wide level. Therefore, various techniques have been developed to coordinate the real and reactive power of multiple inverters with other voltage control devices in distribution systems. These approaches are commonly referred to as active network management (ANM) schemes. Based on their communication requirement, they are broadly classified as local, distributed, decentralised and centralised [19], as shown in Fig. 1.3.

A local control approach only relies on local measurements available to each inverter, is responsive to real-time changes and does not require communication infrastructure. Existing standards on the usage of inverters for voltage regulation [20–23] can all be categorised as local control approaches. They suggest that the real and reactive power of the small-scale residential / commercial inverters should be a function of voltage magnitude or the available real power to the PV systems. Similar functions have been used for decades in the wind and solar farms at medium and high voltage levels to help with voltage and frequency control. We raise the following important question about the local voltage control approaches in distribution systems:

What are the implications of the DSOs solely relying on local voltage control approaches to coordinate the residential / commercial inverters'

outputs for voltage regulation in PV-rich distribution systems?

In answering this question, we will provide insights for the DSOs to determine whether they need to invest in building a communication infrastructure for the safe operation of PV-rich distribution systems, or they can rely on the available resources to maintain the networks within the operational limits. Our analysis will investigate the efficacy of available standards and new innovative local control approaches in dealing with the voltage rise problem and indicate their limitations.

We learn from our studies that since local control approaches lack a system-wide perspective, their performance is often far from optimal. Also, these approaches often will not be able to efficiently handle all scenarios in our networks. The reason is that to guarantee network security in all scenarios, they have to curtail real power (or inject reactive power) more than necessary, leading to an overly conservative outcome. Hence, with the increasing uptake of PV systems in the distribution systems, it is highly suggested that the DSOs invest in a communication infrastructure to coordinate inverters with other existing voltage control devices.

1.1.2 Operation of Future Distribution Networks Equipped with Communication Infrastructure

Assuming that communication infrastructure exists in distribution systems, the rest of the control architectures depicted in Fig. 1.3 can be realised. Centralised approaches bring the inverter / meter measurements to a central location, make a control decision, and then relay that information back to the inverters in the field. They have the potential to make the best decisions due to their system-wide perspective. However, they run into computation and communications problems in highly volatile settings where the controllers need to be coordinated frequently (usually in tens of seconds for reliable operation in distribution systems) [24]. Also, the underlying assumption in these approaches is that DSOs have access to the inverter controller of all the customers and hence, can solve a central optimisation problem to coordinate the voltage control devices in the grid. Decentralised [25] and distributed [26] approaches can mitigate the computational and single point of failure problems of centralised approaches. They also can eliminate the need for direct control of inverters by the DSOs. However, they typically will have to forgo solution quality when implemented, and since their convergence is highly dependent on the convexity of the problem, they are less attractive in real-time voltage control applications [27].

Instead of a purely local or central approach, the possibility of a combined central-local approach to coordinate inverter outputs is start-

ing to be explored in the literature [27–30]. The idea is to benefit from both the system-wide coordination of centralised approaches and the fast response of local approaches. Hence, the focus of this thesis is to answer the following key question:

How to design a combined central-local voltage control approach for PV-rich distribution systems?

We identify the following main challenges in such designs:

- The optimisation in the central layer aims to coordinate thousands of residential and commercial inverters along with other installed voltage control devices. This is especially problematic since the optimisation problem needs to be solved frequently (usually every 15 minutes). Hence, the proposed design must be sufficiently scalable to solve such a large problem within the available time. However, the power flow equations representing the flow of electric power in an interconnected system are non-convex, making the optimal power flow (OPF) problem intractable and difficult to solve for large distribution systems.
- The response time of voltage control devices ranges from a couple of minutes, e.g. capacitor banks, to less than a second in residential inverters. Hence, any applicable proposed design should factor in the time-scale difference in these devices and simultaneously coordinate their actions.
- The uncertain and volatile nature of the PV generation and demand behaviour has increasingly made the decision-making for control devices more difficult. Under such a highly volatile setting, the deterministic approaches that neglect the uncertain nature of the problem often fail to provide reliable control signals [31].

The main focus of this thesis is to design a combined central-local voltage control approach that addresses the above challenges. In each chapter, we gradually build up a model to satisfy every criterion.

1.2 Thesis Outline and Contributions

In this thesis, we first investigate the capability of local control approaches in dealing with the voltage rise problem in PV-rich distribution systems (Chapter 2). Next, Chapter 3 introduces two-stage combined central-local voltage control approach structures. It then describes how we can apply affinely adjustable robust counterpart (AARC) methodology to realise such a two-stage scheme to coordinate inverter

reactive powers in balanced distribution systems. Chapter 4 extends the modelling to three-phase unbalanced distribution systems, coordinating inverter real and reactive powers simultaneously, and incorporating historical data. Chapter 5 further extends the modelling to distinguish between the hard and soft constraints, using a joint chance-constrained program. Finally, Chapter 6 concludes the findings of this thesis. In what follows, we provide a more detailed summary of our main contributions in this thesis and outline how the thesis is organised.

- Chapter 2 investigates the efficacy of different standards and available approaches in the literature to design local control algorithms in dealing with voltage rise in PV-rich distribution systems. Also, here we propose a novel local control approach, which prevents overvoltage / undervoltage by determining dynamic set points of PV inverters based on online measurements of connection point voltage. We then show that, although our proposed approach outperforms the alternative local control approaches, it still fails to keep all the voltages within the desired band in all operating scenarios. Hence, we argue the need for a communication infrastructure for voltage regulation in distribution systems.

- Chapter 3 details the structure of combined central-local voltage control approaches. It also presents our approach to model uncertain parameters within an OPF problem. Since we are interested in guaranteeing safe operation, this chapter focuses on robust optimisation (RO), which allows the modeller to ensure that all constraints are satisfied as long as uncertain parameters are within a bounded interval. In this chapter, we also propose two novel two-stage volt/var control schemes based on the AARC methodology to mitigate the over-voltage issues while reducing the over-conservatism of traditional RO. To cope with different grid code requirements, our first approach formulates the unused capacity of residential inverters to provide reactive power support based on real power deviation, while the second approach formulates this capacity based on voltage magnitude deviation. Although these approaches can alleviate the over-voltage issues, there is only so much they can do before reaching the inverter limits or causing other problems for the network through increased currents. Moreover, the high resistance to reactance ratio in distribution systems' lines further limits the reactive power-based approaches ability to prevent voltage violations. Hence, in Chapter 4, we extend our modelling to include the real power curtail-

ment functionality of the inverters.

Our main contribution in this chapter is the development of a novel formulation of the volt/var problem that, unlike alternative AARC-based approaches, allows us to directly include the voltage and inverter limit constraints at the early stages of developing the control algorithm. Our simulations show that our approach, compared to the state of the art, leads to fewer voltage violations and significantly decreases inverter reactive power usage, network real-power loss, and line congestion.

- Chapter 4 builds on our proposed modelling approach in Chapter 3 and allows us to simultaneously control the real power curtailment and reactive power compensation of inverters. Whereas the models in Chapters 2 and 3 assume balanced load, the power flow in three-phase distribution networks is intrinsically unbalanced, especially in networks with highly unbalanced DER penetration. Hence, in this chapter, we extend our modelling approach to capture the three-phase unbalanced energy flows. Moreover, we show that if in AARC-based approaches, the controller parameters are obtained based on the worst-case realisations, this may lead to over-conservative results when uncertainty realises away from the worst-case. To close this gap, we extend AARC to allow exploiting probabilistic uncertainty information within the optimisation problem. This results in controller parameters that not only secure the worst-case but also work better in expectation. However, despite the improvement in the performance, since our modelling requires a 100% guarantee that all the voltages are within limits for all the possible realisations, even if it is highly unlikely that they ever occur, the approach often leads to making over-conservative decisions. Hence, in Chapter 5, we build upon our model in this chapter to alleviate this problem.

  Our main contribution in this chapter is a novel extension to the conventional AARC methodology that enables us to benefit from available information about the distribution of uncertain parameters. Through extensive numerical simulations, we show that our approach improves the performance of the conventional AARC up to 60%.

- Chapter 5 extends our model in Chapter 4 by distinguishing between hard and soft constraints in the optimisation stage. The hard constraints should be satisfied for all possible realisations of uncertainty. An example of such constraint is the voltage limit on a critical node in the system where the disconnection of the node

from the grid is too costly or consequential. Conversely, the soft constraints allow some network limits to be violated in extreme scenarios, if the benefit of allowing such violations for improbable scenarios outweighs the decisions guaranteeing their satisfaction for all the possible realisations. An example of such constraint is the voltage limit on a common node in the grid. We show that allowing a small probability of constraint violation can change the problem solution significantly, and result in a significant improvement of the optimal value for those instances that remain feasible.

Our main contribution in this chapter is a novel approach that combines the application of adjustable robust optimisation and scenario optimisation for coordinating the fast-acting and slow-acting voltage control devices in three-phase distribution systems. Through numerical simulations, we show that our approach by combining the adjustable robust optimisation and scenario optimisation approaches outperforms them by 86% and 88%, respectively.

- Chapter 6 concludes the findings of this thesis and discusses future developments.

Chapter 2

Local Active Network Management

The main goal of this chapter is to provide the background material that sets the context and motivation for our problem. This chapter focuses on local active network management schemes, and their strengths and limitations in dealing with the voltage rise problem. It also answers one of our preliminary questions in this thesis of whether DSOs should solely rely on local voltage control approaches for voltage regulation in PV-rich distribution systems or not.

First, in Section 2.1, we explain why the uptake of rooftop PV panels into distribution systems has led to a voltage rise problem, and how the utilisation of PV inverters might present a solution to this problem. Then, in Section 2.2, we present some of the available standards and innovative approaches in the literature that use PV inverters to deal with the voltage rise problem. Next, in Section 2.3, we present a novel heuristic approach for local voltage control. For a point of comparison, Section 2.4 introduces a centralised solution to the voltage regulation problem, assuming that communication infrastructure exists in distribution systems. Section 2.5 reports simulation results showing the performance of our approach relative to the alternative approaches. Finally, Section 2.6 concludes this chapter.

This chapter presents an edited and extended version of our work [32], published as a conference paper and presented at the 2019 IEEE Milan PowerTech Conference.

2.1 Voltage Rise Problem in Distribution Systems

The overvoltage problem caused by high PV penetration in distribution systems can be explained through a simple two-node system, shown in

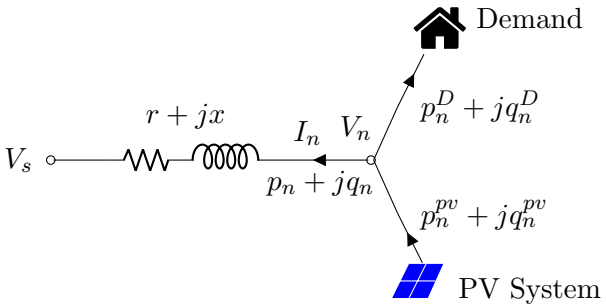

Figure 2.1: Diagram of a single-phase two-node distribution feeder

Fig. 2.1. This system consists of a node with grid connected PV system and electrical demand, a line connecting the two nodes, and a slack node with constant voltage. In Fig. 2.1, r and x are the grid resistance and reactance seen from the point of common coupling (PCC), and V_n and V_s are the voltages at the PCC and the slack node. Also, p_n^D and p_n^{pv} denote the demand and PV real power generation while $p_n = p_n^{pv} - p_n^D$ denotes the injected real power from node n into the grid. Similarly, q_n^D and q_n^{pv} denote the reactive power demand and PV reactive power generation while $q_n = q_n^{pv} - q_n^D$ denotes the injected reactive power from node n into the grid.

The sensitivity of the PCC voltage of a PV system for either real power or reactive power can be derived theoretically. The voltage deviation along the feeder due to the current injected from the PCC into the grid is:

$$\Delta V = V_n - V_s = (r + jx)I_n, \tag{2.1}$$

where I_n is the injected current from the PCC into the grid and is calculated using the complex power equation at the PCC as follows:

$$s_n = V_n I_n^* \tag{2.2a}$$

$$p_n + jq_n = V_n I_n^* \tag{2.2b}$$

$$I_n = \frac{p_n - jq_n}{V_n^*}. \tag{2.2c}$$

Substituting (2.2c) in (2.1), the voltage deviation can be written as:

$$\Delta V = \frac{rp_n + xq_n}{V_n^*} + j\frac{xp_n - rq_n}{V_n^*}. \tag{2.3}$$

Considering V_n as the reference angle, i.e. $V_n = |V_n|\angle 0$, the voltage at

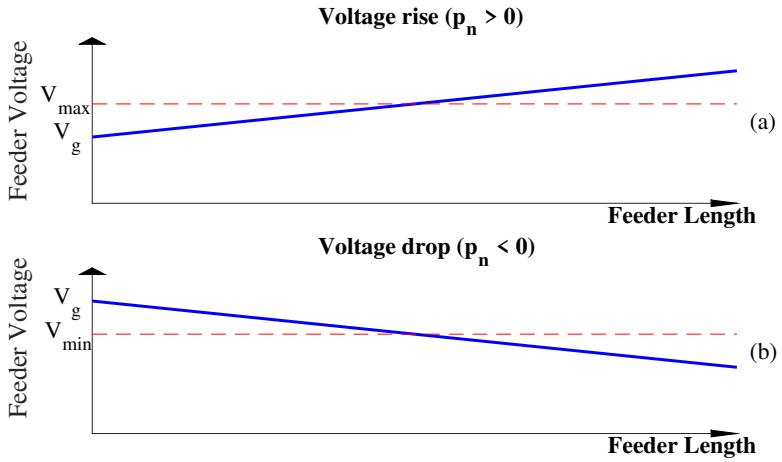

Figure 2.2: Voltage profile along a distribution feeder assuming unity power factor at the load. This figure is sourced from [14].

the grid side can be expressed as follows:

$$V_s = (|V_n| - \frac{rp_n + xq_n}{|V_n|}) + j(\frac{xp_n - rq_n}{|V_n|}). \tag{2.4}$$

Since, in short distribution systems, the imaginary part of V_s is much smaller than its real part, substituting (2.4) into (2.1), the voltage deviation along the feeder can be approximated as follows:

$$|\Delta V| = |V_n - V_s| \approx \frac{rp_n + xq_n}{|V_n|}. \tag{2.5}$$

During PV peak generation, assuming unity power factor at the load, when PV generation is typically more than the demand [33], the direction of the real power flow will be from the PCC to the grid, i.e. $p_n > 0$, which will increase the voltage at the PCC. On the other hand, in the peak load period when the amount of load usually is greater than the PV generation, the direction of power flow is toward the PCC, and the voltage at PCC will decrease. The voltage profile along the distribution system is shown in Fig. 2.2. The nodal voltage magnitudes along a feeder must always remain within $[V_{min}\ ,\ V_{max}]$, which we refer to as the safe operating region. If the voltage magnitude at a node goes beyond the safe operating region, it can cause malfunction of household and network devices, and may result in the node being disconnected from the grid.

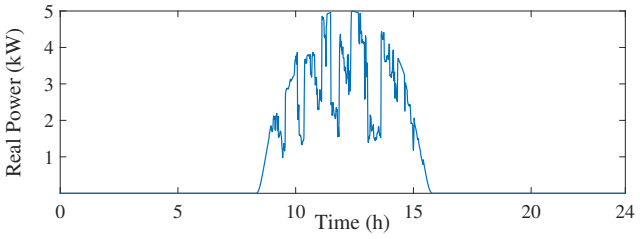

Figure 2.3: Residential PV power output in a cloudy day

The voltage rise problem has become a critical challenge in the operation of distribution systems due to the synchronised behaviour and sudden changes in PV generation in multiple houses. To illustrate, let us use the following example. Fig. 2.3 shows the generation of a 5-kW PV system on a cloudy day [34]. We can see that at midday, the PV generation can change by more than 55% in one minute. Since the solar panels in the same feeder exhibit similar fluctuations in their generation, their collective generation significantly changes the system operating point. This is in contrast with the behaviour of distribution system demand. Fig. 2.4.a shows the fluctuation in demand at three randomly chosen nodes out of the 55 nodes with consumption from the data of the European test feeder [35], and Fig. 2.4.b shows the aggregated demand of all the 55 nodes. We can see that although the changes in demand of an individual house can be up to 80% from one minute to the next, as their fluctuation is not synchronised, their aggregated fluctuation in one minute is less than 15%. Hence, the system operators could use the mechanically switched devices, such as OLTC, a few times a day (typically four times per day [36]) to keep the system voltage within a safe operating region. However, these devices are not designed to keep the system safe in the case of intermittent and synchronised PV generation, as their continuous actions can significantly reduce their life expectancy [36].

Fortunately, based on (2.5), we can see that the voltage rise / drop along the feeder can be controlled by controlling the real and reactive power injected into the grid via the real power curtailment and reactive power compensation capabilities of PV inverters. The following sections discuss how these resources can be utilised in a communication-less distribution system.

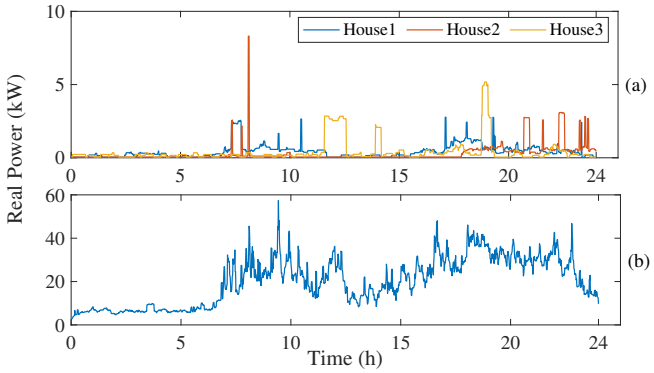

Figure 2.4: Electrical demand extracted from the European test feeder [35]. (a) shows the fluctuation in demand at 3 randomly chosen nodes. (b) shows the aggregated demand of all the 55 nodes with electrical consumption.

2.2 Local Voltage Control Approaches

PV systems are interfaced with LV grids through power electronic inverters. An inverter can be controlled to inject / absorb active and reactive power into / from the grid [37]. In local voltage control approaches, the decision of how much real and reactive power compensation is needed from each inverter is taken using only the locally available information. Indeed, these approaches can be classified into two groups based on what information they use as shown in Fig. 2.5. The first group uses behind-the-meter real power information (p^*) such as the amount of demand and available energy for generation via the solar panel as the input to the controller, while the second group uses voltage magnitude at the PCC as the input. Then, based on certain pre-specified rules, they calculate how much real and reactive power should be injected into the grid at any point in time. In what follows, we present some of the available standards and innovative local voltage control approaches available in the literature.

2.2.1 Available Standards for Local Voltage Control Using Inverters

Various standards in different countries exist that promote the use of inverters to assist in regulating voltage in distribution systems by adapting their real and reactive output powers [20–22]. Despite their differences, their modes of operation can be broadly categorised as voltage-reactive power mode, real-reactive power mode and voltage-real power mode. In the following, we present a summary of these

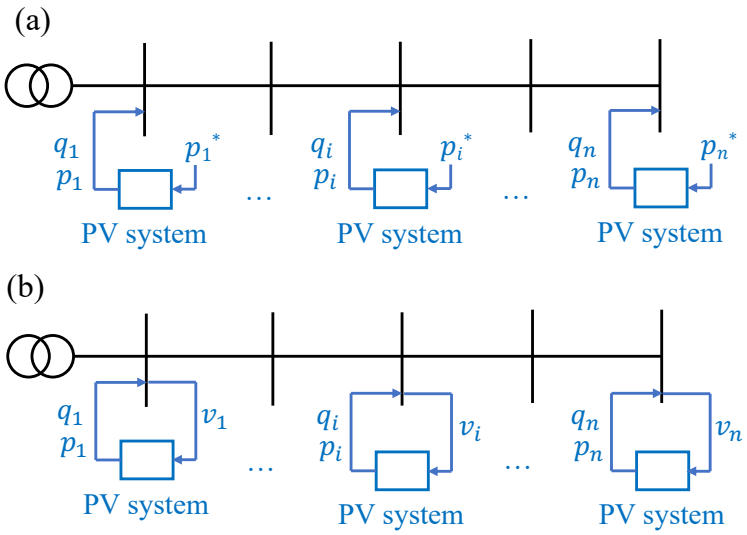

Figure 2.5: Schematic of different control local voltage control schemes in residential PV inverters.

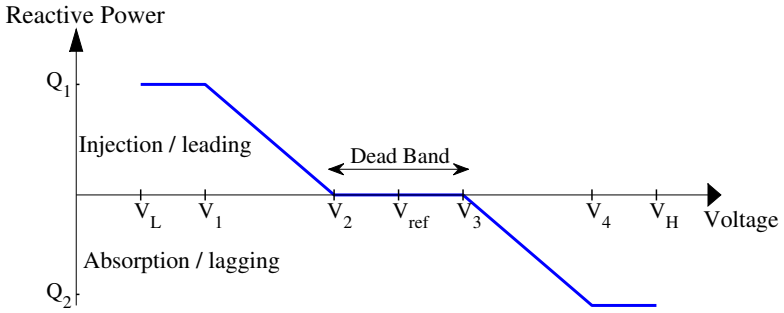

Figure 2.6: An example of a standard piecewise linear volt/var curve [21].

modes of operations.

- ***Voltage-Reactive Power Mode (volt/var):*** When in this mode, the inverter shall actively control its reactive power output as a function of locally measured voltage magnitude following a voltage-reactive power piecewise linear function. An example of such a piecewise linear function is shown in Fig. 2.6, and its parameters are shown in Table 2.1. This mode of operation is commonly referred to as volt/var, and is described in [20–22].

- ***Voltage-Real Power Mode (volt/watt):*** When in this mode, the inverter shall actively limit the PV panel real power generation as a function of the locally measured voltage following a voltage-real power piecewise linear function. An example of such a piecewise linear function is shown in Fig. 2.7. Unlike volt/var, the default setting in most inverters disables the volt/watt function. This is the case since the volt/watt function effectively throws away surplus renewable generation that reduces the value to the PV owners.

- ***Real-Reactive Power Mode (watt/var):*** When in this mode, the inverter shall actively control the reactive power output as a function of the real power output following a target piecewise linear real power-reactive power function. An example of such a piecewise linear function is shown in Fig. 2.8. Similarly to the volt/var operation mode, the settings should be designed considering the connection voltage level and grid code requirements. Notice that the left-hand side of Fig. 2.8 only applies to devices capable of absorbing real power, e.g., a battery storage system installed with the PV system. Hence, in our studies, we only care about the right-hand side of this curve. Table 2.2 shows the IEEE 1547 standard suggested parameters for the watt/var droop, where P'_{rated} and P_{rated} denote the maximum real power a DER can absorb and inject, respectively.

- ***Voltage-Reactive-Real Power Mode (volt/var/watt):***

  When in this mode, the inverter shall actively control the reactive power of the inverter and limit the PV panel's real power generation, both as a function of the locally measured voltage. Activating this mode is the same as considering the volt-watt and volt-var functions are simultaneously enabled. Thus, the reactive and real power output of the inverters should follow the piecewise linear functions in Figures 2.6 and 2.7, respectively. Also, the parameters of these functions are the same as the ones used in the volt-watt and volt-var functions, which are reported in Table 2.1. The parameters in this standard are chosen so that the PV inverters give priority to real power generation.

Table 2.1: Parameters suggested by the Australian standard on the grid connection of energy systems via inverters [20] for volt/var and volt/watt controllers. The reactive power values are the percentage of the installed inverter rated capacity.

	V_1	V_2	V_3	V_4	Q_1	Q_2
volt/var	207 V	220 V	240 V	258 V	44%	66%
volt/watt	-	-	253 V	260 V	-	-

Table 2.2: Parameters suggested by the IEEE standard 1547 [20] for watt/var controllers. The reactive power values are the percentage of the installed inverter rated capacity.

	p_1	p_2	p_3	p_4	Q_1	Q_2
watt/var	P'_{rated}	$0.5P'_{rated}$	$0.5P_{rated}$	P_{rated}	44%	44%

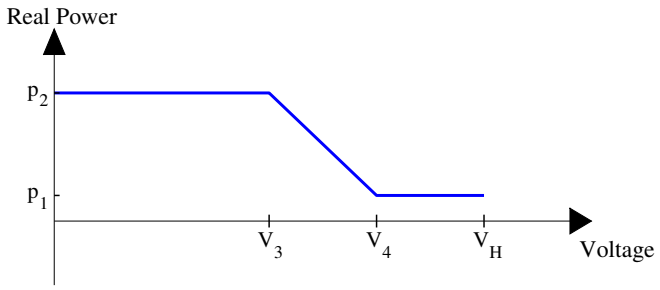

Figure 2.7: An example of a standard piecewise linear volt/watt curve [21].

2.2.2 Innovative Approaches in the Literature for Local Voltage Control Using Inverters

The above standards propose a characteristic curve to support voltage profiles via a PV system's real and reactive powers. However, their suggested curves do not change with time and are obtained irrespective of network characteristics. Hence, the control actions in each inverter are determined according to an identical characteristic for each PV system, independently of its location in the grid and the overall state of the network.

Our numerical simulations in Section 2.5 indicate that usage of the standard static characteristic curves in some scenarios leads to unnec-

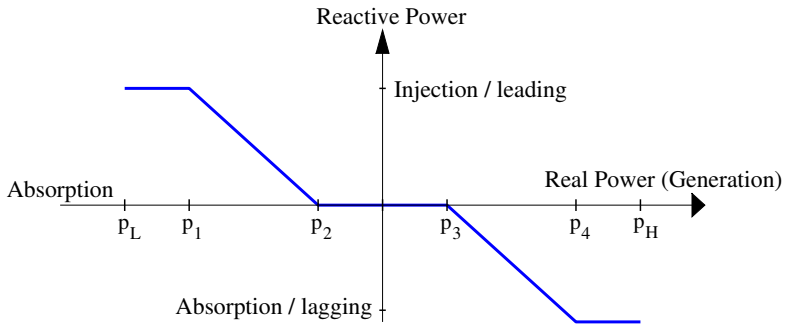

Figure 2.8: An example of a standard piecewise linear watt/var curve [21].

essary reactive power consumption / absorption by PV systems and unnecessary real power curtailment. Considering the large number of PV systems in grids, their excessive collective reactive power usage increases the total line losses. Also, real power curtailment is not desired by the PV owners as it leads to a loss of potential revenue for the owners. In other scenarios, using the static characteristic curves lead to overvoltage / undervoltage in the system, while the inverters could have kept the system safe if their actions were better coordinated.

To overcome the above shortcomings, the available literature on the voltage regulation problem focuses on developing methods that can provide a coordinated, systematic characteristic for each PV system along a feeder coherent with each network specification. The literature, however, mostly assumes that there is communication infrastructure in distribution systems. Much of the literature assumes that there is an underlying communication infrastructure that can coordinate inverters — a setting that we cover in Chapters 3–5. It also assumes the existence of an accurate distribution network model down to residential customers, which is not available in practice. Here we focus on the model-free works that do not require communications and thus, can be more readily implemented for a large range of network settings at a lower deployment cost.

The use of rule-based algorithms to efficiently utilise piecewise linear curves is investigated in [13, 16, 38–43]. A frequently used approach in these works is the use of the voltage sensitivity to real and reactive nodal injections[1]. For example, the authors in [13] calculate volt/watt droop parameters based on a voltage sensitivity matrix, approximated about a particular operating point, to coordinate multiple PV systems.

[1]The voltage sensitivity can be obtained using the Jacobian matrix inverse from a solved power flow case, which provides an accurate way to calculate droop slopes [39].

However, this fails to accurately account for the sensitivities when the operating point is far away from the assumed operating point. To overcome this, authors in [39] propose a fitting function-based sensitivity approach that develops a nonlinear function to describe dependencies between the voltage of a node and its PV real and reactive power injections and then calculates the slopes based on the function. Their approach requires about 135000 scenarios which are often not available in practice, and their suggested function should be altered for any changes in the network configuration.

In addition to the above shortcomings, the authors in [37, 42, 44, 45] identify another significant concern about the operation of multiple volt/watt and volt/var control approaches. They have reported an undesired oscillatory behaviour in the response of these inverters to operating point deviations. Thus, authors in [44] propose two incremental local volt/var control schemes based on the sub-gradient and pseudo-gradient algorithms, respectively. In their approaches, instead of sudden changes in reactive power output in response to voltage deviations, reactive power is gradually adjusted based on the changes made at previous times. They show that in doing so, their approaches prevent the undesired oscillatory behaviour and achieve better dynamical properties. Similar approaches have been suggested by the authors in [42] based on the Gradient Projection algorithm to further improve the dynamic response of the volt/var control approaches. However, although these approaches can mitigate the oscillatory behaviours, they still converge to the same solution[2] as a simple volt/var droop, shown in Fig. 2.6. Hence, they will not improve the steady-state performance of such control designs and will still face similar problems as the existing standards.

To overcome the above shortcomings, in the following section, we propose a local rule-based control approach to coordinate residential inverters' real and reactive power to mitigate the voltage rise problem in PV-rich distribution systems. Our proposed approach is based on an incremental procedure where the real and reactive power of the inverters are updated gradually over time. Therefore, the voltages gradually converge towards the desired region through each control action. Hence, our proposed approach enjoys similar dynamical properties as those in [42] and [44]. Furthermore, our numerical simulations, in Section 2.5 show that our control proposal keeps the voltages inside the desired region in a wider range of scenarios in comparison with alter-

[2] In Appendix A, we provide a detailed analysis on why and when volt/var and volt/watt control approaches will cause oscillations in the network voltages. Also, we discuss the trajectories of the gradient projection algorithm and its steady-state solution relative to the simpler droop approach.

native approaches.

2.3 Proposed Local Voltage Control Approach

In this section, we provide details of our proposed approach. The proposed approach consists of three modes of operation. At any point in time, based on the measured connection point voltage, one of the modes of the controller will be activated. Then, in each control mode, the real and reactive powers of the PV inverter are determined based on the online local voltage measurements and a set of control rules. Also, similarly to the IEEE volt/var/watt standard, here prioritise the use of reactive power over real power curtailment by defining a time delay in the response of the inverters. *Mode 1* is activated when the connection point voltage exceeds the upper voltage limit. In this mode, reactive power consumption and real power curtailment are utilised to bring the connection point voltage back to the desired region. *Mode 2* is activated when the connection point voltage is below the lower voltage limit. In this mode, reactive power injection is utilised to push the voltages to the desired region. Finally, *Mode 3* is activated when the voltage is within the desired region. This mode is responsible for normal operation and restoration of the real and reactive powers. The details of each mode of operation are presented in the following sections.

2.3.1 *Mode 1*: Overvoltage

When the connection point voltage exceeds the upper desired limit (V_3), the inverter reactive power consumption increasingly adjusts as a function of its connection point voltage, as shown in Fig. 2.9.a, until either it reaches its maximum amount, limited by the apparent power of the inverter, or the voltage is mitigated. Thus, the reactive power at node n and time t is:

$$q_n^{pv}(t) = \left[q_n^{pv}(t-1) + \Delta q_n^{pv}(t)\right]_{\underline{q_n}}^{\overline{q_n}} \tag{2.6a}$$

$$\Delta q_n^{pv}(t) = \begin{cases} m_1(V_n(t) - V_3) & \text{if} \quad V_n(t) \geq V_3 \\ 0 & \text{if} \quad V_2 \leq V_n \leq V_3. \end{cases} \tag{2.6b}$$

where $\Delta q_n^{pv}(t)$ denotes the change in the reactive power output of the inverter connected to node n at time t. m_1 is the rate of change of the reactive power, and is obtained from the slope of the curve in Fig. 2.9.a. In Fig. 2.9, V_1 and V_4 are parameters of our design which are used to adjust the rate of change of the real and reactive powers. Also, operator

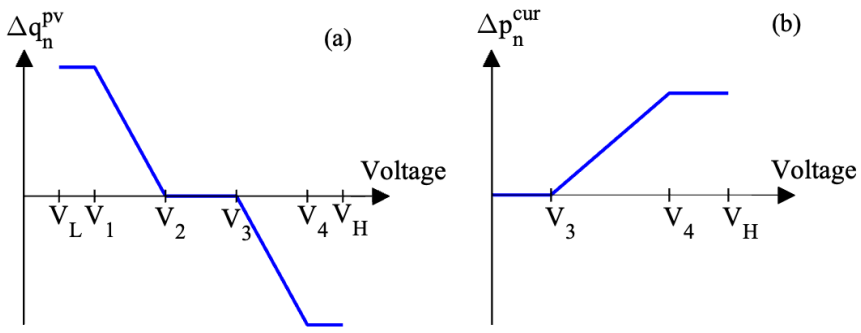

Figure 2.9: The schematics of local real and reactive powers management in the overvoltage and undervoltage modes of operation; (a) change in reactive power of the inverter; (b) change in PV real power curtailment.

[.] denotes the mapping of the reactive power in each time-step to the range $[\overline{q_n}, \underline{q_n}]$, which enforces the inverter capacity limit. $\overline{q_n}$ and $\underline{q_n}$ are the maximum and minimum reactive power available at each node and time-step, which are limited by the inverter size and the real output power of the PV.

If the reactive power consumption cannot alleviate the overvoltage, the output real power is curtailed as a function of its connection point voltage. However, since normally the voltage deviation is larger for nodes located at the end of the feeder, according to (2.6), the rate of increase in reactive power consumption in these nodes is larger. Therefore, they often reach their limits sooner than the other nodes, and hence, they start to curtail real power sooner than the rest. To use the full potential of other nodes and avoid unnecessary real power curtailment at nodes located at the end of the feeder, another starting criterion ($Crit_{start}$) is defined. For each node, the starting criterion is true when the voltage exceeds the upper desired limit for a predefined number of consecutive time steps. The number of consecutive time steps is tuned based on the trial and error method[3]. Thus, the real PV

[3]The trial and error experiments are done to heuristically find the time delay that is smaller than the guidelines for the sustained over-voltage, where the inverters need to be disconnected from the grid, and is long enough to see the impact of reactive power of compensation of other inverters.

power generation at node n and time t is controlled as follows:

$$p_n^g(t) = p_n^{pv}(t) - p_n^{cur}(t) \tag{2.7a}$$

$$p_n^{cur}(t) = \Big[p_n^{cur}(t-1) + \Delta p_n^{cur}(t)\Big]_0^{p_n^{pv}(t)} \tag{2.7b}$$

$$\Delta p_n^{cur}(t) = \begin{cases} m_2(V_n(t) - V_3) & \text{if} \quad V_n(t) \geq V_3 \quad \text{and} \quad q_n^{pv}(t-1) = \overline{q_n} \\ & \quad \text{and} \quad Crit_{start} = True \\ 0 & \text{if} \quad \text{Otherwise.} \end{cases} \tag{2.7c}$$

where $p_n^{cur}(t)$ and $p_n^{pv}(t)$ denote the inverter real power curtailment and available real power for generation at node n and time t, respectively. Also, m_2 is the rate of change of the real power curtailment and is obtained from the slope of the curve in Fig. 2.9.b.

2.3.2 Mode 2: Undervoltage

When the connection point voltage is smaller than the lower desired limit (V_2), the inverter reactive power injection increasingly adjusts as a function of its connection point voltage until either it reaches its maximum amount, limited by the apparent power of the inverter, or the undervoltage is mitigated. Thus, we define the following control rule:

$$q_n^{pv}(t) = \Big[q_n^{pv}(t-1) + \Delta q_n^{pv}(t)\Big]_{\underline{q_n}}^{\overline{q_n}} \tag{2.8a}$$

$$\Delta q_n^{pv}(t) = \begin{cases} m_3(V_n(t) - V_2) & \text{if} \quad V_n(t) \leq V_2 \\ 0 & \text{if} \quad V_2 \leq V_n(t) \leq V_3, \end{cases} \tag{2.8b}$$

m_3 is the rate of change of the reactive power, and is obtained from the slope of the curve in Fig. 2.9.a.

2.3.3 Mode 3: Restoration

When the connection point voltage is within the desired region, we check whether curtailment has been applied in previous times in order to avoid unnecessary curtailment and harvest as much energy as possible from the PV. If so, the curve in Fig. 2.10.b is used to decrease the unnecessary real power curtailment at each node. Also, to prevent voltage oscillation around the upper desired limit, we define a deadband controlled by V_3'. Similarly to V_4 in Fig. 2.9, V_3'' is defined to adjust

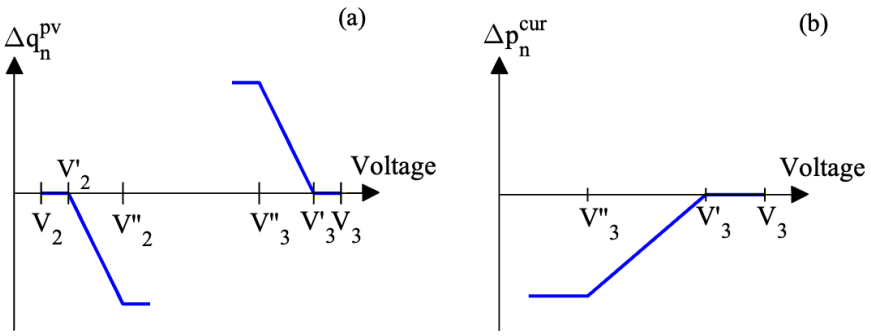

Figure 2.10: The schematics of local real and reactive powers management in the restoration mode; (a) change in reactive power of the inverter; (b) change in PV real power curtailment.

the rate of decrease in real power curtailment. Hence, the potential extra PV real power gradually augments as a function of the connection point voltage, as shown in Fig. 2.10. The process of real power restoration continues until the real power curtailment is decreased to zero or the voltage reaches the upper desired limit. This control rule for the real power curtailment restoration is defined as follows:

$$p_n^g(t) = p_n^{pv}(t) - p_n^{cur}(t) \tag{2.9a}$$

$$p_n^{cur}(t) = \left[p_n^{cur}(t-1) + \Delta p_n^{cur}(t)\right]_0^{p_n^{pv}(t)} \tag{2.9b}$$

$$\Delta p_n^{cur}(t) = \begin{cases} m_3(V_n(t) - V_3') & \text{if } V_n(t) \le V_3' \\ 0 & \text{if } \textit{Otherwise.} \end{cases} \tag{2.9c}$$

If the real power generation reaches the available power time t, i.e., $p_n^{pv}(t)$, and the voltage is still smaller than V_3', then to avoid unnecessary reactive power consumption, the extra reactive power is gradually decreased according to the following:

$$q_n^g(t) = \left[q_n^g(t-1) + \Delta q_n^{pv}(t)\right]_{\underline{q_n}}^{\overline{q_n}} \tag{2.10a}$$

$$\Delta q_n^{pv}(t) = \begin{cases} m_4(V_n(t) - V_3') & \text{if } V_n(t) \le V_3' \text{ and } p_n^g(t) = p_n^{pv}(t) \\ 0 & \text{if } \textit{Otherwise.} \end{cases} \tag{2.10b}$$

Similarly, another curve is defined to prevent unnecessary reactive power injection when moving from the undervoltage mode to restora-

tion mode, i.e., when the voltage becomes greater than V_2' after being lower than V_2 (details omitted to avoid repetition).

2.4 Centralised Solution Using Optimal Power Flow

Assuming that communication infrastructure exists in distribution systems, and computation time and communication delay are not an issue, a centralised approach can be realised, which provides the optimum solution to the voltage regulation problem [46]. This approach provides a perfect but unachievable baseline in which an optimal power flow (OPF) problem is solved to coordinate the real and reactive power of multiple PV systems connected to the grid. Although unachievable due to excessive computational requirements, the OPF still provides insight into the performance of different voltage control schemes.

We use the *Distflow* model to represent the power flow equations, as the *Distflow* formulation is well-suited for radial distribution systems with a tree structure, as shown in [47]. In the *Distflow* formulation, a power network is represented by a connected graph $\mathcal{G} = (\mathcal{V}, \mathcal{B})$, where $\mathcal{V} = \{0, ..., n\}$ denotes the set of nodes with cardinality $|\mathcal{V}| = n + 1$ and $\mathcal{B} \subseteq \mathcal{V} \times \mathcal{V}$ denotes the set of branches. For every node $i \in \mathcal{V}$, let v_i denote the squared voltage magnitude, $p_i = p_i^{pv} - p_i^{cur} - p_i^D$ be the real power injected into the grid at node i, and $q_i = q_i^{pv} - q_i^D$ be the reactive power injected into the grid at node i. Also, let S_i denote the inverter capacity connected at node i. For every branch $(i, j) \in \mathcal{B}$, let $z_{ij} = r_{ij} + jx_{ij}$ denote the complex impedance of the line, and l_{ij} denote the squared current magnitude between node i and node j. Also, let P_{ij} and Q_{ij} denote the real and reactive powers sending from node i to node j. It is also assumed that the substation voltage (slack node) set-point v_0 is given. Moreover, the inverter capacity and voltage limit constraints are incorporated in the *Distflow* model. What follows is

the OPF formulation:

$$\min \quad \sum_{(i,j)\in\mathcal{B}} r_{ij} l_{ij} + \sum_{i\in\mathcal{V}} p_i^{cur} \tag{2.11a}$$

$$p_j = \sum_{k:j\to k} P_{jk} - (P_{ij} - r_{ij} l_{ij}) \qquad \forall j \in \mathcal{V} \tag{2.11b}$$

$$q_j = \sum_{k:j\to k} Q_{jk} - (Q_{ij} - x_{ij} l_{ij}) \qquad \forall j \in \mathcal{V} \tag{2.11c}$$

$$v_j = v_i - 2(r_{ij}P_{ij} + x_{ij}Q_{ij}) + (r_{ij}^2 + x_{ij}^2) l_{ij} \qquad \forall (i,j) \in \mathcal{B} \tag{2.11d}$$

$$v_i l_{ij} \geq P_{ij}^2 + Q_{ij}^2 \qquad \forall (i,j) \in \mathcal{B} \tag{2.11e}$$

$$p_j = p_j^{pv} - p_j^{cur} - p_j^D \qquad \forall j \in \mathcal{V} \tag{2.11f}$$

$$q_j = q_j^{pv} - q_j^D \qquad \forall j \in \mathcal{V} \tag{2.11g}$$

$$(p_j^{pv} - p_j^{cur})^2 + {q_j^{pv}}^2 \leq S_j^2 \qquad \forall j \in \mathcal{V} \tag{2.11h}$$

$$v_j^{min} \leq v_j \leq v_j^{max} \qquad \forall j \in \mathcal{V}, \tag{2.11i}$$

where objective (2.11a) is minimising total real power loss in a distribution system that includes the power loss due to the real power curtailment and line losses (because of the current flowing through lines). In other words, we wish to maximise the power throughput of the grid and harvest as much PV generation as possible. Please note that if we only focus on the latter, we end up with the solution of injecting massive amount of reactive power, and thus excessive current, into the grid, which, aside from creating high losses in the lines, creates additional problems, such as line overheating, and transformer congestion. Furthermore, it will lead to complications for the transmission system operators as the injected reactive power is sent through the transmission system that needs to be absorbed by the generators or reactors, and it might lead to overvoltage problems as the transmission system commonly have much higher reactance to resistance ration than distribution systems. In (2.11), constraints (2.11b)-(2.11g) denote the *Distflow* equations, (2.11h) enforces the inverter capacity constraint, and (2.11i) denotes the voltage limitations. Note that (2.11e) is a conic relaxed version of the original quadratic equality constraint. This is a tight relaxation as the objective function includes l_{ij}, which prevents excessive deviation from the equality (our simulations show that relaxing this constraint introduces less than 0.5% error in the constraint). Please note that in this chapter, we assume a balanced three-phase network and solve OPF (2.11) problem for the single-phase equivalent model. We build on this modelling in Chapters 4 and 5 by removing this assumption and modelling a three-phase unbalanced distribution system.

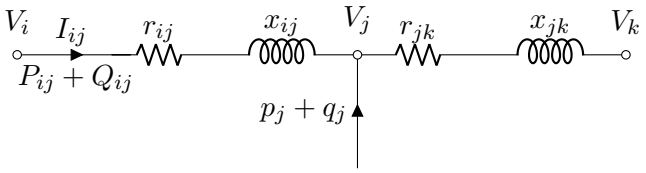

Figure 2.11: Diagram of a single-phase two-node distribution feeder

2.5 Results and Discussion

2.5.1 Case Study

We test the performance of our proposed method using simulations on a real 30-node modern underground LV feeder with $R/X \approx 2$, located in Hobart, Australia, and shown in Fig. 2.12. We use the Australia New Zealand Standard: Grid connection of energy systems via inverters, Inverter requirements, AS/NZS, 4777.2 [20] to specify the nominal voltage and voltage limits in our study. Thus, we consider the nominal voltage of the feeders 230V and the base power 1kW. We also assume the inverters can remain connected to the grid as long as the voltages are within 216V to 253V.

Our simulations assume a balanced loading condition and a high PV penetration scenario by pairing each load with a 10 kVA PV system[4]. Each of the 30 different residential customers has a different load pattern, and the rooftop PV systems are assumed to have a correlated solar input. We extract from [34] PV generation and load consumption data for five consecutive days at the resolution of one step change per minute. We arbitrarily select 15-19 January and consider houses to have 4-6 residents. The often large instantaneous transitions between minutes provide a good way to test the response of our control approach and allow us to observe the settling time and behaviour (we consider the controller voltage sampling rate to be one second). The controller and simulation parameters are summarised in Table 2.3. Notice that

[4]The Australian energy council in [48] report a rapid increase in solar panel installations and their average system from July 2013 to December 2021 in Australia. Their data (please see figure 1 in [48]) shows that the average PV system size has increased from 4 kW to almost 9 kW during this period. Also, the International Renewable Energy Agency, in its 2019 report, anticipated that the increase in PV system installation will continue to grow until at least 2050. Thus, although the current grid code in some states prevents higher PV capacity installations, the 10 kW PV system installation that we consider in our study will likely happen in the future.

Table 2.3: Controller and Simulation Parameters

Parameter	Value (pu)	Parameter	Value (pu)
V_1	0.5	V_2'	0.92
V_2	0.9	V_2''	0.96
V_3	1.1	V_3'	1.08
V_4	1.5	V_3''	1.02

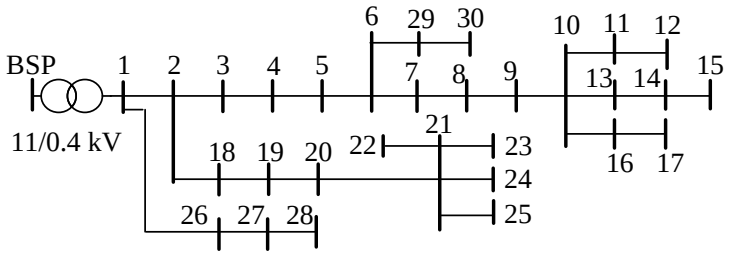

Figure 2.12: 30-node low-voltage feeder.

the upper and lower voltage limits are 0.94 pu and 1.1 pu in our studies. All the experiments are carried out using Python scripts. Also, the optimisation model is developed using the Pyomo package [49].[5]

2.5.2 Detailed Results for Some Scenarios

This section demonstrates the detailed performance of our approach in dealing with overvoltage / undervoltage scenarios in a couple of scenarios. Average results over the five days are later reported in Section 2.5.3. Fig. 2.13 shows the real and reactive power and the voltage profile at *Node 15* which is located at the end of the feeder, with and without voltage management at minute 600. We can see that when the voltage at this node exceeds 1.1pu, *Mode 1* of its controller is activated. Hence, the reactive power is increasingly consumed based on (2.6) until it brings the voltage to the desired region after 45s. Also, we can see that since the reactive power compensation is enough to

[5]We use an exact power flow model to calculate the voltage magnitudes, using the Backward-Forward technique [50]. We also use the OpenDSS simulation environment [51], an electric power distribution system simulator, to verify our implementation of the Backward-Forward technique.

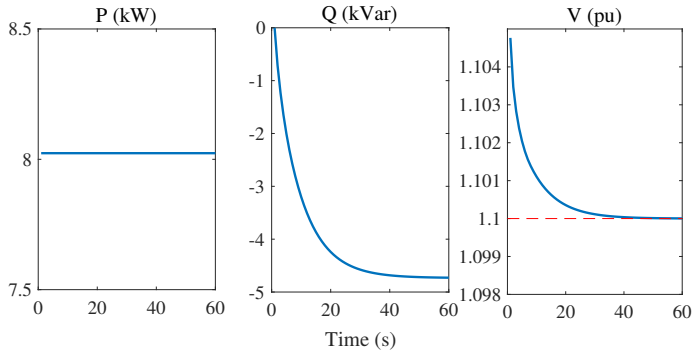

Figure 2.13: Detailed performance of the proposed approach at *Node 15* in minute 600. The overvoltage at this minute is mitigated using only the reactive power consumption of the inverter.

bring the voltage back to the region, the real power generation of the PV does not change in this scenario.

Fig. 2.14 shows the results at minute 690. Similarly to minute 600, the inverter increasingly consumes reactive power to bring the voltage to the desired limit. However, because only a limited capacity of the inverter remains unused (the rest of the capacity is used to generate 9.86 kW real power), it cannot bring the voltage to the safe limit, and the overvoltage persists. At this stage, as described in Section 2.3.1, the controller waits to see the impact of other nodes for 26 seconds, and then starts to curtail the real power output and increase the reactive power consumption.

Fig. 2.15 shows the results at minute 725, where a sudden decrease in the real power generation of the PV systems leads to a drop in the voltage magnitudes. Thus, *Mode 3* of the operation of the controller is activated at *Node 15*. Based on (2.10), the controller gradually decreases the reactive power consumption until it reaches the upper voltage limit in the restoration mode (V_3'). Similarly, in scenarios with high demand, the controller gradually increases the reactive power injection to prevent undervoltage, which we do not include here to avoid repetition.

2.5.3 Average Results Over Multiple Scenarios

This section compares, over five days, the performance of our proposed approach with the standard volt/var, volt/watt and watt/var

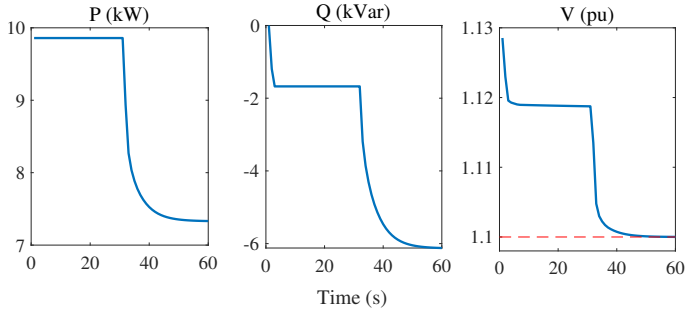

Figure 2.14: Detailed performance of the proposed approach at *Node 15* in minute 690. The overvoltage at this minute is mitigated using a combination of the reactive power consumption and the real power curtailment of the inverter.

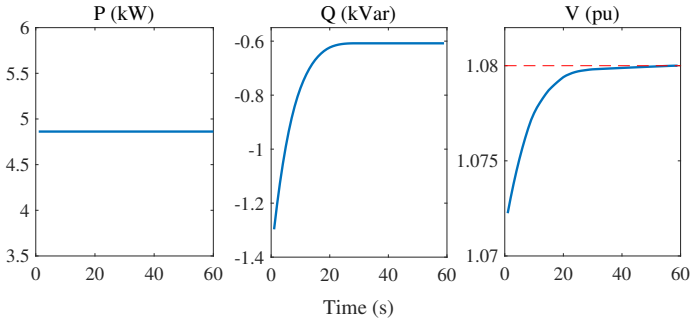

Figure 2.15: Detailed performance of the proposed approach at *Node 15* in minute 725. The unnecessary reactive power consumption is decreased to prevent excessive line losses.

control approaches described in Section 2.2.1[6]. We also implement a case where the inverters do not use any control approach, i.e., they work with unity power and do not curtail real power. In addition, we implement the optimal power flow method described in Section 2.4 as a perfect but unachievable baseline. This method assumes that computation and communication time are not an issue, and we can collect the demand and generation data, solve an OPF problem and send the control actions to the inverters every minute. In our experiments, we assume that when a sustained overvoltage / undervoltage occurs in a scenario at a node, the inverter connected to that node will be disconnected during that scenario. Also, we consider the voltage limits to be 0.94pu and 1.1pu, and consider 60 seconds as the duration for

[6]We provide a detailed discussion on how these approaches can be implemented in a distribution system, and their potential instability problem in Appendix A

Table 2.4: Summary of the simulation results. NVV denotes the number of voltage violations, and EL denotes the energy loss.

	EL (kWh)	NVV
No control	860.35	3562
volt/var	538.1	1347
volt/watt	488.2	836
watt/var	432.3	740
volt/var/watt	331.9	81
Proposed	181.2	5
OPF	27.8	0

a sustained overvoltage / undervoltage scenario. We then report how much real power is lost due to the inverter disconnection, line losses and inverter-controlled real power curtailment. We also report how many voltage violations occur in the experiments.

Table 2.4 shows the simulation results over the five days. When none of the inverters uses any control approach, the network faces 3562 overvoltage cases, which means that in only five days, the inverters in our experiment will get disconnected from the grid 3562 times. Their disconnection will lead to a significant loss of energy, and the sudden change in their output to the grid could result in stability issues in networks [52]. However, activating any of the local control approaches will decrease the number of voltage violations and the amount of energy losses. Moreover, we can see that our proposed approach outperforms the alternative standard approaches by decreasing the number of voltage violations and real power loss compared to the best alternative (volt/watt/var) by more than 95% and 45%, respectively.

An important observation of Table 2.4 is that although our approach manages to decrease the number of voltage violations and real power loss compared to alternative approaches, there is still a significant difference between its performance and the optimal baseline. Indeed, because the local control approaches lack a system-wide perspective, their decisions are made blindly regarding the grid as a whole. Hence, with more and more uptake of PV systems in the distribution systems, it is necessary to invest in communication infrastructure to coordinate multiple control devices in the grid. The advantage of such communication infrastructure will be for both the DSOs to more reliably operate the network and the consumers to increase their revenue by preventing repeated inverter disconnections from the grid.

2.6 Summary

This chapter presents an analysis of how the uptake of PV systems in distribution systems can cause the voltage rise problem and discusses how the smart inverters have the potential to mitigate this problem. It also provides a comprehensive literature review on the state-of-the-art and established standards for control approaches in a communication-less grid.

Moreover, in this chapter, a novel decentralized rule-based control approach is proposed to mitigate overvoltage/undervoltage in a high PV penetrated distribution network using residential inverters. Based on online measured connection point voltage, dynamic setpoints of PV smart inverters are determined, and the voltage gradually converges toward the desired region. The proposed approach consists of three modes of operation, overvoltage, undervoltage and restoration modes, and each mode is responsible for a range of connection point voltages.

To assess the performance of the local control approaches in managing the voltages, we conducted numerical experiments on a real 30-node high PV penetrated LV distribution network in Hobart, Australia. The results highlight that although our proposed approach acts closer to the optimal, without the need for communication, full network observability and heavy offline computations; there is still a considerable difference between the local control approaches and the optimal. Thus, in the next chapters, we investigate how communication infrastructure can reduce this gap.

Chapter 3

Robust Central-Local Volt/Var Control

3.1 Introduction and Literature Review

In Chapter 2, we discussed how the massive uptake of residential photovoltaic (PV) panels has led to overvoltage problems in operating distribution systems. We also explained how using smart inverter capabilities to provide reactive power support and real power curtailment presents a low-cost solution to this problem. Moreover, we showed that using local control approaches, which allow the inverters to determine their real and reactive power contributions to the voltage regulation problem based on only locally available information, is inadequate. Hence, we argued the necessity of a communication infrastructure for the coordination of these devices. This chapter explores the use of communication infrastructure in coordinating the reactive power output of smart inverters to mitigate the overvoltage / undervoltage problem. Later on, in Chapters 4 and 5, we extend our work to simultaneously coordinate the real and reactive power of PV inverters.

As introduced in Chapter 1, the coordination techniques for the installed residential inverters in the literature, based on their communication requirements, can be broadly classified as centralised, decentralised, and local [53]. Centralised approaches bring the inverter / meter measurements to a central location, make a control decision, and then relay that information back to the inverters in the field. They have the potential to make the best decisions, due to their system-wide perspective, but they run into computation and communications problems in highly volatile settings where the controllers need to be coordinated very frequently (in a matter of seconds) [24]. By foregoing some solution quality, decentralised approaches can mitigate the computational

and single point of failure problems that a centralised approach has. However, the convergence of such approaches is highly dependant on the convexity of the problem, making them less attractive in real-time voltage control applications [27]. Unlike centralised and decentralised approaches, a local control approach only relies on local measurements available to the inverter. However, because a local controller lacks a system-wide perspective, its actions can be far from optimal [28].

To overcome the shortcomings of these approaches, we propose to use a combined local and centralised approach. The idea is to benefit from both the system-wide coordination of centralised approaches and the fast response of local approaches. We use a timescale decomposition technique [29] to combine the two approaches and form a two-timescale scheme. This should be intuitive as there exist slow-acting and fast-acting voltage control devices working together in distribution systems. In these approaches, a discrete controller periodically takes measurements throughout the network and sends corrective adjustments to the local layer. Then in real-time, the local controller takes recourse actions after the uncertainty is realised [27–30]. Using such a scheme, we can extend the period between two consecutive updates of the centralised layer, making it practical for use in large distribution systems.

Moreover, we make use of the affinely adjustable robust counterpart (AAR C) methodology introduced in [54] to ensure that the voltage limits are not violated between two consecutive updates. This is achieved by factoring in the impact of uncertainty in the centralised layer when the controller parameters are calculated and communicated to the local layer. In AARC, similarly to a linear feedback controller, the output of the controllers can be constantly updated as the uncertain parameters are revealed. In our context, such an AARC approach is in the spirit of a combined centralised and local control approach, where the system-wide decisions (known as "here-and-now" values) are made through a centralised optimisation, while the "wait-and-see" control action are made locally to tune the "here-and-now" values.

The application of AARC, or equivalently, linear decision rules (LDR) in voltage control has been investigated in the literature [55], [30], [27]. In [55], the coordination of residential battery energy storage systems is formulated as an AARC problem and solved using a distributed optimisation algorithm. A linear decision rule is assigned to each battery relating uncertain household real power consumption to battery charge / discharge response. [30] proposed using LDR for adjusting the reactive power of multiple inverters in response to local changes in real power injection. The parameters in the decision rules are obtained based on linearised power flow equations. This work is

extended in [27] by presenting a closed-form solution to the AARC of volt/var problem.

Note that the above literature designs the decision rules without actually incorporating the voltage limits in their model. The decision rules in [27] and [30] are designed to keep the voltages close to (ideally the same as) the voltage references. Thus, there is no guarantee that their results lie within the voltage safe limits. Also, [27] and [30] use as much reactive power as they can to keep the voltages the same as the reference value. This not only leads to over-consumption of reactive power, which can potentially lead to an increase of real power losses, but also (as we show in Section 3.5) can increase line congestion in the distribution system.

To address these shortcomings, in this chapter, we propose two novel volt/var control schemes based on AARC to keep voltages within predefined limits using residential inverters. To cope with different grid code requirements, our first approach formulates the reactive power of inverters based on their real power deviation, while the second approach formulates them based on voltage magnitude deviation. In the first stage of both schemes, we propose to decouple the AARC of the volt/var problem into convex quadratically constrained programming (QCP) and linear programming (LP) sub-problems. The QCP sub-problem is a centralised optimal power flow with the objective of minimum real power loss subject to voltage limit constraints. The LP sub-problem is used to optimise the linear relation between the inverters' reactive power and real power deviation in the first scheme, and voltage magnitude deviation in the second scheme. The second stage is a local feedback controller that determines the inverter reactive power, using the provided linear functions and local measurements.

Numerical analysis is used to compare our proposed methods with the existing volt/var control techniques in the literature, including two purely local control approaches, i.e., fixed droop based volt/var control suggested by IEEE standard 1547 [21], and the incremental droop control presented in Chapter 2; also, the state of the art in volt/var control based on AARC proposed in [27], and the optimal solution that has knowledge of the eventual realisation of uncertainty. Our analysis shows that factoring the actual network voltage limits into the decision-making process will significantly decrease excess reactive power usage and real power loss in the system. It should be noted that with increasing voltage issues in distribution systems, it is predicted that new ancillary service markets will emerge to incentivise consumers to provide reactive power support [56]. In such a situation, the excessive use of reactive power puts an unnecessary economic burden on the dis-

tribution system operator. Another strength of our approach is that the two AARC formulations facilitate the integration of such control approaches with existing regulations and grid code requirements. For example, the German grid code mandates that the reactive power of residential inverters be a function of real power [22], and the Australian grid code mandates that the reactive power of residential inverters be a function of voltage magnitude [57]. The major contributions of this chapter are:

- an AARC of volt/var problem that formulates the inverters' real-time reactive power response as a linear function of voltage magnitude;
- a novel formulation that improves the state-of-the-art solution [27] to the volt/var problem, which uses AARC to formulate the inverters' real-time reactive power response as a linear function of their real power deviation. We modify the formulation by incorporating the voltage and inverter limit constraints directly in the formulation at the early stages of developing the linear function. Our simulations show that our approach, compared to [27], leads to fewer voltage violations and significantly decreases the inverter's reactive power usage, network real-power loss, and line congestion;
- a Monte-Carlo-based comparison between our proposed approaches and 4 alternative volt/var techniques in small and large scale distribution systems. Our experiments demonstrate that not only our approaches can keep the voltages inside the accepted limits for a wider range of scenarios, but also significantly decrease the reactive power usage, real power loss, and line congestion compared to the alternative approaches.

The rest of this chapter is organised as follows. In Section 3.2 a short summary of the AARC technique is presented. In Section 3.3 our proposed methods are introduced. A short summary of other volt/var techniques are presented in Section 3.4, and simulation results are reported in Section 3.5. Scalability to large distribution systems is investigated in Section 3.6. Finally, Section 3.7 concludes this chapter.

This chapter presents an edited and extended version of our work [46], published as a journal paper in IEEE Transactions on Power Systems.

3.2 AARC Methodology

Ben-Tal and et al. originally designed adjustable robust counterpart algorithm in [54] to deal with uncertainty in real-time. For this purpose, they introduced an affinely adjustable robust counterpart (AARC) variant in which the variables are modelled as linear functions of the uncertain parameters. They showed that the AARC approach is not only computationally tractable, but also that it is significantly less conservative compared to conventional Robust Counterpart approaches. Their affine function can be written as follows:

$$X(\epsilon) := \beta + \alpha\epsilon, \tag{3.1}$$

where $X(\epsilon)$ is the control variable, comprising a non-adjustable part β and an adjustable part $\alpha\epsilon$. ϵ is the uncertain parameter in the original problem, while β and α are the decision variables in the robust counterpart problem. Fixing β and α in real-time operation allows the variable X to affinely tune itself to the volatility of the uncertain parameter ϵ. In other words, similarly to a linear feedback controller, the value of X can be constantly updated as uncertain parameters are revealed. In what follows, we present the AARC methodology on a general adjustable robust linear optimisation problem to provide the required setup on which we build our approach[1] in Section 3.3, whose result is published in [46]

Let $\boldsymbol{\epsilon}$ be a random vector with convex polyhedral sample space $\mathcal{E} := \{\boldsymbol{\epsilon} \in \mathbb{R}^m : \boldsymbol{W}\boldsymbol{\epsilon} \leq \boldsymbol{h}\}$, where $\boldsymbol{W} \in \mathbb{R}^{\nu \times m}$ and $\boldsymbol{h} \in \mathbb{R}^{\nu}$ are known parameters of the polyhedron. Also, let $f : \mathcal{E} \to \mathbb{R}^n$ be a function whose range are the variables of an optimisation problem that can take recourse actions in response to the uncertainty realisation. We also define $f \in \mathcal{F}$, where $\mathcal{F}$ is the set of all possible/acceptable functions mapping the sample space $\mathcal{E}$ to $\mathbb{R}^n$. Consider a general adjustable robust linear optimisation problem as:

$$\min_{f \in \mathcal{F}} \ \boldsymbol{c}^{\intercal} f(\boldsymbol{\epsilon}) \tag{3.2a}$$

$$\boldsymbol{A} f(\boldsymbol{\epsilon}) \leq \boldsymbol{B}\boldsymbol{\epsilon} + \boldsymbol{d} \quad \forall \boldsymbol{\epsilon} \in \mathcal{E}, \tag{3.2b}$$

where $\boldsymbol{c} \in \mathbb{R}^n$, $\boldsymbol{A} \in \mathbb{R}^{w \times n}$, $\boldsymbol{B} \in \mathbb{R}^{w \times m}$ and $\boldsymbol{d} \in \mathbb{R}^w$ are parameters of the optimisation.

As discussed in [54], solving problem (3.2), and finding function f for a general case is computationally intractable. Also in practice, we

[1] Throughout Chapters 3 to 5, we repeatedly use linear programming, duality theory and their applications in obtaining the robust counterpart of an optimisation problem. Hence, to make it easier to follow for the reader, we provide a brief overview of these topics in Appendix B.

might want to restrict f to belong to a particular family of functions for simplicity or stability reasons. If we restrict $\mathcal{F}$ to be the set of affine functions from $\mathcal{E}$ to $\mathbb{R}^n$, we can solve the optimisation problem (3.2) offline, and then just have to evaluate a simple affine function in real-time. We can apply this affine restriction directly to f:

$$f(\boldsymbol{\epsilon}) \coloneqq \boldsymbol{\beta} + \boldsymbol{\alpha}\boldsymbol{\epsilon}, \tag{3.3}$$

where $\boldsymbol{\beta} \in \mathbb{R}^n$ and $\boldsymbol{\alpha} \in \mathbb{R}^{n \times m}$ are the decision variables of the offline optimisation, and parameters of the affine function. We then, substitute the affine function (3.3), which we will refer to as LDR, in the optimisation model (3.2). Notice that the objective function (3.2a) contains uncertain parameters. The common technique in robust optimisation to deal with an uncertain objective is to evaluate the objective function at the worst-case by writing the equivalent epigraph model with certain objective [54]. To do so, we introduce auxiliary variables (x_a), and then shift the uncertain parameters from the objective to multiple additional constraints as follows:

$$\min_{x_a, \boldsymbol{\beta}, \boldsymbol{\alpha}} \quad x_a \tag{3.4a}$$

$$\boldsymbol{c}^\intercal(\boldsymbol{\beta} + \boldsymbol{\alpha}\boldsymbol{\epsilon}) \leq x_a \qquad \forall \boldsymbol{\epsilon} \in \mathcal{E} \tag{3.4b}$$

$$\boldsymbol{A}(\boldsymbol{\beta} + \boldsymbol{\alpha}\boldsymbol{\epsilon}) \leq \boldsymbol{B}\boldsymbol{\epsilon} + \boldsymbol{d} \qquad \forall \boldsymbol{\epsilon} \in \mathcal{E}, \tag{3.4c}$$

Introducing vector $\boldsymbol{\beta}_1 = [x_a, \boldsymbol{\beta}^\intercal]^\intercal$ and collecting constraints (3.4b) and (3.4c) in a set of constraints, we obtain:

$$\min_{\boldsymbol{\beta}_1, \boldsymbol{\alpha}} \quad \boldsymbol{c}_1^\intercal \boldsymbol{\beta}_1 \tag{3.5a}$$

$$\boldsymbol{A}_1(\boldsymbol{\beta}_1 + \boldsymbol{\alpha}\boldsymbol{\epsilon}) \leq \boldsymbol{B}_1\boldsymbol{\epsilon} + \boldsymbol{d}_1 \qquad \forall \boldsymbol{\epsilon} \in \mathcal{E}, \tag{3.5b}$$

where $\boldsymbol{c}_1$, $\boldsymbol{A}_1$, $\boldsymbol{B}_1$ and $\boldsymbol{d}_1$ are known matrices with appropriate sizes. Notice that the constraints in (3.5b) need to be satisfied for any realisation of uncertainty within the sample space $\mathcal{E}$, which leads to an infinite number of constraints. To overcome this, the *max* protection function is used to robustify (3.5b) against the worst uncertainty realisation within $\mathcal{E}$ as follows:

$$\max_{\boldsymbol{\epsilon} \in \mathcal{E}} \{(\boldsymbol{A}_1\boldsymbol{\alpha} - \boldsymbol{B}_1)\boldsymbol{\epsilon}\} \leq -\boldsymbol{A}_1\boldsymbol{\beta}_1 + \boldsymbol{d}_1. \tag{3.6}$$

We then use the duality technique to replace (3.6) with a finite set of linear inequality constraints:

$$\exists \boldsymbol{\lambda} : \boldsymbol{h}^\intercal \boldsymbol{\lambda} \leq -\boldsymbol{A}_1\boldsymbol{\beta}_1 + \boldsymbol{d}_1,\ \boldsymbol{W}^\intercal \boldsymbol{\lambda} \geq \boldsymbol{A}_1\boldsymbol{\alpha} - \boldsymbol{B}_1, \tag{3.7}$$

where $\boldsymbol{\lambda} \in \mathbb{R}^{\nu}_{\geq 0}$ is the vector of dual variables associated with the bounding constraints in the sample space $\mathcal{E}$. Hereinafter, we refer to the optimisation problem with objective (3.5a) subject to constraint (3.7) as the conventional AARC model, which is a linear programming problem and can be solved efficiently using solvers such as Gurobi [58].

3.3 Proposed Combined Central-Local Volt/Var Control Approach

In this section, we propose an affinely adjustable robust counterpart of the volt/var problem based on real powers (AARBP) and an affinely adjustable robust counterpart of the volt/var problem based on voltage magnitude (AA RBV). Fig. 3.1 shows an overview of our proposed two-stage process. The two stages in our proposed approach are differentiated from each other using the black-dotted line, and the data required to initialize the first stage is shown in the ovals on top. In the first stage of our control approaches, we obtain the inverter parameters, which are then communicated to the inverters through a communication channel. Since both of our proposed approaches are linear, they remain computationally tractable for networks with large numbers of PV inverters. We assume we have a reliable communication infrastructure that allows us to send the smart inverter parameters at regular intervals. Such communication infrastructure is an essential feature of smart grids, and various research and standards have been published to help realise it [59]. In the second stage, using the updated parameters and local measurements, the inverter reactive power set-points are calculated. The real power set-points are obtained using the maximum power point tracker (MPPT) included in the PV system to maximise power extraction under all conditions (note that the MPPT functionality is not the focus of our work). A regular inverter feedback controller is then used to achieve and maintain these set points on the AC side. Also, note that our approaches only require the inverters to measure the connection to the grid voltages, which the already installed inverters can measure in real-time. Thus, there is no need for a hardware upgrade in the PV / inverter systems. However, the inverters require a firmware update so that they follow our suggested control strategy.

Our first stage optimisation is done periodically in the background (in our simulation, we solve the optimisation problem every 5 minutes), while the local controllers in the second stage work in real-time. We update the controller parameters when we have a new output from our optimisation problem. The two blocks in Fig. 3.1 are detailed in the following subsections.

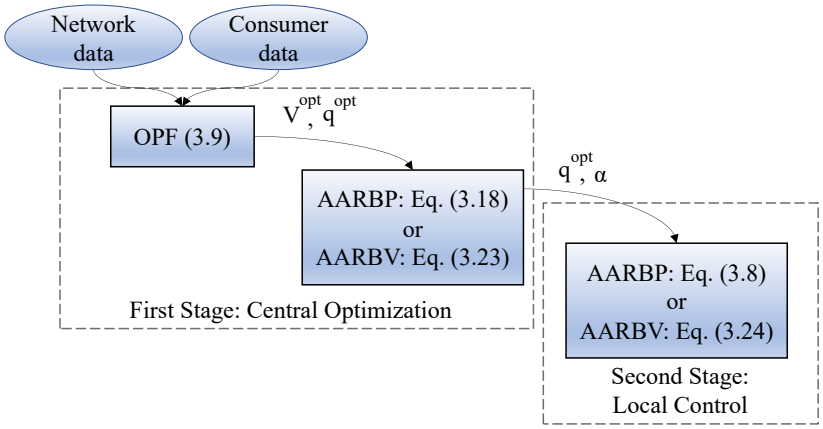

Figure 3.1: High-level structure of our proposed central-local control system.

3.3.1 AARC of the Volt/Var Problem Based on Real Power (AARBP)

In line with the German grid code[2], coordination of the reactive power contribution of PV inverters can be achieved using a linear relation between their real and reactive powers. To do this, we consider that measurements are made periodically throughout the network. Then, using these measurements, an optimal power flow (OPF) with the objective of minimizing real power loss is solved to obtain the ideal reactive power contribution of each inverter. Finally, to deal with operating point deviations in each period, we suggest to use a linear relation between the change in reactive power contribution and the real power deviation from the value measured at the start of the period by each inverter as follows:

$$q_i^{pv}(\Delta p_i^{pv}) = q_i^{opt} + \alpha_i \Delta p_i^{pv}, \tag{3.8}$$

where q_i^{pv} is the inverter reactive power connected to node i, q_i^{opt} is the optimal reactive power obtained from the OPF at the beginning of each period, Δp_i is the real power deviation from the measurement,

[2]The German grid code mandates the grid-connected inverters to provide reactive power support to keep the voltages within acceptable limits in cases of slow changes in connection voltage magnitudes. It suggests a linear relationship between the power factor and PV generation, which mathematically can be mapped to a linear relationship between the reactive and real power generation. Please note that a similar strategy is also proposed in the Australian standard [20], where a relationship between the real and reactive power is suggested. We have covered this in Section 2.2.1 under the name "Real-Reactive Power Mode (watt/var)". Also, note that the difference between the Australian and the German grid code is the addition of the dead-band in the Australian standard.

and α_i is the slope of the linear decision rule. The affine function (3.8) includes a bi-linear term $\alpha_i \Delta p_i^{pv}$, and thus the resulting AARC problem would be difficult (if at all possible) to solve. However, the uncertain parameter Δp_i^{pv} has a bounded polyhedral uncertainty set and provided that the rest of the problem is linear, we can use duality theory to obtain a linear AARC model. Unfortunately, this is not the case in our problem as our approach features a nonlinear OPF model. To resolve this, we decoupled the problem into two subproblems. In the first one, we use a convex conic relaxed OPF model to calculate the values of q_i^{opt}. In the second one, we linearise the power flow equations about the OPF solution of the first stage. This two-stage approach has the benefit of both accounting for the nonlinear power flow equations, and a tractable AARC model.

How to obtain the Non-Adjustable Parts of the Decision Variables

As in Chapter 2, we use the Distflow model to represent the power flow equations. To facilitate the task of the reader in keeping track of the equations we used, we repeat the model here. Recall that the $\mathcal{V}$ and $\mathcal{B}$ are the set of nodes and branches, respectively. For every node $i \in \mathcal{V}$, v_i denotes the squared voltage magnitude, also, p_i^D and p_i^{pv} denote the real power demand and PV generation. For every branch $(i,k) \in \mathcal{B}$, $z_{ik} = r_{ik} + jx_{ik}$ denotes the complex impedance of the line, and l_{ik} denotes the squared current magnitude between node i and node k. Also, P_{ij} and Q_{ij} denote the real and reactive powers sending from node i to node j. Thus, the Distflow model is written as follows:

$$\min \quad \sum_{(i,j)\in\mathcal{B}} r_{ij} l_{ij} \tag{3.9a}$$

$$p_j = \sum_{k:j\to k} P_{jk} - (P_{ij} - r_{ij} l_{ij}) \qquad \forall j \in \mathcal{V} \tag{3.9b}$$

$$q_j = \sum_{k:j\to k} Q_{jk} - (Q_{ij} - x_{ij} l_{ij}) \qquad \forall j \in \mathcal{V} \tag{3.9c}$$

$$v_j = v_i - 2(r_{ij}P_{ij} + x_{ij}Q_{ij}) + (r_{ij}^2 + x_{ij}^2) l_{ij} \qquad \forall (i,j) \in \mathcal{B} \tag{3.9d}$$

$$v_i l_{ij} \geq P_{ij}^2 + Q_{ij}^2 \qquad \forall (i,j) \in \mathcal{B} \tag{3.9e}$$

$$p_j = p_j^{pv} - p_j^D \qquad \forall j \in \mathcal{V} \tag{3.9f}$$

$$q_j = q_j^{pv} - q_j^D \qquad \forall j \in \mathcal{V} \tag{3.9g}$$

$$p_j^{pv^2} + q_j^{pv^2} \leq S_j^2 \qquad \forall j \in \mathcal{V} \tag{3.9h}$$

$$v_j^{min} \leq v_j \leq v_j^{max} \qquad \forall j \in \mathcal{V}. \tag{3.9i}$$

Solving the optimisation problem (3.9), we obtain the optimal value for the reactive power of each inverter, i.e., q_i^{pv} which is the non-adjustable part of the reactive power in our design, and is equivalent to the q_i^{opt} in the decision rule (3.8).

How to obtain the Adjustable Parts of the Decision Variables

The variable α_i is used to deal with voltage deviations due to the uncertainties in inverter real powers. A linear relation between the voltage deviation, and deviations in real and reactive power of inverters can be obtained by linearising the power flow equation about an operating point [39] as follows:

$$\Delta V_i = \sum_{k=1}^{n} K_{ik}^p \Delta p_k^{pv} + K_{ik}^q \Delta q_k^{pv} \qquad \forall i \in \mathcal{N} \tag{3.10a}$$

$$K_{ik}^p = \frac{\partial V_i}{\partial p_k^{pv}}, \quad K_{ik}^q = \frac{\partial V_i}{\partial q_k^{pv}}, \tag{3.10b}$$

where $\mathcal{N} = \mathcal{V} - \{0\}$ denotes the set of all nodes expect the slack node. Substituting $\Delta q_k^{pv} = \alpha_k \Delta p_k^{pv}$ from (3.8) into (3.10a), we can obtain the voltage deviations in terms of the uncertain parameter, i.e., real power of the inverter, as follows:

$$\Delta V_i = \sum_{k=1}^{n} (K_{ik}^p + \alpha_k K_{ik}^q) \Delta p_k^{pv}. \tag{3.11}$$

Remember that our goal here is to deal with uncertainties to prevent voltage violation. This can be formulated as follows:

$$V^{min} \leq V_i \leq V^{max}. \tag{3.12}$$

For any small changes around the operating point we can write the two equivalent linear equations:

$$V_i^{opt} + \Delta V_i \leq V^{max}, \quad V_i^{opt} + \Delta V_i \geq V^{min}, \tag{3.13a}$$

where V_i^{opt} is the voltage magnitude obtained from the centralised OPF at the beginning of each interval at node i. Considering the linear decision rules, the voltage deviation term can be replaced with (3.11) as follows:

$$V_i^{opt} + \sum_{k=1}^{n} (K_{ik}^p + \alpha_k K_{ik}^q) \Delta p_k^{pv} \leq V^{max} \tag{3.14a}$$

$$V_i^{opt} + \sum_{k=1}^{n} (K_{ik}^p + \alpha_k K_{ik}^q) \Delta p_k^{pv} \geq V^{min}. \tag{3.14b}$$

We use a polyhedral uncertainty set to model the deviation of PV power from a forecast:

$$\Delta p_i^{pv} \in \mathcal{U} = [\Delta p_i^{min}, \Delta p_i^{max}] \tag{3.15a}$$

$$\Delta p_i^{min} \leq 0 \leq \Delta p_i^{max}. \tag{3.15b}$$

Such an uncertainty set notifies that the PV power can deviate from its forecast in either a positive or negative direction, which is representative of how PV power behaves in practice. We only consider the uncertainty in PV generation. This is in line with the state of the art [27] to enable us to compare our approach with the recent related works. Regarding the uncertainty of loads, since we run our optimisation model and obtain the AARC control parameters every 5 minutes, at every run, we take the latest (most accurate) load forecast into account.

Now we can rewrite (3.14) as the following optimisation problem. We consider the objective to be equal to the minimum of aggregated values of $|\alpha_i|$. The idea is to obtain the minimum aggregate change from the optimal reactive power values in all the nodes that can keep the voltages in the accepted limits, for all operating point deviations. Also, to obtain practical values for α_i we consider the inverter capacity constraint.

$$\min \quad \sum_{i=1}^{n} \alpha_i^{aux} \tag{3.16a}$$

$$\text{(3.14a), (3.14b)} \qquad \forall i \in \mathcal{N} \tag{3.16b}$$

$$p_i^{pv^2} + q_i^{pv^2} \leq S_i^2 \qquad \forall i \in \mathcal{N} \tag{3.16c}$$

$$\alpha_i^{aux} \geq \alpha_i, \quad \alpha_i^{aux} \geq -\alpha_i \qquad \forall i \in \mathcal{N}, \tag{3.16d}$$

where (3.16d) is used to linearise the absolute value of α_i in the objective function. To avoid repetition, these two constraints are not included in the formulations in the rest of this chapter, instead only the absolute value over α_i is used. (3.16c) is a circle in (p_i^{pv}, q_i^{pv}) coordinates, which can be linearised using a set of linear equalities as follows:

$$(cos(\phi) + sin(\phi))q_i^{pv} + (cos(\phi) - sin(\phi))p_i^{pv} \leq \sqrt{2}S_i \quad \forall i \in \mathcal{N}, \forall \phi \in \mathcal{A}, \tag{3.17}$$

where $\mathcal{A} = \{0, \pi/m, 2\pi/m, ..., (2m-1)\pi/m\}$, and m is an arbitrary integer number. Considering the same box uncertainty set (3.15), and partitioning the real power of the inverter $p_i^{pv} = p_i^{pv_0} + \Delta p_i^{pv}$, we can

obtain the AARC of (3.16), using the duality technique used in [30] as follows:

$$\min \quad \sum_{i=1}^{n} |\alpha_i| \tag{3.18a}$$

$$V^{max} - V_i^{opt} \geq \sum_{k=1}^{n} \theta_{ik}^{'} \Delta p_k^{max} + \theta_{ik}^{''} \Delta p_k^{min} \tag{3.18b}$$

$$\theta_{ik}^{'} + \theta_{ik}^{''} = (K_{ik}^{p} + \alpha_k K_{ik}^{q}) \tag{3.18c}$$

$$\theta_{ik}^{'} \geq 0, \quad \theta_{ik}^{''} \leq 0 \tag{3.18d}$$

$$V_i^{opt} - V^{min} \geq \sum_{k=1}^{n} \lambda_{ik}^{'} \Delta p_k^{max} + \lambda_{ik}^{''} \Delta p_k^{min} \tag{3.18e}$$

$$\lambda_{ik}^{'} + \lambda_{ik}^{''} = -(K_{ik}^{p} + \alpha_k K_{ik}^{q}) \tag{3.18f}$$

$$\lambda_{ik}^{'} \geq 0, \quad \lambda_{ik}^{''} \leq 0 \tag{3.18g}$$

$$\begin{aligned}&(cos(\phi) + sin(\phi))q_i^{opt} + (cos(\phi) - sin(\phi))p_i^{pv_0} \\ &+ \gamma_{i\phi}^{'} \Delta p_i^{max} + \gamma_{i\phi}^{''} \Delta p_i^{min} \leq \sqrt{2} S_i\end{aligned} \tag{3.18h}$$

$$\gamma_{i\phi}^{'} + \gamma_{i\phi}^{''} = (cos(\phi) - sin(\phi)) + \alpha_i (cos(\phi) + sin(\phi)) \tag{3.18i}$$

$$\gamma_{i\phi}^{'} \geq 0, \quad \gamma_{i\phi}^{''} \leq 0 \tag{3.18j}$$

$$j, k \in \mathcal{N}, \quad \phi \in \mathcal{A}, \tag{3.18k}$$

where $\theta_{ik}^{'}$, $\theta_{ik}^{''}$, $\lambda_{ik}^{'}$, $\lambda_{ik}^{''}$, $\gamma_{ik}^{'}$ and $\gamma_{ik}^{''}$ are dual variables. The convex quadratic problem (3.9) and linear problem (3.18) can be solved in polynomial time [58]. We used the *Gurobi* solver in our experiments.

3.3.2 AARC of the Volt/Var Problem Based on Voltage Magnitude (AARBV)

In this section, we propose an AARC formulation of the volt/var problem, which is in line with the IEEE 1547 standard and the Australian grid code. Similarly to the approach described in section 3.3.1, we consider a two-stage approach with periodic measurement throughout the network. In the first stage, after solving OPF (3.9), the following linear decision rule based on the voltage magnitude is used to deal with operating point deviations in each period:

$$q_i^{pv}(\Delta V_i) = q_i^{opt} + \alpha_i \Delta V_i. \tag{3.19}$$

Substituting $\Delta q_i^{inv} = \alpha_i \Delta V_i$ from (3.19) to (3.10a), and considering the same objective as (3.16), we obtain the following optimisation problem:

$$(3.10),\ (3.16a),\ (3.16d),\ (3.17) \tag{3.20a}$$
$$\Delta q_i^{pv} = \alpha_i \Delta V_i. \tag{3.20b}$$

Constraint (3.20b) has a bilinear term, which makes (3.20) non-convex. Note that in (3.8), Δp_i^{pv} is an uncertain parameter while ΔV_i in (3.19) is a variable of the optimisation problem. Thus, unlike in (3.16), the duality technique described in section 3.3.1 cannot be used directly to linearise problem (3.20). Also, other relaxation techniques for bilinear terms, e.g., McCormick's relaxation [60], depend heavily on having tight variable bounds [61]. In fact, general relaxation of bilinear terms is an ongoing research topic in the field of optimisation. In our case, since tight bounds on α_i is not available prior to solving (3.20), using McCormick's relaxation may produce poor results, which would degrade performance of the controller in the second layer. As an alternative, to solve problem (3.20), we propose approximating voltage deviation (3.11) with only the deviation in real power, i.e. ignoring how reactive power changes voltage in the network in the LDR phase. Then, the impact of reactive power on voltage is factored back in at the local control phase, by using (3.19) to change the reactive power at discrete points in time rather than continuously updating it. This is in this sense that the inverter reactive powers are controlled to prevent voltage violation due to changes in real powers. This creates a time difference between the effects of real and reactive power changes in voltage deviation. The idea is to take benefit from the time difference to decouple the voltage deviation caused by changes in inverter reactive powers, from the deviations caused by real powers. The motivation behind this will be further explained later in this section, after introducing the modified discrete version of the voltage-base linear decision rule (equation (3.24)). Applying this approximation, we obtain the following optimisation problem:

$$(3.16a),\ (3.16d),\ (3.17) \tag{3.21a}$$
$$\sum_{k=1}^{n}(K_{ik}^p \Delta p_k^{pv} + \alpha_k K_{ik}^q \sum_{j=1}^{n} K_{ij}^p \Delta p_j^{pv}) \leq V^{max} - V_i^{opt} \tag{3.21b}$$
$$\sum_{k=1}^{n}(K_{ik}^p \Delta p_k^{pv} + \alpha_k K_{ik}^q \sum_{j=1}^{n} K_{ij}^p \Delta p_j^{pv}) \geq V^{min} - V_i^{opt}. \tag{3.21c}$$

Simplifying (3.21) results in:

$$s \min \quad \sum_{i=1}^{n} |\alpha_i| \tag{3.22a}$$

$$\sum_{k=1}^{n} (K_{ik}^{p} + \sum_{j=1}^{n} \alpha_j K_{ij}^{q} K_{jk}^{p}) \Delta p_k^{pv} \leq V^{max} - V_i^{opt} \tag{3.22b}$$

$$\sum_{k=1}^{n} (K_{ik}^{p} + \sum_{j=1}^{n} \alpha_j K_{ij}^{q} K_{jk}^{p}) \Delta p_k^{pv} \geq V^{min} - V_i^{opt} \tag{3.22c}$$

$$\begin{aligned}(cos(\phi) + sin(\phi)) q_i^{opt} + (cos(\phi) - sin(\phi)) p_i^{inv_0} + \\ (cos(\phi) - sin(\phi)) \Delta p_i^{pv} + (cos(\phi) + sin(\phi)) \alpha_i \sum_{j=1}^{n} K_{ij}^{p} \Delta p_j^{pv} \leq \sqrt{2} S_i^{max}.\end{aligned} \tag{3.22d}$$

Considering the same box uncertainty set (3.15), and the same duality technique as used in (3.18) we can obtain the following AARC for (3.22):

$$\text{(3.18a), (3.18b), (3.18d), (3.18e), (3.18g), (3.18h), (3.18j)} \tag{3.23a}$$

$$\theta_{ik}^{'} + \theta_{ik}^{''} = (K_{ik}^{p} + \sum_{j=1}^{n} \alpha_j K_{ij}^{q} K_{jk}^{p}) \qquad \forall i, k \in \mathcal{N} \tag{3.23b}$$

$$\lambda_{ik}^{'} + \lambda_{ik}^{''} = -(K_{ik}^{p} + \sum_{j=1}^{n} \alpha_j K_{ij}^{q} K_{jk}^{p}) \qquad \forall i, k \in \mathcal{N} \tag{3.23c}$$

$$\begin{aligned}\gamma_{ij\phi}^{'} + \gamma_{ij\phi}^{''} = \alpha_i (cos(\phi) + sin(\phi)) K_{ij}^{p} + \\ (cos(\phi) - sin(\phi)) K_{ij}^{q} \qquad \forall i = j \in \mathcal{N}, \forall \phi \in \mathcal{A}\end{aligned} \tag{3.23d}$$

$$\gamma_{ij\phi}^{'} + \gamma_{ij\phi}^{''} = \alpha_i (cos(\phi) + sin(\phi)) K_{ij}^{p} \qquad \forall i \neq j \in \mathcal{N}, \forall \phi \in \mathcal{A}. \tag{3.23e}$$

Solving optimisation problem (3.23) yields values for α_i. Now we introduce the discrete version of the voltage-base linear decision rule as follows:

$$q_i^{inv,n+1} = q_i^{inv,n} + \alpha_i (V_i^{n+1,a} - V_i^{n,b}), \tag{3.24}$$

where n is an index for each discrete change in reactive power, and a and b represent voltage measurements made just before and after the n-th reactive power adjustment, as shown in Figure 3.2. An example is presented here to demonstrate, how based on (3.24) the reactive powers in each instance are calculated. To calculate the reactive powers at instance $n = 2$, the voltage is measured at $n = 2, a$. Then, it is compared with the voltage magnitude at $n = 1, b$, and based on (3.24) a

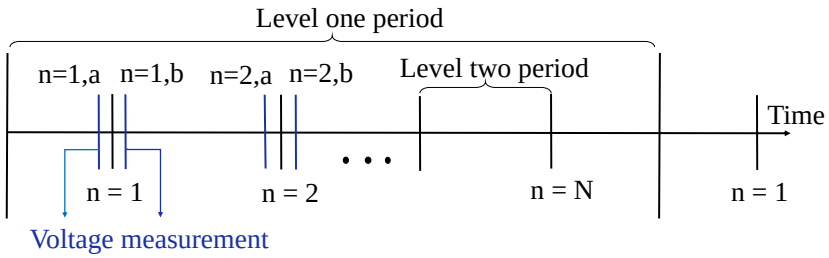

Figure 3.2: A sample of the discrete time definition used in (3.24). The level one period is the time between two consecutive centralised adjustments, and the level two period is the time between two consecutive discrete decisions.

new value for reactive power is obtained. After applying the calculated reactive powers, at $n = 2, b$ the voltage magnitudes are measured and stored to be used in the next instance. This process should be intuitive as it means the calculated values for reactive power at decision time n will not change at decision time $n + 1$, if the operating point has not changed since the actions made at n. Under such a scheme, the voltage deviation caused by changes in inverter reactive powers is decoupled from the deviations caused by real powers, which makes the approximation used in (3.21) possible. Note that this approach is practical under the assumption that changes in network operating point occur more slowly than the time required for the inverter to inject / absorb the calculated value, and measure the new voltage profile. This is a justifiable assumption as the time required for the inverters to do the above mentioned actions is in the order of hundreds of milliseconds, and the PV and load variations are generally in the order of tens of seconds [62].

In order to implement the AARBV approach on the PV inverters, the inverters require a firmware update so that they can follow our suggested control strategy. They need to periodically measure the voltage at the connection point and store the voltage magnitude value until a new a measurement is made. Then following the decision rule (3.19), they generate the inverter reactive power set-point. The parameters of the inverter controllers also need to be updated periodically by solving the optimisation problems (3.9) and (3.23) as described above.

3.3.3 Use of Auxiliary Variables

In general the volt/var problem with hard voltage and inverter capacity constraints may not always have a feasible solution regardless of the approach. In these circumstances we would still like to take an action

that reduces the voltage violation by as much as possible. To achieve this, we convert these to soft constraints by introducing auxiliary variables for the voltage limit constraints ((3.18b) and (3.18e)), and the inverter capacity constraints ((3.18h)). These auxiliary variables are then included in the objective function with large penalty coefficients.

3.4 Alternative Solutions to the Volt/Var Problem

In this section, the three alternative techniques for volt/var control[3], introduced in section 3.1, are briefly summarised. These techniques along with the two proposed techniques, AARBP and AARBV, and the optimal solution considering perfect realisation of uncertainty will be compared in section 3.5.

3.4.1 Fixed Droop-Based Volt/Var Control

This approach is suggested by IEEE standard 1547, where the reactive power of each inverter is calculated as follows:

$$q_i^{pv} = \begin{cases} \big[-\alpha_i (V_i - (V_i^{nom} - \delta_i)) \big]_{q^{min}}^{q^{max}} & V_i < V_i^{nom} - \delta_i \\ 0 & V_i^{nom} - \delta_i \leq V_i \leq V_i^{nom} + \delta_i \\ \big[-\alpha_i (V_i - (V_i^{nom} + \delta_i)) \big]_{q^{min}}^{q^{max}} & V_i > V_i^{nom} + \delta_i, \end{cases} \tag{3.25}$$

where V_i^{nom} is the nominal voltage value, usually considered equal to one per-unit. $2\delta_i$ is the dead-band size, and α_i is the slope of the droop. Operator $[.]_{.min}^{max}$ enforces the inverter reactive power capacity limit.

[3]Please note that this chapter focuses on using only reactive power to deal with the electrical distribution systems' over/under voltage problem. This is a more acceptable solution for the PV owners as it will not curtail their PV generation, i.e., monetarily penalise them for the grid limitation.

3.4.2 Incremental Droop Based Volt/Var Control

In this approach[4] the reactive power of each inverter is calculated as follows:

$$q_n^{pv}(t) = \left[q_n^{pv}(t-1) + \Delta q_n^{pv}(t)\right]_{\underline{q_n}}^{\overline{q_n}} \tag{3.26a}$$

$$\Delta q_n^{pv}(t) = \begin{cases} m_1(V_n(t) - V_3) & if \quad V_n(t) \geq V_3 \\ 0 & if \quad V_2 \leq V_n \leq V_3. \end{cases} \tag{3.26b}$$

where m_1 is the rate of change of the reactive power, V_2 and V_3 are the lower and upper desired voltage limits, and $t \in \mathcal{T} = \{0, 1, .., T\}$ denotes the number of discrete time steps. This approach acts similar to an integral feedback controller, where the reactive power at each time step is a summation of the reactive power at previous time step and the deviation from a reference value. Please note that this approach is not a standard PV inverter control strategy. However, it can be easily implemented using the available technology as it only requires measuring the voltage magnitude at the inverter connection point to the grid. Thus, implementing this approach does not require a hardware upgrade. However, since this approach is not an already built-in functionality of the inverters, a firmware update is required for the inverters to follow this approach's control rule.

3.4.3 State-of-the-Art Linear Decision Rules Based on Real Powers in the Literature

In this LDR approach, proposed by R.A. Jabr in [27] (which we will refer to as AARC-J. hereinafter), the reactive power of each inverter is obtained using the following linear rule:

$$q_i^{pv} = q_i^{opt} + \alpha_i \Delta p_i^{pv}. \tag{3.27}$$

Note that although both (3.27) and AARBP use the same linear decision rule, the optimisation algorithm used to obtain the value of α_i is different. The main difference is that in [27] α_i is determined in a way to minimise the voltage deviation irrespective of the voltage limits. However, AARBP aims to determine α_i to keep the voltage inside the voltage limits. Through numerical simulations, we will show that this change will result in a significant improvement in the performance of the decision rule both in terms of reducing reactive power usage and decreasing scenarios with voltage violations.

[4]This approach is derived from our proposed approach in Chapter 2 which is described in detail in Section 2.3.1. The only difference is that here we are only using its capability to provide reactive power support to have a fair comparison with other approaches.

3.5 Numerical Results and Discussion

We test the performance of the different methods using simulation on a real 27-node underground LV feeder with $R/X \approx 2$ located in Hobart, Australia [32] (the details of the network data and how we assume to have a balanced network are explained in Section 2.5.1 and are repeated here to avoid repetition). Three cases with different system operating points are considered for the comparison. In *Case 1* the voltage profile is well-below the voltage limits, and even in the worst case condition the voltage limits will not be breached. In *Case 2* all the voltages at the measurement time are below the limits. However, under the worst case condition the voltage limits will be breached. In *Case 3* the network is operating at the limit, which means that there is at least one node whose voltage magnitude is equal to the voltage limit at the measurement time. Therefore, any increase in real power injections would result in voltage violation.

We assume that measurements are made throughout the network every 5 minutes, and the resolution of load consumption and PV generation data is one minute. Similarly to Chapter 2, the load data is extracted from [34], where the load consumption varies between 0-5 kW, assuming the houses have 4-6 residents. In all of the cases, PV generation with uniform distribution between 0-4 kW is randomly assigned to each node (the different values associated to PV generation in each node is because of randomly sampling solar system capacity, orientation, soiling, and irradiance all at the same time). In subsection 3.5.1 a detailed result for one scenario, i.e., measurement followed by a change in the operating point, is presented for each case. In subsection 3.5.3 a Monte Carlo simulation is carried out. 250 scenarios are generated between the three cases. Then, each scenario is simulated for 4 minutes, with the decision rules / droops acting every one minute, resulting in a total of 1000 random operating points.

3.5.1 Detailed Results for One Scenario

Fig. 3.3 shows the voltage profile and reactive power usage of the inverters at each node in the three cases using the different volt/var control schemes.

In *Case 1* since (even in the worst condition) the voltage limits will not be violated, ideally it is expected that control schemes make a slight change in response to the operating point deviation, to keep the real power loss at minimum possible. In both AARBP and AARBV approaches, the value that we obtained for α is equal to zero in all the nodes. The reason is that the operating point deviation does not

lead to any voltage violation and thus, there is no need to any change in reactive powers in real-time to guarantee that voltages are within the limits. We can see in Fig. 3.3.d that the results of AARBP and AARBV is almost equal to the optimal solution. On the other hand, the AARC approach of [27] overuses the reactive power resources to keep all voltages at the measurement value (i.e., overusing the reactive power for an unnecessary requirement). Moreover, since the Inc. droop approach keeps all the voltages below 1.02 p.u., as plotted, it over-absorbs more reactive power than necessary.

In *Case 2* the measured values for PV generation indicate that none of the voltages are initially beyond their limits. However, since in some possible realisations of uncertainty over the next 4 minutes the voltage limits can be breached, α in AARBP and AARBV have negative values to absorb reactive power if real power injection increases. It can be seen in Fig. 3.3.e that AARBV has a better performance compared to other techniques and uses much less reactive power while keeping the voltage magnitudes inside the limit.

In *Case 3* the initial values for PV generation is in a way that

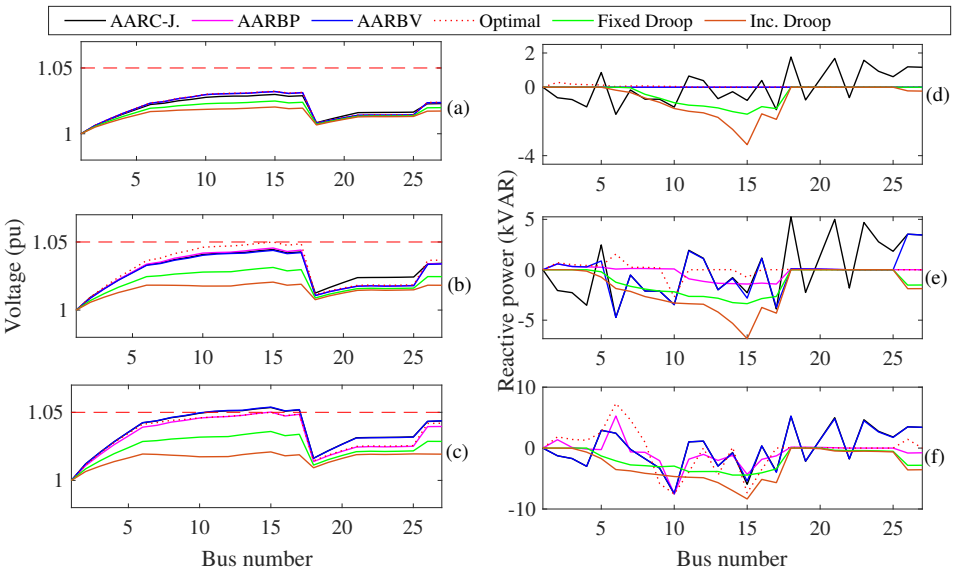

Figure 3.3: Voltage magnitude and reactive power of nodes in the three cases, under different volt/var control. (a), (b) and (c) show the voltage magnitude in *Case 1*, *Case 2* and *Case 3*, respectively. Also, (d), (e) and (f) show the reactive power in *Case 1*, *Case 2* and *Case 3*, respectively. Note that as described in text (a) and (d) AARBP and AARBV lie completely on top of each other. Also, in (c) and (d) and AARC [27] are almost on top of each other.

at least in one node voltage magnitude is beyond its predefined limit. Interestingly, we see that the results from AARC-J. and AARBP act very similarly, unlike in the previous cases. This happens in almost all the other random scenarios that we generated for case 3. This can be explained by observing (3.18). Since there is at least one node whose voltage magnitude is equal to the limit, the value of $V^{max} - V_i^{opt}$ is equal to zero for that node. So in turn the solver in (3.18) tries to minimise the voltage deviation in that node to prevent the big penalty of having non-zero values for the soft voltage constraints. Therefore, the objective function of AARBP and AARC [27] will be close to each other. Moreover, we can see that in both schemes voltage violation occurs. In general for the extreme *Case 3* there are some scenarios where AARBV fails to keep the voltages inside the limits. We suggest an extension to AARBP and AARBV to deal with extreme *Case 3*, which will be introduced in subsection 3.5.2.

3.5.2 Further Improvement in AARBP and AARBV to Handle Extreme Cases

We propose a further improvement to AARBP and AARBV by limiting the reactive power only to negative values, i.e. absorption when extreme operating conditions occur, such as *Case 3*. It is possible to automatically distinguish these extreme conditions from the other cases prior to running the AARC step by comparing the value of V_i^{opt} from solving the OPF with the voltage limits. Note that positive values for reactive power in some nodes can help to decrease total real power loss. This is because the reactive power consumption of lines and loads can be sourced locally from inverters rather than needing to come from the upstream network, reducing current flow throughout the entire system. By applying this improvement, we are foregoing the ability to reduce losses in extreme cases to keep voltages within the limits in more scenarios. Fig. 3.4 shows the voltage profile and the reactive power usage under AARBP and AARBV in the same operating point as chosen in Fig. 3.3.f. It can be seen that the voltages are brought to the limits under both schemes using their improved versions[5].

[5]We use an exact power flow model to calculate the voltage magnitudes, using the Backward-Forward technique [50], in the real-time operation rather than the linearised approximated model. In doing so, we ensure that our experiments are realistic and that the linear power flow model approximation does not affect the number of voltage violations happening in the grid.

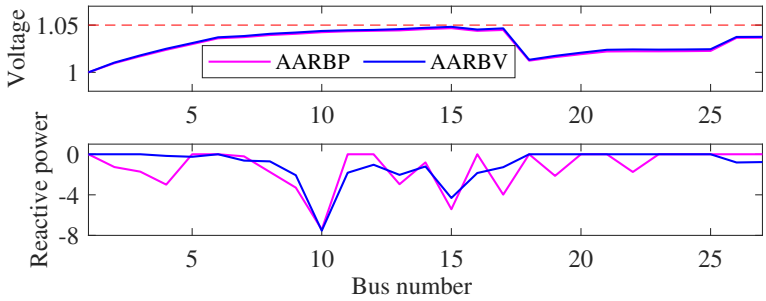

Figure 3.4: Voltage profile and reactive power of nodes under improved versions of AARBP and AARBV in *Case 3*.

3.5.3 Average Results Over Multiple Operating Points

Fig. 3.5 shows the average of real power loss and reactive power usage relative differences between the optimal solution and other approaches, over the thousand operating points. It can be seen that AARBP and AARBV significantly use less reactive power compared to the other techniques. This can be economically beneficial from the distribution system operator's perspective, as discussed in section 3.1. Furthermore, while the improved AARBP and AARBV approaches managed to keep the voltage within the safe limits in almost all scenarios, AARC-J. failed to do so in 213 out of 1000 operating points. We exclude these infeasible results from the average results shown in Fig. 3.5. When

Fig. 3.6 shows the maximum difference in line loading between different control schemes and the optimal scheme. To conduct the comparison, first we calculate the loading on each line (the line current as a percentage of the line rating). Then, we obtain the maximum difference between the loadings for each technique and the optimal approach. We can see that on average AARBP and AARBV act closer to the optimal approach. Incremental droop-based control increases the line currents more than other techniques, with droop-based control and AARC-J. behind it.

From the reported simulations we can conclude that even though purely local approaches (i.e., droop-based and incremental droop-based controls) eliminate the need for communication, they significantly increase the reactive power usage as well as the real power losses, and may create line congestion in heavily loaded lines. Other approaches investigated in this paper require a communication infrastructure and system configuration information. In particular, AARC-J. leads to an excessive use of reactive power which not only might not be able to keep the voltage within the safe limits, but also might create line con-

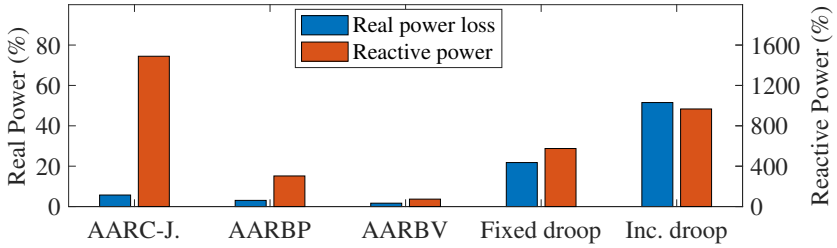

Figure 3.5: Average relative difference in real power loss and inverter reactive power usage (absorption or injection) between different voltage control schemes and the optimal scheme over 1000 operating points in the 27-node system.

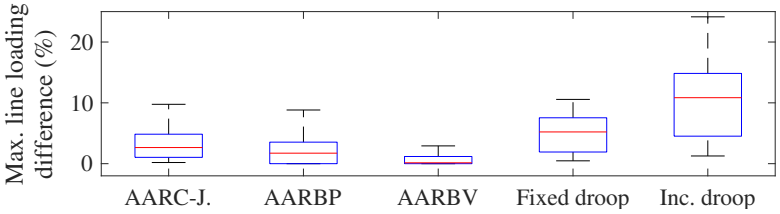

Figure 3.6: Distribution of the maximum line current differences in the 27-node system, using different approaches with the optimal scheme. On each box, the central mark indicates the median, and the bottom and top edges of the box indicate the 25th and 75th percentiles, respectively.

Table 3.1: Summary of the simulation results in the 27-node system

Control technique	Agg. real power loss (MW)	Agg. reactive power usage (MVAR)	No. voltage violation
AARC-J.	1.286	30.876	213
AARBP	1.254	7.834	1
AARBV	1.237	2.284	0
Fixed droop	1.481	13.116	4
Inc. droop	1.843	20.728	0
Optimal	1.263	1.943	0

gestion. On the other hand, AARBP and AARBV could keep the voltage within the safe limits in almost all the investigated operating points, with AARBV having the best performance (almost similar to the optimum yet an unachievable case). A summary of the simulation results is reported in Table 3.1.

3.6 Scaling to Large LV Systems

We implement our models on a modified version of the IEEE European low voltage test feeder [35], which consists of 906 nodes and 55 residential loads. We model a balanced per-phase version of the network by connecting all residential loads to phase A, and a high PV penetration scenario by pairing each load with a 6 kW PV system. To generate load patterns, we first randomly choose 55 load shapes from the IEEE 906-node 1-min resolution data. Then, we select 50 random minutes (the same minutes for every household) between 10 AM and 2 PM. Each selected minute is simulated for 20 scenarios where in each scenario, we randomly set the PV output to a value in the range 0 to 6 kW.

Fig. 3.7 shows the average relative difference in real power loss and reactive power usage between the optimal solution and the other approaches, over the combined thousand scenarios. We can see that similarly to the results that we obtained for the smaller 27-node system, our proposed approaches use significantly less reactive power and manage to decrease real power loss compared to the other techniques. The simulation results are summarised in Table 3.2. Note that due to the limited available reactive power (inverter size is assumed to be 10 KVA), in three scenarios, voltage violation happens in the optimal approach, indicating that the volt/var problem in these scenarios has no solution. Also, we can see that the Inc. droop approach manages to keep the voltage inside the limit in few more scenarios than AARBP and AARBV, but at the cost of a significant increase in real power loss and reactive power usage.

The maximum difference in line loading between different control schemes and the optimal are shown in Fig. 3.8. The results agree with the previous section, indicating that, on average, AARBP and AARBV leads to line loadings that are closer to the optimal. Note that since the IEEE 906-node test system does not provide details about the ampacity of the lines, we used the following approach to obtain a sensible value for each line. First, we calculate the maximum line loading of each line over the whole day; and then we assume each line's ampacity to be three times this amount.

Furthermore, to investigate the scalability of the control schemes, we checked the connection of 10, 25, and 55 loads to the system. Table 3.3 shows the computing time for solving AARC in the three schemes using *Gurobi* [58]. The simulations are carried out on a Dell Latitude 7490 having 1.9 GHz Intel Core i5 processor with a memory of 8 GB.

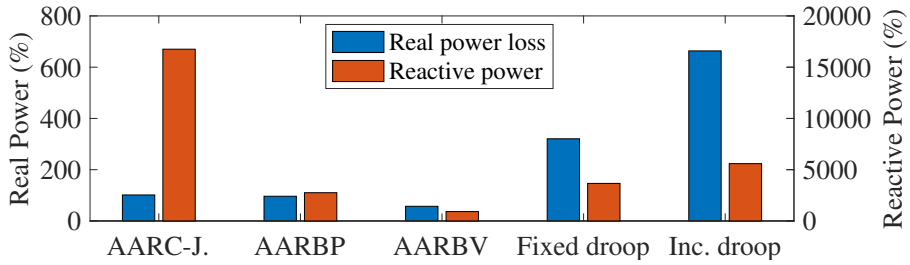

Figure 3.7: Average relative difference in real power loss and inverter reactive power usage (absorption or injection) between different voltage control schemes and the optimal scheme over 1000 operating points in the 906-node system.

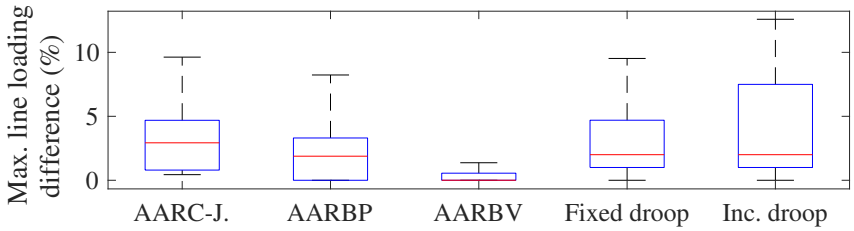

Figure 3.8: Distribution of the maximum line current differences in the 906-node IEEE system, using different approaches with the optimal scheme.

Table 3.2: Summary of the simulation results in the 906-node system

Control technique	Agg. real power loss (MW)	Agg. reactive power usage (MVAR)	No. voltage violation
AARC-J.	0.346	35841	84
AARBP	0.340	6510	8
AARBV	0.274	2132	6
Fixed droop	0.693	7612	11
Inc. droop	1.269	11614	5
Optimal	0.171	225	3

3.7 Summary

We proposed two affinely adjustable robust counterparts, that respond to changes in local real power (AARBP) and voltage magnitude (AARBV), respectively. In these approaches we directly incorporated the voltage limit constraints into a AARC of the volt/var problem. Through numerical simulations we show that our proposed approaches can keep

Table 3.3: Computing time in the 906-node test system

Number of Loads	Time(s)		
	AARC-J.	AARBP	AARBV
10	0.442	0.661	1.331
25	1.613	2.038	5.269
55	7.640	4.225	24.663

the voltages inside the accepted limits for a wider range of scenarios compared to alternative approaches, while significantly decreasing the reactive power usage, real power loss, and line congestion. Moreover since these functions are developed in accordance with different grid codes, they are practical to implement for a wide range of operating distribution systems.

We have identified three main shortcomings of our work in this chapter: *i)* in this chapter, we assumed that the distribution system is balanced, and hence, we developed our models on a single-phase equivalent system. However, the power flow in distribution networks is intrinsically unbalanced, especially in networks with highly unbalanced DER penetration); *ii)* in our modelling, we neglect the real power curtailment capability of PV inverters. However, as we show in our numerical results, there are situations in which, due to limited reactive power available, it is not possible to keep the voltages inside the limits using only reactive power of the residential inverters; *iii)* in our modelling, we make decisions based on the worst-case realisation of uncertainty. However, with more and more available data of PV generation and demand, it might be possible to construct accurate probability distribution functions of these uncertain parameters, and make decisions that not only secure the worst-case but also work better in expectation. In the following chapters, we will explore solutions to address these shortcomings.

Chapter 4

Data-Driven Adjustable Robust Solution to Voltage Regulation Problem

4.1 Introduction and Literature Review

In the previous chapters, we discussed the new technical challenges caused by the uptake of residential photovoltaic (PV) panels in distribution systems. Then, in Chapter 3, we designed a combined central-local approach based on the application of AARC methodology to coordinate the reactive power of inverters to prevent voltage violations in balanced distribution systems. In this chapter, we will build upon our work on Chapter 3 and address its three main shortcomings identified in the Summary section of chapter four (3.7). In what follows, we provide a literature review of other existing solutions to address the shortcoming and what are the limitations of these solutions.

As we showed in Section 3.6, when we are only using the reactive power of inverters for voltage regulation, there are several scenarios where voltage violation cannot be avoided. This happens as limited reactive power resources are available to deal with the over-voltage (the inverter size limits reactive power). Studies have shown that the real power curtailment (RPC) capability of inverters, along with their potential to provide reactive power compensation, can better mitigate voltage issues in LV networks [63]. Also, these resources are already available in LV systems; thus, there is no need for an additional investment cost for the DSO [64]. Existing standards [21, 22, 65] suggest that the real and reactive power of inverters should be a function of voltage magnitude or real power available to the PV. These functions do not change with time and are obtained irrespective of different net-

work characteristics. Such static functions will not be able to efficiently handle all scenarios in our networks. The reason is that to guarantee network security in all scenarios; they have to curtail real power (or inject reactive power) more than necessary, leading to an overly conservative outcome. However, designing criteria for inverter controller parameters specific to each network is complicated due to inherent uncertainties and highly volatile PV generation and demand behaviour. This chapter coordinates multiple PV inverters to prevent voltage violations in three-phase distribution systems while preventing unnecessary RPC and reactive power usage. We focus on the uncertain nature of the problem, and the communication and computation limitations in the operation of distribution systems.

Similarly to our work in Chapter 3, here we use (AARC) methodology to develop controller functions that simultaneously coordinate the real and reactive power of inverters. The AARC method used in the literature, similarly to our work in Chapter 3, only requires the uncertain parameters to belong to a polyhedral uncertainty set. This is useful when no information about the distribution of uncertain parameters is available. However, in many real-world problems, some information does exist, which could be leveraged to achieve statistically better decisions. To enable this, distributionally robust optimisation (DRO) has been introduced in the literature [66–68]. In these works, the modeller uses a chance-constraint formulation to limit the probability of constraint violation instead of guaranteeing a safe operation for all realisations. To accurately capture the underlying distribution of uncertain parameters, DRO requires to use of many samples. However, the authors in [69] have shown that the number of constraints of the DRO problem increases with the number of samples, leading to computationally challenging problems. This is especially problematic in the distribution system operation problem, where a large problem needs to be solved frequently (usually every 15 minutes), and the required control decisions are to be delivered to multiple devices. Plus, these works either overlook DER recourse capability or limit the recourse to affine adjustments only, i.e., underestimating DER flexibility.

To overcome these limitations, we propose DARC – a data-driven adjustable robust counterpart method that extends the conventional AARC method in two main ways: firstly, in DARC, we partition the uncertainty set into a user-defined number of segments along each dimension, and assign a probability to each segment. Secondly, rather than optimising for an affine function, as in AARC, we optimise to find parameters of a piecewise affine function, with each piece associated with one segment. This allows additional probabilistic information

about the uncertain parameters to be exploited, so that better decisions can be made away from just the worst-case scenarios. As we show in Section 4.7, optimising according to the worst-case may fail to find the desired controller parameters for the segments away from the worst-case realisation. Thus, in live operation, when uncertainty realisation is often milder than the worst-case, the controllers' responses might lead to over-conservative results.

Moreover, in the above literature, the application of AARC is neither assessed in three-phase networks (while the power flow in distribution networks is intrinsically unbalanced, especially in networks with highly unbalanced DER penetration) nor extended to the inverter dispatch problem, i.e., simultaneously coordinating real and reactive power output of inverters. To close the gap in the literature, this chapter proposes a two-stage combined central-local approach to coordinate multiple residential inverters' output to prevent voltage violations in three-phase distribution systems. Fig. 4.1 shows the high-level structure of our proposed solution approach. In the first / central stage, we periodically (every 15 minutes) collect the most accurate forecast of PV generation and demand from a forecasting agency and households, respectively. Then, depending on the number of segments (designed by the modeller), collected forecasts and their historical data, we construct a segmented uncertainty set (described in Section 4.4). Then, through solving an optimal power flow problem, parameters of piecewise affine (PWA) functions are obtained that take the local PV generation and demand as input, and output the control signals for real and reactive power of the corresponding inverter. In the second / local stage, within each period, the local controllers use the provided functions and real-time local measurements to determine their output until an updated function is sent.

We use Monte-Carlo simulations to assess the performance of our method by implementing our approach on both IEEE 37-bus MV and 906-bus LV networks. We compare our approach with the optimal solution that has knowledge of the eventual realisation of uncertainty, and three alternative optimisation-based approaches. Our experiments show that our approach can successfully keep the voltages within a desired band in all scenarios, while decreasing RPC compared to the other approaches and performing near-optimally. We also show that our approach is superior to the conventional AARC method in performance without significantly increasing the computing time, and is robust to errors in identifying the distributions underlying the uncertain parameters.

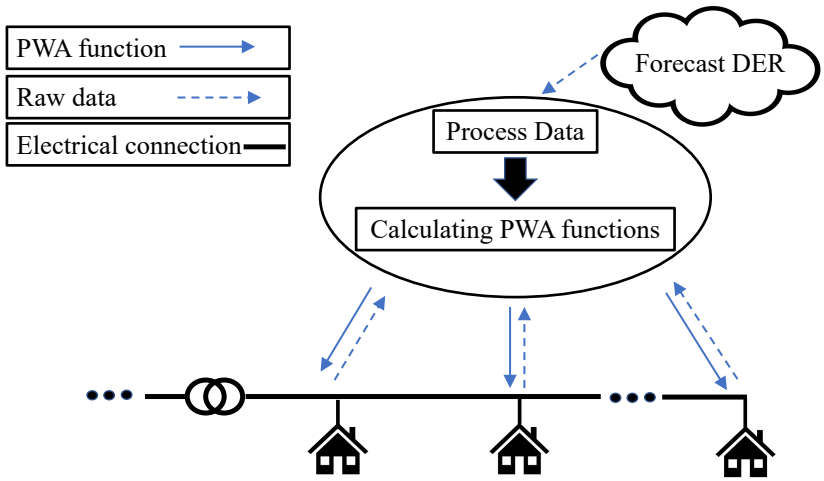

Figure 4.1: High-level structure of our proposed solution approach in the voltage regulation problem.

The main contributions of this chapter are:

- A novel extension to the conventional AARC methodology that enables us to benefit from available information about the distribution of uncertain parameters. Unlike [46, 54, 70–72] that optimise for an affine function based on the worst-case realisation of uncertainty, our approach optimises to find parameters of a piecewise affine function, with each piece associated with one segment in the uncertainty set. Also, instead of optimising based on the worst-case realisation, our approach optimises for the expected realisation over each segment of the uncertainty set. Thus in live operation, when uncertainty realisation is often milder than the worst-case, our controllers' responses prevent over-conservative results and reduce real power curtailment. Through extensive numerical simulations, we show that our approach improves the performance of the conventional AARC up to 60%.
- An adjustable robust counterpart of the voltage regulation problem in three-phase distribution systems, which formulates the inverters' output as a piecewise affine function of the available PV and demand. Contrary to [30, 55, 73, 74] that assume a balanced distribution system, our formulation considers unbalanced three-phase distribution systems and models the effect of lines' mutual impedances on the voltage magnitudes.
- Discussions and numerical experiments on the trade-off between the exactness and computational burden of modelling approaches

to deal with equality constraints in the voltage regulation problem that contain uncertain parameters. Our discussion provides insight into the advantages and disadvantages of two popular linear three-phase power flow models in uncertain OPF-based studies.

The rest of this chapter is organised as follows: Section 4.2 formulates a three-phase power flow model as well as the deterministic voltage regulation problem. A summary of the conventional AARC approach is presented in Section 4.3 to provide the required setup to build our DARC methodology in Section 4.4. We then investigate the application of DARC on the voltage regulation problem in Section 4.5. Alternative approaches and an illustrative example are given in Sections 4.6 and 4.7, respectively. Section 4.8 reports the simulation results, and Section 4.9 presents a discussion on the important considerations in implementing our approach on real-world networks. Finally, Section 4.10 concludes the chapter.

This chapter presents an edited version of our work [75], published as a journal paper in the International Journal of Electrical Power & Energy Systems.

4.2 Problem Formulation

In this section, we first introduce our three-phase distribution system mathematical modelling. Then, we present the deterministic model of the voltage regulation problem.

4.2.1 Modelling Notation

A three-phase distribution network can be represented by a connected graph $\mathcal{G}=(\mathcal{V},\mathtt{E})$, where $\mathcal{V}=\{0,...,i,j,k,...,N\}$ denotes the set of nodes, while $\mathtt{E}\subseteq\mathcal{V}\times\mathcal{V}$ denotes the set of edges where (i,j) represents an edge from node i to node j. Node 0 is considered as the slack node, and it is connected to the upstream network. Let $\phi\in\Phi$, where $\Phi=\{a,b,c\}$, denote the phase of each edge and each node in a three-phase network. For node i and phase ϕ, the complex line to neutral voltage is denoted by V_i^ϕ. Vector $\mathbf{V}_i=[V_i^a,V_i^b,V_i^c]^\intercal$ denotes the complex voltages on all phases of node i. Let $s_i^\phi=p_i^\phi+jq_i^\phi$ denote the net complex power injection at node i. Vector $\mathbf{s}_i=[s_i^a,s_i^b,s_i^c]^\intercal$ denotes net complex power on all phases of node i. For every edge (i,j), let $S_{ij}^\phi=P_{ij}^\phi+jQ_{ij}^\phi$ denote the complex power from node i to node j on phase ϕ, and vector $\mathbf{S}_{ij}=[S_{ij}^a,S_{ij}^b,S_{ij}^c]$ collect the line currents in all phases. Let $z_{ij}^{\phi\phi'}=r_{ij}^{\phi\phi'}+jx_{ij}^{\phi\phi'}$ denote the complex impedance between phases ϕ and

ϕ' of that edge, and $\mathbf{Z}_{ij}$ denotes the 3×3 impedance matrix between nodes i and j.

4.2.2 Power Flow Model

We use the linear power flow model introduced in [76] to approximate the power flow equations in a three-phase network as follows:

$$\mathbf{U}_j = \mathbf{U}_i - 2(\tilde{\mathbf{R}}_{ij}\mathbf{P}_{ij} + \tilde{\mathbf{X}}_{ij}\mathbf{Q}_{ij}) \tag{4.1a}$$

$$\mathbf{S}_{ij} = \sum_{k:j\to k} \mathbf{S}_{jk} - \mathbf{s}_j \tag{4.1b}$$

$$\tilde{\mathbf{R}}_{ij} + j\tilde{\mathbf{X}}_{ij} = (\boldsymbol{w}\boldsymbol{w}^H)^\intercal \odot \mathbf{Z}_{ij} \tag{4.1c}$$

$$\boldsymbol{w} = [1e^{j0}, 1e^{-j2\pi/3}, 1e^{j2\pi/3}]^\intercal, \tag{4.1d}$$

where $\mathbf{U}_i = [U_i^a, U_i^b, U_i^c]^\intercal$ denotes the vector of squared voltage magnitude at node i in all phases, and matrices $\tilde{\mathbf{R}}_{ij}$ and $\tilde{\mathbf{X}}_{ij}$ are defined to approximate the power flow equations (for more details on the assumptions and derivation process of model (4.1), please refer to [76]). Operators $(.)^H$, $(.)^\intercal$ and $\odot$ denote conjugate transpose, transpose and element-wise multiplication, respectively. As shown in [77], the linear power flow model (4.1) has a superior performance for capturing voltages in unbalanced systems, which is the focus of our work, compared to the SOC relaxation of the power flow constraints. Plus, the linear approximation allows us to cast the problem as a linear programming problem.

4.2.3 Deterministic Voltage Regulation Problem

The voltage regulation problem can be formulated as the following deterministic optimisation:

$$\min \quad \sum_{(i,\phi)\in\mathcal{V}_G} p_{i,\phi}^{cur} + \varepsilon|q_{i,\phi}^{pv}| \tag{4.2a}$$

$$\text{s.t. power flow model (4.1)} \tag{4.2b}$$

$$p_i^\phi = p_{i,\phi}^{pv} - p_{i,\phi}^{D} - p_{i,\phi}^{cur} \tag{4.2c}$$

$$q_i^\phi = q_{i,\phi}^{pv} - q_{i,\phi}^{D} \tag{4.2d}$$

$$0 \le p_{i,\phi}^{cur} \le p_{i,\phi}^{pv} \tag{4.2e}$$

$$q_{i,\phi}^{pv\,2} + (p_{i,\phi}^{pv} - p_{i,\phi}^{cur})^2 \le \overline{S}_{i,\phi}^2 \tag{4.2f}$$

$$\underline{U}_i^\phi \le U_i^\phi \le \overline{U}_i^\phi, \tag{4.2g}$$

where the set $\mathcal{V}_G$ denotes the nodes and phases with PV generation. The parameters $p^D_{i,\phi}$ and $q^D_{i,\phi}$ denote the real and reactive demand at node i and phase ϕ, respectively. $p^{pv}_{i,\phi}$, $p^{cur}_{i,\phi}$ and $q^{pv}_{i,\phi}$ denote the available solar power for generation, the real power curtailment and the reactive power generation at node i and phase ϕ, respectively. $\overline{S}_{i,\phi}$ denotes the inverter capacity at node i and phase ϕ. Parameter ε is a small coefficient used to prioritise the reactive power usage over the RPC. Also, $\underline{U}^{\phi}_i$ and $\overline{U}^{\phi}_i$ denote the lower and upper limits on the squared voltage magnitude. We assume our PV systems and loads have single phase connections, and neutral conductor is treated implicitly in our model.

4.3 A Review of the AARC Formulation

In what follows, we present a summary of the AARC approach on a general adjustable robust linear optimisation problem to point out its limitations and provide the required setup on which we build our DARC approach.

Consider a general adjustable robust linear optimisation problem as:

$$\min_{f\in\mathcal{F}} \ \mathbb{E}\big(\boldsymbol{c}^{\intercal} f(\tilde{\boldsymbol{\epsilon}})\big) \tag{4.3a}$$

$$\boldsymbol{A} f(\boldsymbol{\epsilon}) \leq \boldsymbol{B}\boldsymbol{\epsilon} + \boldsymbol{d} \quad \forall \boldsymbol{\epsilon} \in \mathcal{E}, \tag{4.3b}$$

where operator $\mathbb{E}$ denotes the expected value, $\tilde{\boldsymbol{\epsilon}}$ is an m-dimensional random vector with values $\boldsymbol{\epsilon} \in \mathcal{E} \subseteq \mathbb{R}^m$, and convex polyhedral sample space $\mathcal{E} := \{\boldsymbol{\epsilon} \in \mathbb{R}^m : \boldsymbol{W}\boldsymbol{\epsilon} \leq \boldsymbol{h}\}$, and and $\boldsymbol{A} \in \mathbb{R}^{w\times n}$, $\boldsymbol{B} \in \mathbb{R}^{w\times m}$ and $\boldsymbol{d} \in \mathbb{R}^w$ are parameters of the optimisation. Recall that in Chapter 3, we defined $f : \mathcal{E} \to \mathbb{R}^n$ as a function whose range are the variables of an optimisation problem that can take recourse actions in response to the uncertainty realisation. We also defined $f \in \mathcal{F}$, where $\mathcal{F}$ is the set of all possible/acceptable functions mapping the sample space $\mathcal{E}$ to $\mathbb{R}^n$.

We then took the following two steps: *i*) restrict $\mathcal{F}$ to be the set of affine functions from $\mathcal{E}$ to $\mathbb{R}^n$ and define

$$f(\boldsymbol{\epsilon}) \coloneqq \boldsymbol{\beta} + \boldsymbol{\alpha}\boldsymbol{\epsilon}, \tag{4.4}$$

replace $f(.)$ in (4.3); *ii*) shift the uncertain parameters from the objective function through writing the epigraph model with certain objective which is equivalent to evaluating the objective function at the worst-

case scenario. Thus, we obtained:

$$\min_{x_a,\boldsymbol{\beta},\boldsymbol{\alpha}} \quad x_a \tag{4.5a}$$

$$\boldsymbol{c}^\intercal(\boldsymbol{\beta}+\boldsymbol{\alpha}\boldsymbol{\epsilon}) \leq x_a \qquad \forall \boldsymbol{\epsilon} \in \mathcal{E} \tag{4.5b}$$

$$\boldsymbol{A}(\boldsymbol{\beta}+\boldsymbol{\alpha}\boldsymbol{\epsilon}) \leq \boldsymbol{B}\boldsymbol{\epsilon}+\boldsymbol{d} \qquad \forall \boldsymbol{\epsilon} \in \mathcal{E}, \tag{4.5c}$$

We then use the duality technique[1] to obtain a linear optimisation problem that outputs $\boldsymbol{\beta}$ and $\boldsymbol{\alpha}$ such that the problem's constraints hold for any realisation of $\boldsymbol{\epsilon} \in \mathcal{E}$. Hereinafter, we refer to this approach as the conventional AARC. In the next section, we will revisit our two steps above and show how they may result in over-conservative decisions, and propose our DARC approach to address them.

4.3.1 Equality Constraints in Robust Optimisation

Similarly to (4.2), an optimisation problem may have equality constraints. As discussed in [78], the equality constraints containing uncertain parameters often restrict the feasible region drastically, and therefore should be transformed into inequality constraints. We can use the following two approaches to deal with equality constraints; *i) Elimination and Substitution (E&S)*: eliminate the equality constraints by substituting the variables in the inequality constraints, and *ii) Relaxation*: relax the equality constraint into an inequality constraint (in Section 4.5, we explain how these approaches can be used in our problem, and in section 4.8, we provide a numerical comparison between them). Regardless of which approach is selected, we can obtain all the constraints in the general form (4.5), and use the *max* protection function to robustify the constraints against the uncertainty realisation.

4.4 Data-Driven Adjustable Robust Counterpart (DARC)

In many real-world problems, information about the distribution of uncertain parameters can be derived from the historical data. Such information can be incorporated into the sample space $\mathcal{E}$ to obtain more informed decisions. Here, we modify the AARC formulation to benefit from the probabilistic information around the uncertain parameters' distribution.

Unlike the AARC formulation, where $\mathcal{F}$ is restricted to be the set of affine functions from $\mathcal{E}$ to $\mathbb{R}^n$, here we bring more flexibility to the

[1] For more details, please refer to 3.2.

decision rules by allowing $\mathcal{F}$ to be a set of piecewise affine functions. To do so, we partition the uncertainty set into L consecutive segments and define our piecewise variables to have L pieces, each associated with one segment in the sample space. Next, rather than optimising according to the worst-case in the sample space, as in AARC, we utilise the occurrence likelihood of each segment in the sample space to optimise for the slope of every affine piece within our piecewise functions. Our approach fine-tunes the decisions based on the available probabilistic information and reduces the overconservativeness of the worst-case based AARC. In what follows, we first present the probabilistic information, and then provide details of our proposed model.

4.4.1 Probability Information

Let ϵ_i denote the i-th element in vector $\boldsymbol{\epsilon}$, and $\bar{\epsilon}_i$ and $\underline{\epsilon}_i$ denote the maximum and minimum values of ϵ_i in the set $\mathcal{E}$, respectively. Assuming that the interval $[\underline{\epsilon}_i, \bar{\epsilon}_i]$ consists of L segments, we define $\mathcal{E}_{il}$ as the sample space for l-th segment of the uncertain parameter ϵ_i, and $\mathcal{P}_{il} \coloneqq \mathrm{P}(\epsilon_i \in \mathcal{E}_{il})$ as the marginal probability of a particular i-th element of the random vector being in the l-th segment. Based on historical/forecasted data, let us assume we have access to the marginal probability of the uncertain parameters with the following relation:

$$\sum_{l=1}^{L} \mathcal{P}_{il} = 1 \qquad \forall i \in \{1, ..., m\}. \tag{4.6}$$

Remark: To obtain the marginal probability $\mathcal{P}_{il}$, we need the probability density function (PDF) of the random variables. There are different techniques in the literature to obtain the PDF of DER output and demand in power systems [79]. Notice that obtaining an accurate PDF for the uncertain parameters is not the focus of this chapter, and we simply assume that such information is available. However, we investigate the impact of using an incorrect estimation of PDF on DARC outcome and compare it with a case when the exact PDF is available in section 4.8.

4.4.2 Proposed DARC Model

Let vector $\boldsymbol{x} = f(\boldsymbol{\epsilon}) \in \mathbb{R}^n$ denote the adjustable variables of the optimisation problem. Also, let $\mathcal{N} = \{1, ..., n\}$ and $\mathcal{M} = \{1, ..., m\}$ denote the sets of number of the decision and random variables, respectively. A piecewise affine function mapping different segments in $\boldsymbol{\epsilon}$ to $\boldsymbol{x}$ can be

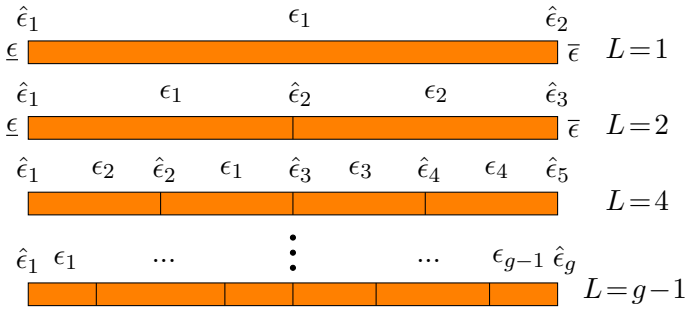

Figure 4.2: Proposed partitioning of the sample space along one dimension.

obtained using the following mixed-integer linear constraints [80]:

$$x^k = \sum_{i=1}^{m} \sum_{l=1}^{L+1} t_{il} \hat{x}_{il}^k \qquad \forall k \in \mathcal{N} \tag{4.7a}$$

$$\epsilon_i = \sum_{l=1}^{L+1} t_{il} \hat{\epsilon}_{il} \qquad \forall j \in \mathcal{M} \tag{4.7b}$$

$$\sum_{l=1}^{L+1} t_{il} = 1, \ \sum_{l=1}^{L} \chi_{il} = 1 \qquad \forall i \in \mathcal{M} \tag{4.7c}$$

$$t_{i1} \leq \chi_{i1}, \ t_{i,L+1} \leq \chi_{iL} \qquad \forall i \in \mathcal{M} \tag{4.7d}$$

$$t_{il} \leq \chi_{il} + \chi_{i,l-1} \qquad \forall i \in \mathcal{M}, \forall l \in \{2, ..., L\}, \tag{4.7e}$$

where $\hat{x}_{il}^k$ and $\hat{\epsilon}_{il}$ denote "x-axis" and "ϵ-axis" breakpoints for each variable and uncertain parameter in the $\epsilon - x$ plane (our goal is to optimise $\hat{x}_{il}^k$ while we consider $\hat{\epsilon}_{il}$ are known). $t_{il} \in [0, 1]$ and $\chi_{il} \in \{0, 1\}$ are variables used to encode the position of x and ϵ in the sample space.

Next, we incorporate (4.7) into (4.3b), and similarly to (4.5), robustify the resulting constraint against uncertainty realisation using a *max* protection function as follows:

$$\max_{(\boldsymbol{\epsilon}, \boldsymbol{x}) \in (4.7), \boldsymbol{\epsilon} \in \mathcal{E}} \{\boldsymbol{A}\boldsymbol{x} - \boldsymbol{B}\boldsymbol{\epsilon}\} \leq \boldsymbol{d}. \tag{4.8}$$

Equation (4.8) represents an MILP problem and thus it is not possible to directly use duality theory and reformulate it, and therefore, a similar approach as in (4.5) will not work here. Notice that if we relax the binaries, the solution will be greater than or equal to the LHS of (4.8). This means that if we utilise the binary relaxed formulation in order to obtain the dual, our solution will still be robust. We also transform the definition x^k and ϵ_i in (4.7a) and (4.7b) to the following

form where we use the central tendency and deviation from the central tendency to present the uncertain parameters (one can show the bijection between the following model and (4.7), when the binary variables are relaxed in (4.7)). The resulting formulation is simpler to relate to in practical power systems applications, as in most cases the forecast / measurement data can be used as the central tendency of the uncertain parameters. To this end, let us define uncertain parameter ϵ_{il} which denotes the uncertainty of realisation i-th uncertain parameter in l-th segment. We also define decision variables β^k and α^k_{il} which are parameters of an affine function that maps uncertain parameter ϵ_{il} to decision variable x^k. Hence, the following relations are defined:

$$x^k := \beta^k + \sum_{i=1}^{m}\sum_{l=1}^{L} \alpha^k_{il}\epsilon_{il} \qquad \forall k \in \mathcal{N} \tag{4.9a}$$

$$\epsilon_i := \epsilon_{i0} + \sum_{l=1}^{L} \epsilon_{il} \qquad \forall i \in \mathcal{M}, \tag{4.9b}$$

where ϵ_{i0} denotes the central tendency of the i-th uncertain parameter. An example of such a design is shown in Fig. 4.2. Notice that choosing $L=1$ leads to the same formulation as the conventional AARC formulation. Incorporating (4.9) into (4.8), results in a set of linear inequality constraints which we then robustify for all realisations of $\epsilon_{il} \in \mathcal{E}_{il}$, using the same duality technique as used in Section 4.3.

Next, we modify the objective (4.3a) so that it can utilise the segmented probability information $\mathcal{P}_{il}$. Remember that we define $\mathcal{P}_{il}$ as the marginal probability of a particular i-th element of the random vector being in the l-th segment. We evaluate the objective at multiple points, one per segment of the elements in the random vector.

$$\min_{f} \sum_{k=1}^{n} c^k \Big(\sum_{i=1}^{m}\sum_{l=1}^{L} \mathcal{P}_{il} f^k(\epsilon_{il}) \Big). \tag{4.10}$$

Also, inspired by the epigraph form of the objective in (4.3), where the objective is assessed for the worst-case in the sample space, we evaluate the objective at the extreme distance of the central tendency in each segment. More specifically, using definition (4.9), objective (4.10) can be written as follows:

$$\min_{\beta^k, \alpha^k_{il}} \quad \sum_{k=1}^{n} c^k \Big(\beta^k + \sum_{i=1}^{m}\sum_{l=1}^{L} \mathcal{P}_{il}\alpha^k_{il}\Gamma(\epsilon_{il}) \Big), \tag{4.11}$$

where $\Gamma(\epsilon_{il})$ denotes the maximum distance of ϵ_{il} from the central tendency of i-th uncertain variable (ϵ_{i0}).

4.5 DARC Implementation on the Voltage Regulation Problem

In this section, we model the voltage regulation problem based on the DARC methodology presented in Section 4.4. In what follows, the details of the implementation process are described.

4.5.1 Uncertainty Modelling

We begin by presenting a detailed formulation of the sample space $\mathcal{E}$, where we consider the random variables to be the available PV for generation and demand. Similarly to (4.9b), we first introduce the central tendency and deviation from central tendency of the random variables. Let $p_{i,\phi}^{pv^0}$ and $p_{i,\phi}^{D^0}$ denote the central tendency of the PV generation and demand, respectively. These values in practice are the measurement made and provided to the central solver at the beginning of each time interval. Also, let $\Delta p_{i\phi l}^{pv}$ and $\Delta p_{i\phi l}^{D}$ denote the deviation from the central tendency, and be random variables corresponding to l-th segment in available PV and demand at node i and phase ϕ. We consider the extremes of the solar and demand random parameters are independent, i.e., our sample space is a hypercube. Hence, we define $\underline{\Delta p_{i\phi l}^{pv}}$, $\overline{\Delta p_{i\phi l}^{pv}}$, $\underline{\Delta p_{i\phi l}^{D}}$ and $\overline{\Delta p_{i\phi l}^{D}}$ as constants, denoting the bounds of the hypercube. Thus, we define the following:

$$p_{i,\phi}^{pv} \coloneqq p_{i,\phi}^{pv^0} - \sum_{l=1}^{L} \Delta p_{i\phi l}^{pv} \quad , \quad p_{i,\phi}^{D} \coloneqq p_{i,\phi}^{D^0} - \sum_{l=1}^{L} \Delta p_{i\phi l}^{D} \tag{4.12a}$$

$$\underline{\Delta p_{i\phi l}^{pv}} \leq \Delta p_{i\phi l}^{pv} \leq \overline{\Delta p_{i\phi l}^{pv}} \quad , \quad \underline{\Delta p_{i\phi l}^{D}} \leq \Delta p_{i\phi l}^{D} \leq \overline{\Delta p_{i\phi l}^{D}}. \tag{4.12b}$$

Similarly to (4.9a), the RPC of each inverter at each node is written as a piecewise affine function of the uncertain parameters that can be measured at that node:

$$p_{i,\phi}^{cur}(\Delta p_{i\phi l}^{pv}, \Delta p_{i\phi l}^{D}) \coloneqq \beta_{i,\phi}^{cur} + \sum_{l=1}^{L} \alpha_{1i\phi l}^{cur} \Delta p_{i\phi l}^{pv} + \alpha_{2i\phi l}^{cur} \Delta p_{i\phi l}^{D} \tag{4.13}$$

where $\beta_{i,\phi}^{cur}$, $\alpha_{1i\phi l}^{cur}$ and $\alpha_{2i\phi l}^{cur}$ are parameters of the function. In the first stage, we optimise the parameters of the functions, given the uncertain parameters $\Delta p_{i\phi l}^{pv}$ and $\Delta p_{i\phi l}^{D}$. In the second stage, the parameters of the functions are fixed at the obtained values, and the functions output the suitable recourse in response to the uncertainty realisation. Unlike RPC, for simplicity, we do not replace the reactive power generation of inverters ($q_{i,ph}^{pv}$) with a piecewise affine function. Yet, the same technique can be applied to the reactive power as well.

4.5.2 Equality Constraints

We use the constraint-wise robust counterpart construction technique, described in Section 4.3, to robustify our deterministic problem (4.2) against the uncertainty. To do so, we first deal with the equality constraints using *E&S* and *Relaxation* techniques. In the next two subsections, we provide the details on how these approaches can be applied in our problem.

Elimination and Substitution

In this approach, we eliminate the analysis variables in the equality constraints and substitute them in other inequality constraints. More specifically, we eliminate the real and reactive power injection variables, i.e., p_i^ϕ and q_i^ϕ, in the constraints (4.2c) and (4.2d), respectively. We then use the physical tree structure of the distribution systems, to express U_i^ϕ directly by the decision variables and uncertain parameters.

Let vectors $\mathbf{p}_i = [p_i^a, p_i^b, p_i^c]^\intercal$ and $\mathbf{q}_i = [q_i^a, q_i^b, q_i^c]^\intercal$ denote the real and reactive power injection at all the phases of node i, respectively. Let $\boldsymbol{p} = [\mathbf{p}_1^\intercal, ..., \mathbf{p}_N^\intercal]^\intercal$ and $\boldsymbol{q} = [\mathbf{q}_1^\intercal, ..., \mathbf{q}_N^\intercal]^\intercal$ be $3N\times 1$ vectors denoting the injected real and reactive powers at every node and phase, respectively. Also, let $\boldsymbol{U^0} = [\mathbf{U}_0^\intercal, ..., \mathbf{U}_0^\intercal]^\intercal$ be a $3N\times 1$ vector, where $\mathbf{U}_0$ is a 3×1 vector denoting the squared voltage at the slack node. We then write the relation between the injected real and reactive powers and the nodal squared voltage magnitudes as follows:

$$\boldsymbol{U} = \boldsymbol{R}\boldsymbol{p} + \boldsymbol{X}\boldsymbol{q} + \boldsymbol{U^0}, \tag{4.14}$$

where, $\boldsymbol{R}$ and $\boldsymbol{X}$ are $3N\times 3N$ matrices, and their elements denote the sensitivity of squared voltage magnitude at node i and phase ϕ to real and reactive power changes at node j and phase φ, respectively. We obtain their elements as follows:

$$R_{j,\varphi}^{i,\phi} = \frac{\partial U_i^\phi}{\partial p_j^\varphi}, \qquad X_{j,\varphi}^{i,\phi} = \frac{\partial U_i^\phi}{\partial q_j^\varphi}. \tag{4.15}$$

Applying the voltage limit constraint (4.2g) to (4.14), which is now expressed in terms of the decision variables and uncertain parameters, we can transform all the equality constraints to the inequality constraints in the form of (4.5).

Relaxation

In this approach, where possible, we relax the equality constraints to inequality constraints. Given that in our problem we focus on over-voltage scenarios, we can relax the injection at each node, i.e. the LHS

of (4.2c), to be greater than or equal to the true injection at the node, i.e., the RHS of (4.2c). Since more real power injection will often make the voltage limit constraints more binding, we expect our relaxation to tightly represent the equality constraint (4.2c).

$$p_i^{\phi} \geq p_{i,\phi}^{pv} - p_{i,\phi}^{D} - p_{i,\phi}^{cur}. \tag{4.16}$$

Now that all constraints that include uncertain parameters are represented as inequality constraints[2], we can go ahead and use the LDR definition (4.13) and the uncertainty model (4.12) to rewrite problem (4.2) in the general form (4.5). In section 4.8, we provide a comparison on the the above approaches, and present a discussion on the computational burden of using the *E&S* approach and the tightness of the *Relaxation* approach.

4.5.3 Detailed Formulation

In what follows, we derive the detailed formulation for the voltage regulation problem, where the Relaxation approach is used. A similar process can be used to develop the formulation using the *E&S* approach, which is not included to avoid repetition. We first begin by incorporating the LDR definition (4.13) and the uncertainty model (4.12) in constraint (4.16), and obtain

$$p_i^{\phi} \geq p_{i,\phi}^{pv^0} - p_{i,\phi}^{D^0} - \beta_{i,\phi}^{cur} + \sum_{l=1}^{L} \Big((1 - \alpha_{1i\phi l}^{cur}) \Delta p_{i\phi l}^{pv} - (1 + \alpha_{2i\phi l}^{cur}) \Delta p_{i\phi l}^{D} \Big). \tag{4.17}$$

Similarly, constraint (4.2e) is reformulated as follows:

$$\beta_{i,\phi}^{cur} \geq - \sum_{l=1}^{L} (\alpha_{1i\phi l}^{cur} \Delta p_{i\phi l}^{pv} + \alpha_{2i\phi l}^{cur} \Delta p_{i\phi l}^{D}) \tag{4.18a}$$

$$p_{i,\phi}^{pv^0} - \beta_{i,\phi}^{cur} \geq \sum_{l=1}^{L} \alpha_{1i\phi l}^{cur} (1 - \Delta p_{i\phi l}^{pv}) + \alpha_{2i\phi l}^{cur} \Delta p_{i\phi l}^{D}. \tag{4.18b}$$

Next, we linearise the inverter limit thermal constraint (4.2f) as follows [46]:

$$\big(\cos\theta + \sin\theta\big) q_{i,\phi}^{pv} + \big(\cos\theta - \sin\theta\big)(p_{i,\phi}^{pv} - p_{i,\phi}^{cur}) \leq \sqrt{2}\overline{S}_{i,\phi} \qquad \forall \theta \in \Theta, \tag{4.19}$$

[2]Notice that since the rest of the equality constraints in (4.2) do not contain uncertain parameters, they can remain as they are in the robust reformulation.

where $\Theta = \{0, \pi/\nu, 2\pi/\nu, ..., (2\nu-1)\pi/\nu\}$, and $\nu \geq 2$ is an arbitrary integer number. Then, similarly to (4.17), the LDR and uncertainty definitions are incorporated in (4.19) as follows:

$$(\cos\theta+\sin\theta)q^{pv}_{i,\phi} + (\cos\theta-\sin\theta)\Big(p^{pv^0}_{i,\phi} - \beta^{cur}_{i,\phi} + \sum_{l=1}^{L}(1-\alpha^{cur}_{1i\phi l})\Delta p^{pv}_{i\phi l} - \alpha^{cur}_{2i\phi l}\Delta p^{D}_{i\phi l}\Big) \leq \sqrt{2}\overline{S}_{i,\phi}. \tag{4.20}$$

Now that all the uncertainty-affected constraints in (4.2) are reformulated as an inequality constraint, we can robustify them against the parameter uncertainty, using the duality technique described in Section 4.3. We did not include the detailed formulation in the chapter to avoid repetition.

We next update the objective (4.2a), based on (4.11) as:

$$\min_{\beta^{cur},\alpha^{cur},q^G} \sum_{(i,\phi)\in\mathcal{V}_G} \Big(\beta^{cur}_{i,\phi} + \varepsilon|q^{pv}_{i,\phi}| + \sum_{l=1}^{L}\mathcal{P}^{pv}_{i\phi l}\alpha^{cur}_{1i\phi l}\Gamma(\Delta p^{pv}_{i\phi l}) + \mathcal{P}^{D}_{i\phi l}\alpha^{cur}_{2i\phi l}\Gamma(\Delta p^{D}_{i\phi l})\Big), \tag{4.21}$$

where $\mathcal{P}^{pv}_{i\phi l}$ and $\mathcal{P}^{D}_{i\phi l}$, similar to the marginal probability in (4.6), denote the probability of PV and demand realisation, at node i and phase ϕ, in the l-th segment of their uncertainty interval. Also, $\Gamma(\Delta p^{pv}_{i\phi l})$ and $\Gamma(\Delta p^{D}_{i\phi l})$, similarly to $\Gamma(\epsilon_{ij})$ in (4.11), denote the maximum distance of random variable from their central tendency, i.e., $p^{pv^0}_{i,\phi}$ and $p^{D^0}_{i,\phi}$, respectively. The objective function (4.21) consists of two parts: the first part is the cost of recourse control actions, i.e., $\beta_{i,\phi}$ and $|q^{pv}_{i,\phi}|$, where they will be used continually in real-time irrespective of uncertainty realisation. Hence, their coefficients are equal to unity in the objective function (the probability of these actions being active is one). The second part is the cost of adjustable control actions, i.e., $\mathcal{P}^{pv}_{i\phi l}\alpha^{cur}_{1i\phi l}\Gamma(\Delta p^{pv}_{i\phi l})$ and $\mathcal{P}^{D}_{i\phi l}\alpha^{cur}_{2i\phi l}\Gamma(\Delta p^{D}_{i\phi l})$, where they model the expected cost of real power curtailment through recourse decisions. These terms model how much the inverter connected to node i and phase ϕ will change its real power curtailment if their uncertain parameters PV generation and demand realise in their associated l-th segment. Also, notice that the coefficients of these recourse decisions are equal to the probability of the realisation of the uncertain parameters in their corresponding segments, i.e., $\mathcal{P}^{pv}_{i\phi l}$ and $\mathcal{P}^{D}_{i\phi l}$.

To summarise, we implement the DARC methodology on the voltage regulation problem and obtain a linear optimisation problem with

objective (4.21) subject to constraints (4.2b), (4.2d), (4.2g) and the robust counterpart of constraints (4.17), (4.18a), (4.18b) and (4.20).

4.6 Alternative Approaches

We compare the performance of our approach with 5 alternative approaches. These approaches provide affine or piecewise affine policies to adjust the controllable variables in real-time to deviations in uncertain parameters. In what follows, we briefly summarise these approaches.

4.6.1 AARC

Using the methodology described in section 4.3, we define the RPC policy based on the AARC approach as follows:

$$p^{cur}_{i,\phi} = \beta^{cur}_{i,\phi} + \alpha^{cur}_{1i\phi}\Delta p^{pv}_{i,\phi} + \alpha^{cur}_{2i\phi}\Delta p^{D}_{i,\phi}. \tag{4.22}$$

4.6.2 Limit on Power Generation (LPG)

In the LPG approach [81], we use the following decision rule:

$$p^{g}_{i,\phi}(t) = \min\big(p^{pv}_{i,\phi}(t), p^{pv}_{i,\phi}(t_0) - p^{cur}_{i,\phi}(t_0)\big), \tag{4.23}$$

where $p^{g}_{i,\phi}(t)$ denotes the PV generation at t-th period, $p^{pv}_{i,\phi}(t)$ denotes the available PV in period t, and $p^{pv}_{i,\phi}(t_0)$ denotes the available PV at the beginning of period t, i.e., the measurement sent from each household to be used in the optimisation (4.2). In other words, decision rule (4.23) dictates that PV generation at each household and at each period should be less than or equal to the optimal PV generation which is sent from the central stage, i.e., the solution to problem (4.2).

4.6.3 Limit on Power Injection to the Grid (LPI)

Our simulations show that implementing the LPG approach does not prevent voltage violation and consequently may lead to inverter tripping off. This is an expected result as the decision rule (4.23) does not account for the uncertainty in demand. Therefore, in scenarios where the demand decreases from the measurement value, it is possible that some of the nodes would face voltage violation. We modify (4.23) as follows to prevent the voltage violation problem:

$$\begin{aligned} p^{g}_{i,\phi}(t) = \min\big(&p^{pv}_{i,\phi}(t), \\ &p^{pv}_{i,\phi}(t_0) - p^{cur}_{i,\phi} + \min(p^{D}_{i,\phi}(t) - p^{D}_{i,\phi}(t_0), 0)\big), \end{aligned} \tag{4.24}$$

where $p^D_{i,\phi}(t_0)$ denotes the demand at the beginning of the period. The added part in the decision rule (4.24) ensures that the injected power at each node will not be more than the optimum injected power obtained in the central stage in each period.

4.6.4 Robust Optimisation-Based Approach (RO)

We also compare our approach with the conventional robust counterpart of (4.2) using the constraint wise construction technique described in [54], while assuming that the uncertain parameters belong to uncertainty set (4.12).

4.6.5 Optimal Solution

Finally, we compare our approach with the optimal solution (we will refer to this approach as Opt) assuming perfect knowledge over the uncertain parameters, i.e., solve (4.2) for every scenario.

4.7 An Illustrative Case Study

In this section, we develop an illustrative example to demonstrate the performance of our proposed method against the conventional AARC and robust approaches.

Consider a single-phase two-bus distribution feeder, shown in Fig. 4.3. Let us assume that inverters are working at the unity power factor. Also, let us assume the voltage magnitude at the head of the feeder, $|V_0|$, is $1pu$ and the maximum allowed voltage is $1.05pu$. Let us also assume that the demand is equal to zero, and the PV generation at the time of measurement is equal to $4pu$ and can vary between $2pu$ to $6pu$. In other words:

$$p^{pv} = p^{pv^0} + \Delta p^{pv} = 4pu \pm 2pu. \tag{4.25}$$

Our objective is to minimise the RPC required to keep the voltages within the acceptable limit in all possible scenarios.

Fig. 4.4 shows the policies we obtain when we use RO, AARC, and our proposed method with $L = 2$, $L = 4$ and $L = 8$. Considering the

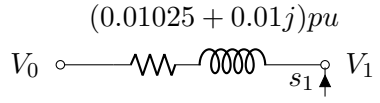

Figure 4.3: Diagram of a single-phase two-bus distribution feeder

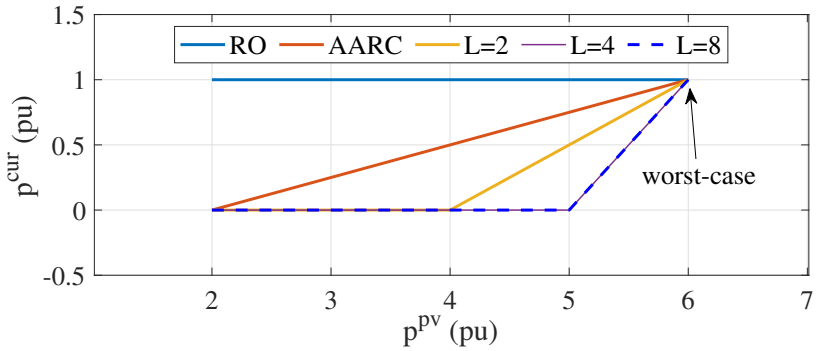

Figure 4.4: Different policies obtained from solving the RPC problem using RO, AARC, and our proposed method with $L=2$, $L=4$ and $L=8$.

power flow model (1), we can see that the real power injection at Bus 1 should not exceed $5pu$:

$$U_1 = \overbrace{U_0}^{1pu} + 2(\overbrace{r}^{0.01025pu} \times p_1) \leq 1.1025pu \rightarrow p_1 \leq 5pu. \tag{4.26}$$

Therefore, when dealing with this problem using the classical robust optimisation approach, the solution is that RPC at this bus should be equal to $1pu$ (since the maximum value of p^{pv} is $6pu$), regardless of uncertainty realisation. By allowing the RPC to adjust itself linearly with the uncertainty, we can improve the performance and prevent unnecessary real power curtailment, shown with a red line as AARC in Fig. 4.4. However, since the RPC should always remain positive, the solution is forced to have a non-zero curtailment, even at the measured value (i.e., at $p^{pv}=4pu$ we will curtail $0.5pu$ while the voltage limit will not be violated for any injection less than $5pu$). We can alleviate this problem by allowing the RPC to be a piecewise affine function of the uncertainty. We can see that by adding more segments to the piecewise affine function, we prevent unnecessary RPC in more possible scenarios through the flexibility provided by the piecewise affine function.

Interestingly, we see that regardless of the chosen approach, the RPC is the same at the worst-case scenario. This is an important observation as it indicates that if we choose to minimise the RPC at the worst-case, the objective will be the same irrespective of whether we allow our decision variables to be affine/piecewise affine function of the uncertainty or not. Hence, the parameters that we will obtain by solving the optimisation problem, with flexible piecewise affine control variables, will not necessarily reflect our expectation shown in Fig. 4.4, if we optimise for the worst-case scenario. By employing our proposed

objective function (4.11), we guide the optimisation problem toward choosing parameters that work better in expectation rather than just for the worst-case.

Furthermore, if we increase the number of partitions from $L = 4$ to $L = 8$, we will see no improvement in the result. This indicates that adding more and more flexibility to the decision variables will not always be beneficial. This is evident in this simple example, as we best decision here is to curtail all the PV generation above $5pu$, and do not curtail any below that. Since both $L = 4$ and $L = 8$ will produce this result, there is no advantage in adding more flexibility to the decision variables. Indeed, the results of our simulations in realistically sized networks agree with our discussion here.

4.8 Numerical Results and Discussion

We test the performance of our proposed method on the IEEE 37-bus MV and the IEEE 906-bus LV test systems [35]. In our simulations, to imitate the real-world situation, we assume that when an over-voltage occurs at a node, the inverter connected to that node will be disconnected for the rest of the period[3]. We experiment on three different distributions for the uncertain parameters, but in each case, we solve the DARC assuming a normal distribution. This enables us to evaluate the performance, when there is a mismatch in identifying the true underlying distribution. Also, we conduct an experiment, assuming we have access to the "true distribution" of the uncertain parameters, when solving the DARC, and show the benefits of having a more accurate PDF on the performance of the DARC.

4.8.1 Experiments on the IEEE 37-Bus MV Network

Simulation Data

We perform three experiments: using 1-minute data generated from a solar/demand model, using a normal distribution to model the uncertainty in a period, and finally, using a uniform distribution to model uncertainty.

[3]This is inline with the the Australian/New Zealand Standard [20] which states that the inverters should be disconnected from the grid if the connection point voltages go beyond a certain point. Also, based on this standard, the inverters can reconnect to the grid only after the connection voltage has been maintained within the acceptable range for 60 seconds. However, since we consider the resolution one minute, the system operating condition will change before the inverter reconnection can happen. A future extension of our work can be to consider a time series analysis over a long period where if the system operating condition does not change, the inverters can reconnect to the grid.

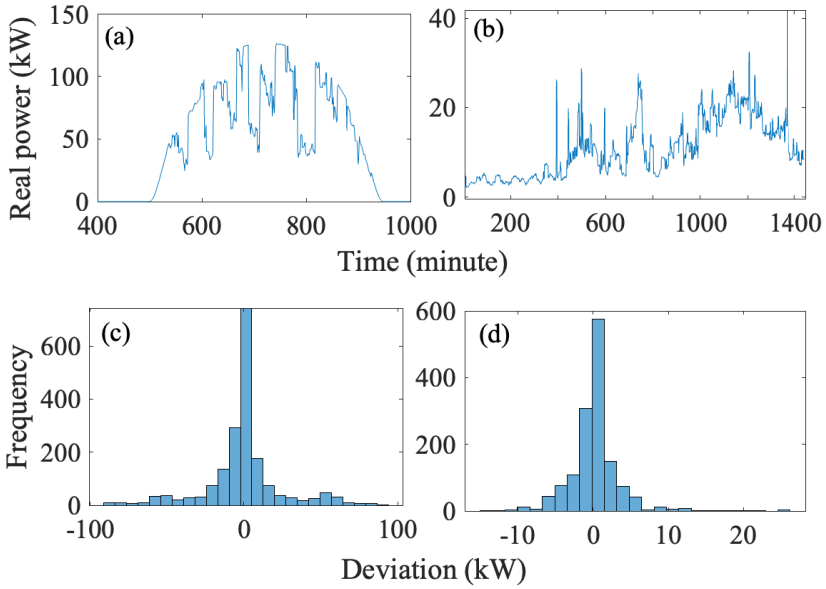

Figure 4.5: (a) and (b) show the PV generation and demand in the first day, respectively. (c) and (d) show the histogram of the PV generation and demand deviations from their measurement values during the week, respectively.

In the first experiment, we use a modified demand profile provided in the IEEE 37-bus datasheet. However, since the demand data is limited to a single operating point, we extend it to a 1-minute resolution data over a day, using the IEEE 906-bus demand data. To generate load coefficients for each of the 32 loads in the 37-bus network, we randomly select 20 load shapes from the available 100 load shapes in the 906-bus system datasheet, and then aggregate and per-unitise them to have a better estimate of an MV load shape. To generate 1-minute resolution PV generation data in a PV-rich system, we assign a PV system to each node, thrice their maximum demand. Then, we use [34] to generate a shape coefficient over a day to obtain 1-minute resolution PV data. We repeat the same process to obtain the 1-minute resolution PV and load data over a week. We also consider a 15-minute period between two consecutive measurements and simulate the LDR functions obtained at the beginning of each period over the next 15 minutes. A sample of the real data used in the simulation is presented in Fig. 4.5.

In the second experiment, we use the demand and PV power of 200 random minutes, sampled from 9 AM to 4 PM from the data that we obtained in the first experiment. Then for each minute, we generate 15 random values for PV generation and demand with a normal distribu-

Table 4.1: Comparison between the *Relaxation* (R) and E&S approaches in terms of their number of variables (NoV), number of non-zeros (NoN) in the Jacobian matrix, average solve time (Avg.T.) and average objective (Avg.O.) of solving the optimisation repeatedly for different operating points.

	NoV	NoN	Avg. T. (ms)	Avg. O.	RPC (MW)
E&S	30604	106041	1024	3.983	17.223
R	3814	9811	129	3.957	17.208

tion which has a mean equal to the sampled value, and three standard deviations equal to 50% of the sampled value. In the last experiment, we use a similar approach, except that we use a uniform distribution with $[-50\%, 50\%]$ deviation from the sampled value at each node.

Simulation Results

We implement DARC with $L = 2$ once using *E&S* and then using the *Relaxation* approach, described in section 4.5. We compare the performance of each technique in dealing with equality constraints on the IEEE 37-bus test system using the real-data. A summary of the simulation results has been reported in Table 4.1, where we compare the two approaches in terms of the number of variables (NoV), number of non-zeros (NoN) in the Jacobian matrix, average solve time (Ave.T.), average objective of solving the optimisation repeatedly for different operating points within the week (Avg.O.), and the RPC obtained by simulating the obtained LDRs from the optimisation in each 15-minute interval. As can be seen, using the *E&S* approach will result in very "dense" constraints, which for the optimisation leads to a large number of non-zeros in the Jacobian matrix. This happens because we have eliminated several useful variables which could account for sub-expressions which now have to be repeated many times. This, in turn, along with a higher number of variables, has increased the solve-time significantly. We can see that, on average, the *Relaxation* approach decreases the number of non-zeros in the Jacobian matrix by more than 90% while it introduces less than 0.7% error in the objective and less than 0.09% error in the RPC. Hence, in the rest of the manuscript, we use the *Relaxation* approach.

Table. 4.2 shows the simulation results on the IEEE 37-bus network using different approaches (NVV denotes the number of voltage violations). We can see that our DARC method reduces RPC compared to

Table 4.2: Summary of the Results in the 37-Bus Network (RPC is in MW)

Approach	Real data		Normal Dist.		Uniform Dist.	
	RPC	NVV	RPC	NVV	RPC	NVV
LPG	415.360	85	85.130	50	831.930	126
LPI	43.541	0	28.180	0	51.482	0
RO	28.435	0	26.252	0	26.252	0
AARC	25.427	0	18.415	0	19.361	0
$L = 2$	17.208	0	8.280	0	10.756	0
$L = 4$	16.831	0	7.569	0	10.529	0
$L = 6$	16.759	0	7.345	0	10.488	0
$L = 8$	16.763	0	7.308	0	10.476	0
Opt	9.022	0	5.296	0	5.835	0

all alternative approaches and acts closer to the optimum yet an unachievable solution. We can also see that the DARC method decreases RPC irrespective of the data distribution. This is an interesting result, as it shows that even if the data distribution is different from what we expect, at least in these experiments, the objective is not harmed by the DARC approach, and we actually manage to improve it relative to the standard AARC. Another interesting observation is that our results here agree with our discussion in Section 4.7, indicating that increasing the flexibility of the control variables continually will not always improve the performance. Also, the simulation results indicate that our proposed approach can successfully keep the voltages in the accepted limits in the experiments while decreasing RPC compared to the conventional AARC by 32%–60% over the experiments.

To illustrate the effectiveness of different approaches in dealing with the voltage rise problem, we have added Fig. 4.6. This figure represents the maximum voltage magnitude of the nodes in the 37-bus feeder when we simulate the real data from hours 7 to 18. We can see that all control approaches, except LPG, manage to bring the voltages back to the desired region. However, as shown in Table 4.2, our DARC method uses 32%–60% less real power curtailment than the best alternative approach (AARC) and acts closer to the optimum yet unachievable solution.

Next, we perform a similar experiment with the real data in the IEEE 37-bus network, except when solving the DARC, we assume to have access to the true distribution of the uncertain parameters. We

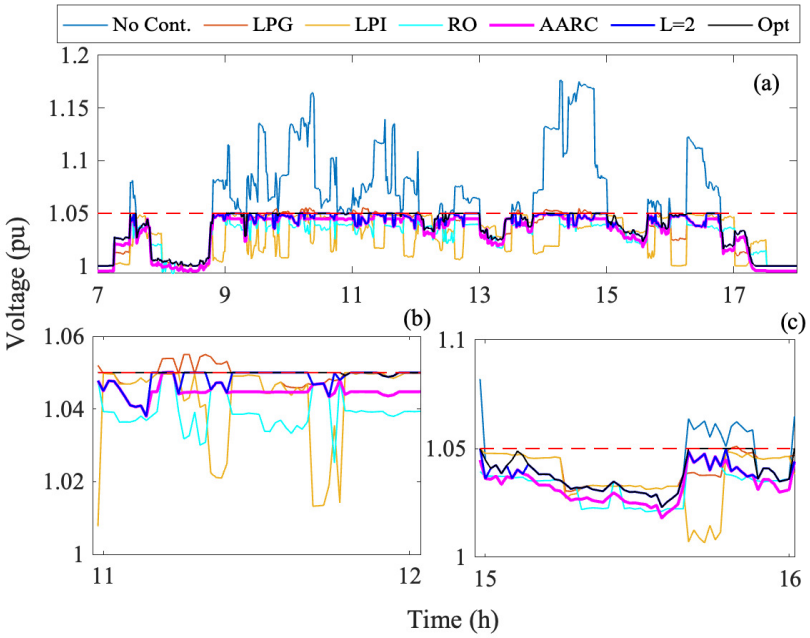

Figure 4.6: (a) Maximum voltage magnitude of the nodes in the 37-bus feeder from hours 7 to 18, using the real data. Also, (b) and (c) zoomed in on the simulation results in hours 11-12 and 15-16, respectively.

Table 4.3: Comparison between the RPC of the conventional AARC and the DARC approaches with different number of segments, when using the real data PDF.

	AARC	$L = 2$	$L = 4$	$L = 6$	$L = 8$
RPC (MW)	25.427	15.143	15.138	15.003	14.983

report the results in Table 4.3. Comparing the results in Tables 4.2 and 4.3, we can see that by using more accurate probability information of the uncertain parameters we manage to further improve the DARC performance.

4.8.2 Experiments on the IEEE 906-Bus Network

Simulation Data

We assume a high PV penetration scenario by pairing each load with a 10 kVA PV system. In the first experiment, we randomly select 55 out of the 100 1-minute resolution load shapes for the 55 houses in the network and use a similar approach as the previous section to generate

1-minute PV generation data. In the other two experiments, we repeat the same approach as the previous subsection to generate random PV and demand power data with normal and uniform distributions at each node, respectively.

Simulation Results

Table 4.4 shows the RPC, using different approaches in the 906-bus network. As can be seen, our simulation results in this section agree with the results in the previous section, showing that our proposed approach can successfully keep the voltages inside the limit in all the scenarios while decreasing the RPC relative to the other approaches. More specifically, it decreases RPC relative to the conventional AARC by 37% to 45% over the experiments.

Table 4.5 shows the average computing time in our approach. The simulations are carried out on a Dell Latitude 7490, having a 1.9 GHz Intel Core i5 processor with 8 GB memory. We can see that increasing the number of segments does not significantly increase the computing time relative to AARC. Also, from these results, we can conclude that increasing the number of segments more than two in the voltage regulation problem is not recommended since it leads to less than 1% benefit at the cost of the extra computation and complexity in the modelling. Note that as discussed in Section 4.7, the benefit obtained from the extra number of segments is related to each specific problem, and hence, a similar study is required to determine the "best" number of segments for a given a problem.

4.9 On the Implementation of DARC on Real-World Networks

This section discusses the key considerations in implementing DARC on real-world networks. In particular, it discusses the computational burden and convergence, communication infrastructure and delays, and synchronised measurement. In the following paragraphs, we separately provide insight on each topic / issue.

Computational burden and convergence: our proposed control scheme is composed of two stages, an optimisation stage that occurs every 15 minutes[4] in the background, and a controller action stage that operates continually in real-time. The controller action time is the time required for the inverter to adjust their real and reactive power

[4]The optimisation can occur in longer or shorter intervals depending on the operators' need.

Table 4.4: Summary of the results in the 906-bus network (RPC is in kW). It shows that our proposed approaches decrease RPC compared to the conventional AARC by 37%–45% over the experiments on the real, normal distribution and uniform distribution data.

Approach	Real data		Normal Dist.		Uniform Dist.	
	RPC	NVV	RPC	NVV	RPC	NVV
LPG	150.323	149	185.940	91	190.689	188
LPI	102.730	0	99.573	0	108.958	0
RO	65.592	0	62.068	0	62.068	0
AARC	55.516	0	52.075	0	52.894	0
$L = 2$	35.290	0	29.019	0	31.958	0
$L = 4$	35.001	0	28.625	0	31.839	0
$L = 6$	34.890	0	28.478	0	31.792	0
$L = 8$	34.940	0	28.414	0	31.800	0
Opt	14.550	0	12.381	0	13.116	0

Table 4.5: Average computing time in the 906-bus test system for different approaches

	Opt	RO	AARC	$L=2$	$L=4$	$L=6$	$L=8$
Time (ms)	236	263	330	353	395	421	439

outputs based on their piecewise affine functions, which given the fast-responding inverter-based technologies, is in the order of hundreds of milliseconds. The optimisation time, however, is the time taken to solve the optimisation problem detailed in Section 4.5.3. Note that we only need to solve the optimisation problem once to update the local controllers' parameters at each 15-minute interval. Also, with the recent advances in computation, linear problems can be solved efficiently using available solvers in polynomial time [82]. For example, as shown in Table 4.5, the solve time of the proposed schemes are in the order of milliseconds– well below the 15 minutes available– for our 906-bus test system on a core i5 laptop computer. Moreover, because our optimisation approach casts the problem as a linear program, it enjoys the guaranteed convergence to its optimal solution [83]. Hence, we expect the proposed approach to be computationally viable for the real-world implementation.

Communication infrastructure and delays: our design assumes the existence of a reliable two-way communication system between a central entity (responsible for updating the control parameters) and consumers that allows sending the smart inverter parameters at regular intervals. Such a communication infrastructure is an essential feature of smart grids, and various research and standards are being developed to help realise it [59]. Regarding communication delays, notice that our controllers are designed to respond to a variety of realisations within an operating interval (uncertainty set). Therefore, in case of a delay, our controllers can still respond to the realisations until the new setting is broadcasted.

Synchronised measurement: in our control scheme, we collect measurement every 15 minutes throughout the network. New technologies, such as micro-phasor measurement unit (μPMU), can measure the synchronised voltage and current values of electric power distribution networks. The synchronised data obtained by μPMU can then be used for monitoring, diagnostic, and control applications [84].

4.10 Summary

We proposed a two-stage central-local approach to coordinate multiple PV systems to prevent voltage violation in three-phase distribution systems. We casted the problem as a linear program and obtain piecewise affine functions mapping the real PV power and demand to inverter output at each household. We also proposed a novel partitioning technique to enable the conventional AARC method to exploit the available probability information. Our simulations confirm that our approach is robust against parameter uncertainty while decreasing RPC compared to alternative approaches.

A further extension to our work in this section is to incorporate soft constraints in our modelling. The soft constraints allow some network limits to be violated in extreme scenarios, if the benefit of allowing such violations for improbable scenarios outweighs the decisions guaranteeing their satisfaction for all the possible realisations. An example of such constraint is the voltage limit on a common node in the grid. As we will show in Chapter 5, allowing even a tiny probability of constraint violation can change the problem solution significantly, and results in a significant improvement of the optimal value for those instances that remain feasible.

Chapter 5

Adjustable Scenario Optimisation Approach

5.1 Introduction

In the previous two chapters, we have presented a two-stage central-local approach to coordinate PV inverters and mitigate overvoltage problems. At the heart of our approach is an uncertain optimal power flow (OPF) problem that we regularly solve to obtain parameters of the local controllers. Our approach to solving the uncertain OPF was to robustify all the constraints against uncertainty realisation regardless of their importance. This chapter revisits this step and discusses how this may lead to over-conservative decisions. It then proposes an approach based on scenario optimisation to reduce the conservativeness of adjustable robust approaches.

An OPF problem in power system operation is often solved to minimise an objective, e.g., generation cost and/or real power losses, while supplying the required demand and adhering to network constraints and engineering limits [85]. In an OPF problem, depending on the nature and importance of different constraints, they can be modelled as hard or soft constraints. The hard constraints should be satisfied for all possible realisations of uncertainty. An example of such a constraint is the voltage limit on a critical node in the system, where the disconnection of this node from the grid due to an overvoltage scenario is too costly or consequential. Another example of such a constraint is where its violation is impractical in real-time operation, like the constraint on the real power curtailment (RPC), which states that the RPC should be less than or equal to the available PV power for generation at each node.

Conversely, soft constraints allow some network limits to be violated

in extreme scenarios if the probability of their occurrence is negligible. An example of such a constraint is the voltage limit on a not critical node in the grid, e,g., a residential connection. If the voltage exceeds the limits in an extreme case, the protective relays/fuses will be triggered and disconnect the node from the grid. However, as shown in [86], allowing even a tiny probability of constraint violation can change the problem solution significantly and possibly, result in a significant improvement of the optimisation value for those instances that remain feasible.

In this chapter, we propose an adjustable scenario optimisation approach to coordinate slow- and fast-acting devices to prevent voltage violation in three-phase distribution systems. In our modelling, the hard physical constraints are immunised against the worst-case uncertainty realisation using the adjustable robust optimisation techniques developed in the previous chapters. Conversely, the soft constraints are modelled using a joint chance constrained (JCC) program. The JCC is a formulation of an optimisation problem that ensures that the probability of meeting a set constraint is above a certain level. However, since JCC programs are typically hard to solve [86], we reformulate them using scenario optimisation, which directly takes empirical data and provides bound on the risk of constraint violation. We allow fast-acting control devices to take live recourse actions by modelling their response through a piecewise affine function which takes the real-time local measurement as input and outputs the control signal. The response of slow-acting devices, on the other hand, due to their physical limits are fixed for each discrete optimisation time interval with no recourse. To the best of our knowledge, this is the first work that combines the adjustability of fast-acting devices and the scenario optimisation approach to deal with JCC problems in distribution system operation.

The available literature on scenario optimisation, e.g., [86–88], suggests a minimum number of scenarios, required within the optimisation, to probabilistically guarantee a pre-specified bound on the risk of constraint violation. However, the authors of [89] have shown that the assumptions to obtain this number of scenarios are relatively weak, and that in many engineering problems, the number of required samples to maintain the desired probability levels is far lower in practice. In fact, the unnecessarily large number of samples not only results in conservative solutions but might also cause computational challenges in large problems that need to be solved frequently.

Hence, in this chapter, we additionally propose an approach to approximate the required samples for the scenario optimisation approach.

We show that unlike alternative approaches, our suggested number of samples does not increase with the size of the problem. Unfortunately, this comes at the price of losing the bulletproof probability guarantees; yet, as we show through extensive numerical results, our proposed approximation behaves well in practice and closely maintains the required probability levels. For example, when testing our approach on the IEEE 37-bus system, it reduces the required number of samples from 4497 to only 90, while introducing less than 1.5% error in the given probability level.

The rest of this chapter is organised as follows: Section 5.2, provides a literature review and discusses the motivations behind our work. Section 5.3, presents our approach on a general optimisation problem. Section 5.4 presents our proposed method to approximate the required number of samples used for scenario optimisation, and Section 5.5 an experimental illustration on a small-scale example. Section 5.6 describes the power flow and component models, followed by the implementation of our proposed model of the voltage regulation problem. Section 5.7 presents our numerical results, and finally, Section 5.8 concludes the chapter.

This chapter presents an edited version of our work [90], published as a research article in the IEEE Transaction of Power Systems journal.

5.2 Related Work and Literature Gap

Defining the types of constraints is a crucial modelling question that dictates the formulation and solution algorithm. For hard constraints, the standard technique is the robust optimisation technique where a support is defined for the uncertainty set, which contains all the possible realisations of the uncertainty, and then chooses the value of the decision variables so that they satisfy the constraints for all the realisations. On the other hand, for soft constraints, a common approach is to formulate them as chance-constraint programs (CCP), where the objective is to find the optimum value of the decision variables that satisfy the constraints with a pre-specified probability. More formally, in this chapter, we are interested in the problems of the following form:

$$\min_{x} \; c^{\intercal} x \tag{5.1a}$$

$$x \in \mathcal{X} \tag{5.1b}$$

$$g(x, \epsilon) \geq 0 \qquad \forall \epsilon \in \mathcal{U} \tag{5.1c}$$

$$\mathrm{P}\{f(x, \tilde{\epsilon}) \geq 0\} \geq 1 - \beta, \tag{5.1d}$$

where $x \in \mathbb{R}^n$ denotes the decision variables, $c \in \mathbb{R}^n$ denotes the objective function coefficients and set $\mathcal{X} \subseteq \mathbb{R}^n$ captures the deterministic constraints on x. Also, $\tilde{\epsilon}$ is an m-dimensional random vector with values $\epsilon \in \mathcal{U} \subseteq \mathbb{R}^m$, and P and $\mathcal{U}$ denote a probability measure and an uncertainty set for $\tilde{\epsilon}$, respectively. The setting we consider is where we do not know the precise distribution of $\tilde{\epsilon}$, instead we only have access to a fixed number of samples. Functions $g(x, \epsilon) : \mathbb{R}^n \times \mathbb{R}^m \to \mathbb{R}^{l^r}$ and $f(x, \tilde{\epsilon}) : \mathbb{R}^n \times \mathbb{R}^m \to \mathbb{R}^{l^c}$ are linear in their arguments. The constraint (5.1c) denotes a hard constraint and it enforces that $g(x, \epsilon) \geq 0$ should hold for any possible realisation of ϵ. Also, the constraint (5.1d) denotes a chance constraint and requires a set of l^c uncertainty-affected inequalities to be jointly satisfied with a probability of at least $1-\beta$, where $\beta \in [0, 1]$ is a desired safety factor specified by the modeler. By convention, (5.1d) is referred to as *individual* or *joint* chance constraint, if $l^c = 1$ or $l^c > 1$, respectively.

We will handle the constraints of the form (5.1c), using the adjustable robust counterpart approaches introduced in Chapter 4, which allow the modeller to replace the decision variables with piecewise affine functions of uncertainty, and optimise the parameters of these functions.

Evaluating the JCC of the form (5.1d) requires exact information about the probability distribution P of the random vector ϵ. However, in most practical applications, we do not have access to the exact information, and P needs to be estimated with a limited number of samples from historical data. The common technique in the literature to deal with the chance constraint (5.1d) under limited information is to adopt a distributionally robust chance constrained (DRCC) approach [91–93]. These approaches form a set of possible distributions, commonly referred to as "ambiguity set" and then guarantee to satisfy the chance constraint (5.1d) for all distributions in the ambiguity set. More formally, the constraint (5.1d) is first reformulated as follows:

$$\inf_{\mathrm{P} \in \mathcal{D}} \mathrm{P}\{f(x, \tilde{\epsilon}) \geq 0\} \geq 1 - \beta, \tag{5.2}$$

where $\mathcal{D}$ denotes the ambiguity set. Then, the JCC (5.2) is separated into several individual chance constraints, one for each l^c. Finally, the individual chance constraints are reformulated as an equivalent set of linear (or mixed-integer linear) deterministic constraints through available techniques, such as applying the worst-case conditional value at risk methodology. We argue the need for our study from two angles:

i) How to efficiently separate JCC into several individual chance constraints is a complex task and an ongoing field of research. For example, the authors in [91], suggest equally dividing the safety factor β

amongst l^c individual chance constraints. Although this is a straightforward approach, the authors in [92] show that the quality of this approximation diminishes as l^c increases if the inequalities in the JCC are positively correlated, which is usually the case in most power system applications. Instead, [92] proposes an alternative approach, which characterises the problem of separating the JCC into several individual chance constraints as an optimisation problem, based on some predefined parameters; and show that their approach will always outperform the approach in [91]. The authors in [93] show that the approximation in [92] depends critically on the choice of the predefined parameters, while the problem of finding the best parameters for a general chance constrained program is nonconvex. Instead, they propose an iterative sequential optimisation approach to approximate the JCC. Using such an approach in online applications, where the optimisation needs to be solved periodically, can be quite challenging.

ii) A key element in reformulating (5.1d) to (5.2) is the choice of the ambiguity set $\mathcal{D}$. The ambiguity set is essentially a set of probable predictions of the "true distribution" based on finite available samples. One way to build the ambiguity set is to assume that true distribution will satisfy certain moment constraints obtained from the samples [94]. In these approaches, the moments are estimated from historical data and fixed for all distributions in the ambiguity set, while in reality these moments are not necessarily true for the underlying distribution, and hence, these approaches fail to provide any probability guarantees for the true distribution [95]. An alternative is to define the ambiguity set as a ball in the space of probability distributions by using a probability distance function such as the Wasserstein metric [96]. Although, these approaches can guarantee a confidence bound on the true distribution based on the predefined metrics, they are often too conservative, and hence, complementary methods such as bootstrapping or cross validation are being investigated to reduce their conservativeness [96].

To address the above shortcomings, in this chapter, we use the scenario optimisation approach [86] to deal with the JCC in (5.1d). In this approach, a number of samples are randomly selected from the historical data, and the following reformulation of (5.1d) is applied:

$$f(x, \epsilon^s) \geq 0, \qquad \forall s \in \{1, ..., N\}, \tag{5.3}$$

where the vector ϵ^s denotes the s-th realisation of ϵ, and N denotes the number of samples to be used in the optimisation. This approach firstly does not require separating the JCC into individual chance constraints, and secondly, it does not require building an ambiguity set since it incorporates the empirical data directly into the optimisation

problem. However, a critical question remains regarding the quality of the solution: *Does the optimal solution of the reformulated problem satisfy the chance constraint in the original problem* (5.1)? Notice that if N goes to infinity, the optimal solution will be feasible and close to the solution of solving the problem with the robust counterpart of (5.1d), which will also satisfy the chance constraint, but it will potentially be too conservative. Conversely, if N is chosen too small, the solution might not satisfy the chance constraint.

The authors in [86] propose an interesting approach to answer the above question. They suggest a lower bound for the number of samples to be included in the optimisation problem (5.1) so that constraint (5.1d) is satisfied with the confidence of $1-\gamma$. The authors in [87] extend the results of [86] and prove that the same probability guarantees can indeed be achieved with much fewer samples. The authors in [88] further extend the results and show that given certain structural properties of function f, such as being separable in its arguments, the number of required samples can be further reduced.

Despite all of these efforts, the authors in [89] have shown that in many engineering applications, the actual number of samples required to be used so that (5.3) can closely represent the JCC (5.1d) is often far less than the number of samples suggested by the above theories. Hence, iterative methods have been proposed in [97–99] to gradually get closer to the minimum number of samples that can maintain the probability levels for a given problem. However, these methods lack instructions on what is a suitable starting number of samples for each problem. This is essential, especially in real-time problems where a limited time is available to produce a solution. Through the lens of this literature stream, our approach can be viewed as an estimate on the number of samples required to reformulate a JCC of the form (5.1d) with (5.3).

Scenario optimisation based approaches have been used in power system operation and planning [100], for instance to solve the economic dispatch problem in transmission systems using a DC power flow model [89, 101], the unit commitment problem [102], the transmission expansion planning problem [103] and reserve scheduling problem in transmission systems with a high level of wind penetration [104]. However, the available literature either rely on too many samples which are not available in a practical setting or neglects the capability of fast-acting devices to take live recourse actions.

The main contributions of this work are:

- An adjustable scenario optimisation approach that combines the application of adjustable robust optimisation and scenario opti-

misation for coordinating the fast-acting and slow-acting voltage control devices in three-phase distribution systems. Our approach enables the operators to maintain the soft constraints with a pre-specified probability using a joint chance-constrained program. Through numerical simulations, we show that in doing so, our approach outperforms the adjustable robust optimisation (that immunises all the constraints based on the worst-case realisation of uncertainty, regardless of their importance and the likelihood of their occurrence) by more than 80%. Our approach also enables the fast-acting devices to provide live recourse actions within the scenario optimisation technique. Using numerical simulations, we show that this improves the performance of scenario optimisation by more than 83%.

- An approximation of the required number of samples in the scenario optimisation approach that does not increase with the size of the problem. We show that using the number of samples in the scenario optimisation that provides an analytical guarantee will require many samples that is often not available in practice, and even if it does, it will lead to a computationally hard problem and result in over-conservative decisions. Instead, our approximation provides a trade-off between computational burden and solution quality in the scenario optimisation approach.

5.3 Proposed Method

In this section, we present our proposed approach on a general linear uncertain optimisation problem. We first begin by providing a short summary of our approach in Chapter 4 where we replaced a number of decision variables with piecewise affine functions and dealt with hard constraints of the form (5.1c). Next, we discuss on how to deal with soft constraints of the form (5.1d). Finally, we present our approach to combine the scenario optimisation and adjustable robust methods.

5.3.1 Piecewise Affine Functions

Recall that in the DARC approach, we distinguished between the variables whose values should be decided before the uncertainty realisation, and the variables whose values can be determined after the realisation of uncertainty. Then, we replaced the latter with piecewise affine functions that take the realisation of the uncertainty as an input, and output recourse control actions.

First, we decomposed the vector of decision variables $x \in \mathbb{R}^n$ such that $x = \begin{bmatrix} x^a \\ x^u \end{bmatrix}$ where $x^a \in \mathbb{R}^{n^a}$ and $x^u \in \mathbb{R}^{n^u}$ correspond to adjustable and non-adjustable variables, respectively, while $n = n^a + n^u$. Next, we segmentate the uncertainty set to L segments along each dimension. To do so, for each element in ϵ, we define a vector of variables, $\hat{\epsilon}_j \in \mathbb{R}^L$, whose elements denote the uncertainty of realisation in each segment. We then collect the vectors $\hat{\epsilon}_j$ into the vector $\hat{\epsilon} = [\hat{\epsilon}_1^\intercal, ..., \hat{\epsilon}_m^\intercal]^\intercal$, which has a size of mL.

Next, we define the following relations between the adjustable variables x^a and uncertain parameter ϵ with the uncertain parameter $\hat{\epsilon}$:

$$x^a(\hat{\epsilon}) \coloneqq y + Y\hat{\epsilon} \tag{5.4a}$$

$$\epsilon \coloneqq \mathbf{1}\hat{\epsilon}, \tag{5.4b}$$

where $y \in \mathbb{R}^{n^a}$ and $Y \in \mathbb{R}^{n^a \times (mL)}$ are the new variables in the optimisation stage, and fixed parameters of the piecewise affine function in the real-time operation stage. Also, $\mathbf{1}$ is a block diagonal matrix with dimension $m \times (mL)$, whose diagonal block is a vector of all one with the size of $1 \times L$. We now discuss how to deal with hard constraints of the form (5.1c).

Expanding the linear function $g(x, \epsilon)$, we write:

$$Ax + B\epsilon + d \geq 0 \qquad \forall \epsilon \in \mathcal{U}, \tag{5.5}$$

where A, B and d are known matrices/vectors with appropriate sizes. We then replace the piecewise affine functions (5.4) into (5.1c), and similarly to process described in Chapter 4, use the duality technique to obtain the robust counterpart of (5.5) as a set of linear constraints.

5.3.2 Scenario Optimisation

The scenario optimisation approach states that the JCC (5.1d) can be approximated by (5.3), given that sufficient number of samples are included in the analysis. To obtain the number of samples, [86] suggests to first define Violation Probability as follows:

Let x be a candidate solution to (5.1). The violation probability of x is defined as:

$$V(x) = \mathrm{P}\{\epsilon \in \mathcal{U} : f(x, \epsilon) < 0\} \tag{5.6}$$

Then, borrowing the terminologies from [86], with probability no smaller than $1-\gamma$ ($\gamma \in [0, 1]$), the reformulated problem returns an optimal solution which is β-level robustly feasible. This statement can be formally

written as:

$$\mathrm{P}\{V(x_N^*) > \beta\} \leq \gamma, \tag{5.7}$$

where vector x_N^* denotes the optimal solution obtained from solving the reformulated problem using N samples. Theorem 1 in [87] states that

$$\mathrm{P}\{V(x_N^*) > \beta\} \leq \sum_{i=0}^{n-1} \binom{N}{i} \beta^i (1-\beta)^{N-i}, \tag{5.8}$$

where n is the number of decision variables. Thus, (5.8) implies that if we choose the number of samples (N) such that:

$$\sum_{i=0}^{n-1} \binom{N}{i} \beta^i (1-\beta)^{N-i} \leq \gamma \tag{5.9}$$

holds, then the inequality (5.7) will hold. Hereinafter, we will refer to the number of samples, suggested by Campi et al. [87], that satisfies (5.9) as N^{Cam}. Notice that the number of samples required to satisfy (5.9) will increase with the number of decision variables. Indeed, in Section 5.7, we show that in distribution systems with many nodes, using N^{Cam} samples in a scenario optimisation, leads to an intractable problem. Hence, in Section 5.4, we propose a more effective alternative approach to approximate the number of required samples in the scenario optimisation approach.

5.3.3 Adjustable Scenario Optimisation Approach

In this section, we bring the approaches introduced in 5.3.1 and Sections 5.3.2 together. In what follows, we develop a linear optimisation problem to obtain the parameters of the piecewise affine functions, whose outputs guarantee that the hard constraints are always met as long as the uncertainty realises within the defined uncertainty set. Also, with the confidence $1-\gamma$, it guarantees that the soft constraints are met with probability of at least $1-\beta$.

Similarly to the function $g(x, \epsilon)$, we expand the linear function $f(x, \epsilon^s)$, and re-write (5.3) as follows:

$$Dx + E\epsilon^s + v \geq 0, \qquad \forall s \in \{1, ..., N\}, \tag{5.10}$$

where D, E and v are known matrices/vectors with appropriate sizes. We then partition matrix $D = [D^u, D^a]$, similarly to matrix A, and

incorporate the new decision variables x^u, y and Y into (5.10), and obtain:

$$D^u x^u + D^a(y + Y\hat{\epsilon}^s) + E(\mathbf{1}\hat{\epsilon}^s) + v \geq 0 \quad \forall s \in \{1, ..., N'\}. \tag{5.11}$$

Notice that as we described in Section 5.3.2, based on (5.9), the number of required samples to replace a chance constraint increases with the number of decision variables in the optimisation problem. Hence as we are replacing our decision variable x^a with the affine function $x^a = y + Y\hat{\epsilon}$, we are increasing the number of decision variables (y and Y are the new decision variables), and thus, if we wish to obtain the same probability guarantees, we need to use more samples, i.e., $N' \geq N$.

Note that by defining the new decision variables, we have added uncertain parameters to the objective function. Here we use the sample average approximation technique [105] to reformulate the objective function as follows:

$$c^\intercal x \rightarrow c_u^\intercal x^u + c_a^\intercal \sum_{s=1}^{N'} \left(\frac{y + Y\hat{\epsilon}^s}{N'} \right), \tag{5.12}$$

where $c = [c_u^\intercal, c_a^\intercal]^\intercal$.

To summarise, we reformulate the optimisation problem (5.1) as a linear program with objective (5.12) subject to the constraint (5.1b), the adjustable robust counterpart of constraint (5.5) and constraint (5.11).

5.4 Approximation of the Required Number of Samples

In this section, we present ***Theorem 1*** (and its proof) which gives the number of samples ϵ^s that must satisfy (5.3) for a given decision variable x, for the JCC to hold with probability $1-\beta$ of constraint violation with statistical significance $1-\gamma$.

The proof is given in the context where decision variable x is constant and given *ex-ante*, and the likelihood of JCC satisfaction is then evaluated from the revealed samples. However, as we will show numerically in Sections 5.5 and 5.7, the effectiveness of this theorem is also practical (but not necessarily analytical) in the *ex-post* context where the decision variable x is optimised from the sample information.

Theorem 1: Let us fix the decision variable x and two values $\beta \in [0, 1]$ and $\gamma \in [0, 1]$ which denote the safety factor and confidence

level, respectively. Also, let us consider that there are N samples taken, where:

$$N \geq \frac{\log(\gamma)}{\log(1-\beta)}. \tag{5.13}$$

If all N samples are satisfied in the reformulation (5.3) of the JCC, then with probability no smaller than $1-\gamma$, the solution with decision variables x is β-level robustly feasible.

Proof: We first briefly provide an overview of Hoeffding's inequality to provide the required setup on which we build our approach. Hoeffding's inequality provides an upper bound on the probability that the sum of bounded independent random variables deviates from its expected value by more than a certain amount [106]. It states that given $X_1, ..., X_N$ which are independent and identically distributed (i.i.d.) random variables bounded by the interval $[0, 1]$, the following inequality holds:

$$\mathrm{P}\{X - \mu \geq t\} \leq \Big((\frac{\mu}{\mu+t})^{\mu+t} (\frac{1-\mu}{1-\mu-t})^{1-\mu-t} \Big)^N, \tag{5.14}$$

where $X = \frac{1}{N}\sum_{i=1}^{N} X_i$, $\mu = \mathrm{E}(X)$ is the expected value of X, and $t \geq 0$ is a parameter.

In what follows, we use (5.14) to obtain the required number of samples (5.13). Let us define indicator variables z and z^s that respectively depend on ϵ and ϵ^s as follows:

$$z := \begin{cases} 1 & \text{if } f(x,\epsilon) \geq 0 \\ 0 & \text{if } f(x,\epsilon) < 0 \end{cases}, \qquad z^s := \begin{cases} 1 & \text{if } f(x,\epsilon^s) \geq 0 \\ 0 & \text{if } f(x,\epsilon^s) < 0 \end{cases}$$

Defining random variable $\tilde{z}$ with values z, we rewrite our desired condition (5.1d) as the following:

$$\mathrm{P}\{\tilde{z} = 1\} \geq 1 - \beta. \tag{5.15}$$

Since $\tilde{z}$ is a binary random variable, $\mathrm{P}\{\tilde{z} = 1\} = \mathrm{E}(\tilde{z})$ and (5.15) becomes:

$$\mathrm{E}(\tilde{z}) \geq 1 - \beta. \tag{5.16}$$

Also, let us define the sample average mean of the random variable $\tilde{z}$ as follows:

$$\mathrm{Z} = \frac{1}{N}\sum_{s=1}^{N} z^s. \tag{5.17}$$

We consider Hoeffding's inequality applied to variables z^s.

Hoeffding's inequality bounds the average of random variables X_i in terms of displacement to their mean μ. However it cannot analytically be applied to bound the mean μ with respect to a sampling realisation of the X_i. Therefore, in order to infer information about the mean μ from sampling realisation we turn to statistical null-hypothesis testing [107]. For the task of showing with high confidence that (5.16) is true, we define the following:

$$H_0(\beta) : \mathrm{E}(\tilde{z}) < 1 - \beta \tag{5.18a}$$
$$H_a(\beta) : \mathrm{E}(\tilde{z}) \geq 1 - \beta, \tag{5.18b}$$

where H_0 and H_a denote the null- and alternative- hypothesis, respectively, for a given β. We then write the null-hypothesis test as follows:

$$\mathrm{P}\{\tilde{\mathrm{Z}} \geq K \mid H_0(\beta)\} \leq \gamma, \tag{5.19}$$

where K denotes the observed value of the average of the samples (or in other words, is the percentage of samples that have satisfied the JCC constraint), and γ is the significance level. Also $\tilde{\mathrm{Z}}$ is a random variable with value Z. In this case $\mathrm{P}\{\mathcal{A} \mid \mathcal{B}\}$ is read as the probability that $\mathcal{A}$ is true 'given that' hypothesis $\mathcal{B}$ is true. For small values of γ, usually less than 0.05%, we can reject the null-hypothesis, or equivalently, with confidence $1-\gamma$ we say the alternative hypothesis is true.

Let us start with an auxiliary hypothesis, parametarised by κ:

$$H_{aux}(\kappa) : \mathrm{E}(\tilde{z}) = \kappa \tag{5.20}$$

Using this auxiliary hypothesis, we can restate Hoeffding's inequality (5.14) as the following:

$$\mathrm{P}\{\tilde{\mathrm{Z}} \geq \kappa + t \mid H_{aux}(\kappa)\} \leq$$
$$\Big((\frac{\kappa}{\kappa+t})^{\kappa+t}(\frac{1-\kappa}{1-\kappa-t})^{1-\kappa-t}\Big)^N := \ell(\kappa, t, N), \tag{5.21}$$

Or by rewriting in terms of a parameter $K = \kappa + t$ then:

$$\mathrm{P}\{\tilde{\mathrm{Z}} \geq K \mid H_{aux}(K-t)\} \leq \ell(K-t, t, N), \tag{5.22}$$

This statement tells of the probability that an average of future observations ($\tilde{\mathrm{Z}}$) being greater than a threshold K given that the auxiliary hypothesis is true (where mean μ is equal to K minus t) is upper bounded the function ℓ.

One can show that for constant K, that $\ell(K-t,t,N)$ is a function which is monotonically decreasing with increasing t. Hence:

$$\begin{aligned}\forall y > t \quad \mathrm{P}\{\tilde{\mathrm{Z}} \geq K \mid H_{aux}(K-y)\} &\leq \ell(K-y,y,N) \\ &\leq \ell(K-t,t,N). \end{aligned} \tag{5.23}$$

We can reformulate the hypothesis used here as:

$$\begin{gathered}(\forall y > t, \quad H_{aux}(K-y) : \mathrm{E}(z) = K-y < K-t) \\ \Updownarrow \\ (H_0(1-(K-t)) : \mathrm{E}(z) < K-t)\,. \end{gathered} \tag{5.24}$$

Hence, considering (5.23) and (5.24), it also must be true that:

$$\mathrm{P}\{\tilde{\mathrm{Z}} \geq K \mid H_0(1-(K-t))\} \leq \ell(K-t,t,N). \tag{5.25}$$

Letting $K-t = 1-\beta$, thus:

$$\mathrm{P}\{\tilde{\mathrm{Z}} \geq K \mid H_0(\beta)\} \leq \ell(1-\beta,t,N). \tag{5.26}$$

For all the samples satisfying the JCC constraint[1] $K \to 1$ and so $t \to \beta$ thus:

$$\begin{aligned}&\mathrm{P}\{\tilde{\mathrm{Z}} \geq 1 \mid H_0(\beta)\} \leq \lim_{t\to\beta} \ell(1-\beta,t,N) \\ &= \lim_{t\to\beta} \Big((\frac{1-\beta}{1-\beta+t})^{1-\beta+t} (\frac{\beta}{\beta-t})^{\beta-t} \Big)^N = (1-\beta)^N. \end{aligned} \tag{5.27}$$

Finally, inserting this inequality (5.27) into our hypothesis test (5.19), we obtain the minimum required number of samples in ***Theorem 1*** as follows:

$$(1-\beta)^N \leq \gamma \quad \Longrightarrow \quad N \geq \frac{log(\gamma)}{log(1-\beta)}. \tag{5.28}$$

Therefore, if we take more than or equal to N samples, with confidence level $1-\gamma$ the alternative hypothesis is correct which completes our proof. ■

[1] $\mathrm{Z} \to 1$ is equivalent to finding a solution for the scenario optimisation problem with the samples used in the optimisation. In other words, a feasible solution for the optimisation problem means that all the samples satisfy all the constraints. For $\mathrm{Z} \to 1$ to happen, we should have $K \to 1$, and based on our definition $K - t = 1 - \beta$, we will have $t \to \beta$.

5.4.1 Remarks on *Theorem 1*

In the process of our proof, we assume that different sample values of the random variable $\tilde{z}$ are independent, which is an assumption for the Hoeffding's inequality, and is true in the case where decision variable x is constant and given *ex-ante*. However, in the *ex-post* case, the value z^s is determined by the optimisation decision variable x, i.e., we choose the values of the decision variable x so that we get $\mathrm{Z} = 1$, the random variables are then a function of the decision variable x, and hence not independent. In the following sections, we demonstrate through numerical simulations that the lower bounds for the number of samples (given by ***Theorem 1***) can closely approximate the required number of samples for the desired probability levels in the *ex-post* case. Hence, it can be used *i)* where only a limited time is available to make the decision, and a marginal error in the probability levels is acceptable; *ii)* as a starting point for the number of samples in an iterative scenario optimisation method.

We note that in using ***Theorem 1*** in the *ex-post* case, the decision variable x controlling the constraints is fitted to the sample points, which has the potential to introduce data over-fitting. We also note that this tendency is expected to be more prevalent when the dimension of the decision variable is large relative to the number of samples.

5.5 Small-Scale Experiment

In this section, we conduct a small-scale experiment where the number of variables and the number of uncertain parameters are both 2 (later on, in Section 5.7, we conduct more experiments on problems with more variables and uncertain parameters). For this, we reimplement the first example in Section 5.1 of [86], to investigate the out-of-sample performance of ***Theorem 1***. To make it easier for the readers to follow this chapter, we provide a summary of the example here.

We aim to solve the following linear optimisation problem:

$$\min_{x} \; c^{\intercal} x \tag{5.29a}$$

$$\mathrm{P}\{A(\tilde{\epsilon})x \leq b\} \geq 1 - \beta, \tag{5.29b}$$

where $x \in \mathbb{R}^n$ is the decision variable. Also, $\tilde{\epsilon}$ is a random vector which is uniformly distributed over a ball with radius one, and with values $\epsilon \in \mathcal{U} \subseteq \mathbb{R}^m$. $\mathcal{U}$ is the uncertainty set which is considered to be the direct product of ellipsoids, and $A(.)$ is assumed to be affine in its arguments. Hereinafter, we will refer to the minimum number of samples that satisfies (5.9) and (5.13) as N^{Cam} and N^{T1}, respectively.

Considering the probability levels $\beta = 0.01$ and $\gamma = 0.01$, we obtain N^{Cam} and N^{T1} using (5.9) and (5.13), respectively. To evaluate the out-of-sample performance, we replace (5.29b) with:

$$A(\epsilon^s)x \leq b, \qquad s \in \{1, ..., N\}, \tag{5.30}$$

and randomly select the required number of samples from $\mathcal{U}$. After solving the optimisation problem, we generate another 1e5 samples, and use the indicator function to check whether the optimal solution satisfies the constraints or not. We then calculate the average value (μ) of the indicator function over the samples. Finally, we repeat the process 1e4 times and obtain the histogram of the averages.

For the given β and γ, we solve (5.9) and use ***Theorem 1*** to obtain $N^{Cam} = 662$ and $N^{T1} = 459$, respectively. Fig. 5.1 shows the experiment results with different number of samples used in (5.30). As we increase the number of samples, we can see that the probability of constraint violation decreases. Here, we are looking for a solution that maintains the design probability levels while not being too far away from them. Ideally, we want to obtain such a solution using as few samples as possible. The reason is that increasing the number of samples both makes the problem computationally more challenging, and adds to the conservativeness of the solution[2]. From the numeric results in Fig. 5.1.c, we can see that for N^{T1} samples, the likelihood of the JCC being satisfied for more than 99% of samples is 99.08%, which is almost exactly following the given parameters $\beta = \gamma = 0.01$. In contrast, in Fig. 5.1.d we can see that for N^{Cam} samples, the likelihood of the JCC being satisfied for more than 99% of samples is 99.9% - which is ten times more conservative than necessary. Hence, in this problem, our approach based on ***Theorem 1*** offers a better solution relative to [87].

5.6 Implementation of Our Approach in the Voltage Regulation Problem

In this section, we implement our approach on the voltage regulation problem in three-phase distribution systems. Here we solve an optimisation problem periodically every 15 minutes (using the most up-to-date forecast information) and send out the control parameters to the controllers. Notice that one can increase/decrease the frequency of solving optimisation, depending on their needs. In real-time operation, the fast-acting devices use the control parameters to respond to

[2]Each scenario adds more cuts to the feasible set resulting in a more restricted solution space.

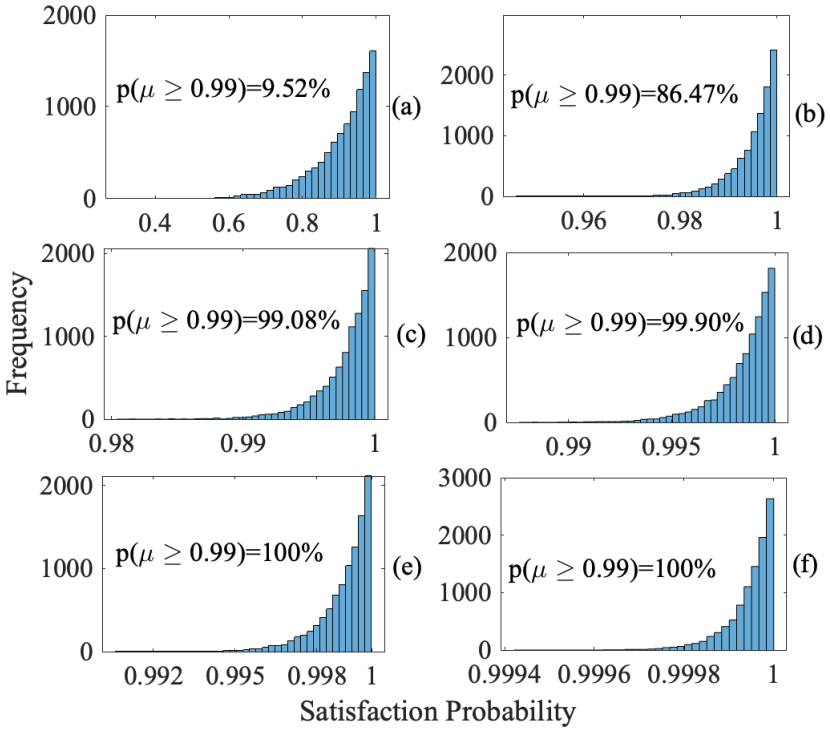

Figure 5.1: Histogram of satisfaction probability using different number of samples in the scenario optimisation. The number of samples in (a)–(f) are $N = 10$, $N = 200$, $N^{T1} = 459$, $N^{Cam} = 662$, $N = 1000$ and $N = 20000$, respectively.

different realisations of uncertainty, while the response of slow-acting devices will remain constant until a new update from the optimisation is sent through. In what follows, we first introduce network and component models. We then describe the details of how to implement our approach.

5.6.1 Network and Component Models

Let vectors $\mathbf{p}_i = [p_i^a, p_i^b, p_i^c]^\intercal$ and $\mathbf{q}_i = [q_i^a, q_i^b, q_i^c]^\intercal$ denote the real and reactive power injection at all the phases of node i, respectively. Let $\boldsymbol{p} = [\mathbf{p}_1^\intercal, \mathbf{p}_2^\intercal, ..., \mathbf{p}_M^\intercal]^\intercal$ and $\boldsymbol{q} = [\mathbf{q}_1^\intercal, \mathbf{q}_2^\intercal, ..., \mathbf{q}_M^\intercal]^\intercal$ be $3M \times 1$ vectors denoting the injected real and reactive powers at every node and phase, respectively. Let $\boldsymbol{U^0} = [\mathbf{U}_0^\intercal, \mathbf{U}_0^\intercal, ..., \mathbf{U}_0^\intercal]^\intercal$ be a $3M \times 1$ vector, where $\mathbf{U}_0$ is a 3×1 vector denoting the squared voltage magnitude at the slack node. Also let $\mathcal{V}$ denotes the set of all the nodes and phases with a power injection connection to the grid. We then establish the relation between the injected real and reactive powers, and the nodal squared voltage

magnitudes as follows:

$$\boldsymbol{U} = \boldsymbol{R}\boldsymbol{p} + \boldsymbol{X}\boldsymbol{q} + \boldsymbol{U^0}, \tag{5.31}$$

where, $\boldsymbol{R}$ and $\boldsymbol{X}$ are $3M \times 3M$ matrices, and their elements denote the sensitivity of squared voltage magnitude at node i and phase ϕ to real and reactive power changes at node j and phase φ, respectively. We obtain their elements as follows:

$$R_{j,\varphi}^{i,\phi} = \frac{\partial U_i^{\phi}}{\partial p_j^{\varphi}}, \qquad X_{j,\varphi}^{i,\phi} = \frac{\partial U_i^{\phi}}{\partial q_j^{\varphi}}. \tag{5.32}$$

We then introduce the uncertain parameters in our problem. Let $p_{i,\phi}^{D^0}$ and $p_{i,\phi}^{pv^0}$ denote the forecasted values of demand and PV output at node i and phase ϕ, respectively. Also, let $\Delta p_{i,\phi}^{D} \in \mathcal{U}^{D}$ and $\Delta p_{i,\phi}^{pv} \in \mathcal{U}^{pv}$ be the uncertain parameters, denoting the deviation from the forecasted values, where $\mathcal{U}^{D}$ and $\mathcal{U}^{pv}$ are the uncertainty sets for their corresponding uncertain parameters. Similarly to section (5.3.1), we segmentate the uncertainty set to L segments and define the following:

$$p_{i,\phi}^{D} = p_{i,\phi}^{D^0} + \sum_{l=1}^{L} \Delta p_{i\phi l}^{D} \tag{5.33a}$$

$$p_{i,\phi}^{pv} = p_{i,\phi}^{pv^0} + \sum_{l=1}^{L} \Delta p_{i\phi l}^{pv}, \tag{5.33b}$$

where $p_{i,\phi}^{D}$ and $p_{i,\phi}^{pv}$ denote the uncertain demand and PV output at node i and phase ϕ, and $p_{i,\phi}^{D^0}$ and $p_{i,\phi}^{pv^0}$ denote the corresponding forecasted values. Also, $\Delta p_{i\phi l}^{D}$ and $\Delta p_{i\phi l}^{pv}$ denote the l-th segment of demand and PV output deviations from the forecasted value at node i and phase ϕ, respectively.

We model the real power curtailment of inverters with adjustable variables using the following piecewise affine function:

$$p_{i,\phi}^{cur} \coloneqq p_{i,\phi}^{cur^0} + \sum_{l=1}^{L} \left(\alpha_{i\phi l}^{pv} \Delta p_{i\phi l}^{pv} + \alpha_{i\phi l}^{D} \Delta p_{i\phi l}^{D} \right). \tag{5.34}$$

The inverter's reactive power can also similarly be modelled. However, to simplify the formulation and reduce the problem's size, we treat the inverter's reactive power as an unadjustable variable.

We also model the voltage control response of OLTCs at the transformer connecting the slack node to the upstream network using [108]:

$$\underline{U} \leq U_0^{\phi} \leq \overline{U} \tag{5.35}$$

where U_0^{ϕ} represents the squared voltage magnitude of the slack node at phase ϕ. The model (5.35) characterises the actions of the OLTC as a slow-acting device, meaning that their value should be determined at the optimisation, and they will remain constant until a new update comes from the optimisation stage. Please note that in [109] a mixed-integer linear model of the optimal power flow problem considering the OLTC is developed. The authors have shown that this mixed-integer problem is solvable in a reasonable time (less than 3 seconds in a 33-bus system in their experiments). Thus, the OLTC model (5.35) can be replaced with their model, which will introduce integer variables in our optimisation problem. Also, note that since in most OLTCs there are a large number of tap positions to cover a wide range of over/under voltage scenarios, the solution obtained from solving the relaxed linear problem is close to the mixed integer linear problem. For example, considering a distribution OLTC with 32 steps that works between 0.9 to 1.1 pu, the maximum error in the voltage magnitude between the mixed integer and linear relaxed solution would be $(1.1pu-0.9pu)/(32\times 2) = 0.0031pu$. Nevertheless, the output of our optimisation will need to be rounded up/down to match the real-world discrete value. A simple workaround solution to prevent extra voltage violations due to this rounding up/down is round-up in cases of over-voltage and round-down in cases of undervoltage scenarios. This way, the integer solution will be at least as robust as the continuous one in practice[3].

We aim to minimise the expected value of RPC, while keeping the voltages within a desired range. We deal with three sets of constraints in our modelling; *i)* the limits on the RPC, *ii)* the inverter thermal limit and *iii)* the voltage limit constraints. We treat the first two as hard constraints, while we model the third as a soft constraint. In what follows, we present the detailed formulation.

The RPC should always be positive and less than or equal to the available PV power for generation. More formally:

$$0 \leq p_{i,\phi}^{cur} \leq p_{i,\phi}^{pv}. \tag{5.36}$$

Also, inverter thermal limit put a cap on how much real and reactive power can be generated at each inverter. The linearised constraint can be written as follows [46]:

$$\big(\cos\theta+\sin\theta\big)q_{i,\phi}^{pv} + \big(\cos\theta-\sin\theta\big)(p_{i,\phi}^{pv}-p_{i,\phi}^{cur}) \leq \sqrt{2}\overline{S}_{i,\phi} \qquad \forall\theta\in\Theta, \tag{5.37}$$

[3]Please note that other control devices, such as capacitor banks as slow-acting, and static var compensators as fast-acting devices can be added to the model in a similar way.

where $\Theta = \{0, \pi/\nu, 2\pi/\nu, ..., (2\nu-1)\pi/\nu\}$, and $\nu \geq 2$ is an arbitrary integer number. Also, $\overline{S}_{i,\phi}$ denotes the inverter capacity at node i and phase ϕ.

We next incorporate the definitions in (5.33) and (5.34) into constraint (5.36) and (5.37), and obtain linear inequality constraints that contain the uncertain parameters $\Delta p^{pv}_{i\phi l}$ and $\Delta p^{D}_{i\phi l}$. Similarly to the process described in Section 5.3.1, using duality theory, we robustify these constraints against the worst-case realisation of the uncertainty within the uncertainty sets, i.e., $\mathcal{U}^{pv}$ and $\mathcal{U}^{D}$. The detailed formulation are not included in the chapter to avoid repetition.

We then deal with the voltage limit constraints. The voltage limit constraint states that the squared voltage magnitude should be within a desired bound, i.e., $U_i^{\phi} \in [\underline{U}, \overline{U}]$. Using the power flow model (5.31), we write the following for the upper bound on voltage magnitudes:

$$\sum_{(j,\varphi)} \Big(R^{i,\phi}_{j,\varphi}(p^{pv^s}_{j,\varphi} - p^{D^s}_{j,\varphi} - p^{cur^s}_{j,\varphi}) + X^{i,\phi}_{j,\varphi}(q^{pv}_{i,\phi}) \Big) + U_0^{\phi} \leq \overline{U} \quad \forall s \in \{1, ..., N\}, \tag{5.38}$$

where

$$p^{D^s}_{i,\phi} = p^{D^0}_{i,\phi} + \sum_{l=1}^{L} \Delta p^{D^s}_{i\phi l}, \quad p^{pv^s}_{i,\phi} = p^{pv^0}_{i,\phi} + \sum_{l=1}^{L} \Delta p^{pv^s}_{i\phi l} \tag{5.39a}$$

$$p^{cur^s}_{i,\phi} = p^{cur^0}_{i,\phi} + \sum_{l=1}^{L} \big(\alpha^{pv}_{i\phi l} \Delta p^{pv^s}_{i\phi l} + \alpha^{D}_{i\phi l} \Delta p^{D^s}_{i\phi l} \big). \tag{5.39b}$$

Parameters $p^{D^s}_{i\phi l}$ and $p^{pv^s}_{i\phi l}$ denote the uncertainty realisations in the s-th sample. Similarly to (5.38), we model the lower bound on the squared voltage magnitudes. However, to avoid repetition, we have not included the detailed formulation.

Finally, similarly to (5.12), we reformulate the objective function using the sample average approximation technique as follows:

$$\min_{p^{cur^0}_{i,\phi}, \alpha^{D}_{i\phi l}, \alpha^{pv}_{i\phi l}, q^{pv}_{i,\phi}} \frac{1}{N} \sum_{s=1}^{N} \sum_{(i,\phi)} \Big(p^{cur^0}_{i,\phi} + \sum_{l=1}^{L} \big(\alpha^{pv}_{i\phi l} \Delta p^{pv^s}_{i\phi l} + \alpha^{D}_{i\phi l} \Delta p^{D^s}_{i\phi l} \big) + \varepsilon |q^{pv}_{i,\phi}| \Big), \tag{5.40}$$

where ε is a small coefficient used to prioritise the reactive power usage over the RPC. Note that although there is no cost associated with reactive power, the extra reactive power usage (injection or absorption) will result in higher currents flowing through the lines, increasing the real power loss in the system. Hence, to avoid real power losses in the lines, we minimise the reactive power usage.

5.7 Numerical Results

We test the performance of our proposed method on the IEEE 37-bus three-phase test system, which contains 32 nodes with power injection / absorption [110]. We use the snapshot demand data in [110] as the forecasted value for demand. We model a high PV penetration network by pairing each load with a PV system five times the demand value, which results in a total of 12.28 MW PV installation capacity. We conduct two experiments; in the first experiment, we assume that the PV and demand deviations from their forecasted values at each node come from a normal distribution with mean equal to zero and three standard deviation equal to 30% of the forecasted value, or more formally $\tilde{\epsilon} \sim \mathcal{N}\big(\epsilon^0, (0.1\epsilon^0)^2\big)$. In the second experiment we assume that the deviations are from a uniform distribution between -30% to 30% of the forecasted value. In each experiment, we randomly select N^{Cam} (or N^{T1}) samples from the distribution and solve the optimisation problem. We then take another 1e4 samples from the distribution to investigate the out-of-sample performance. Each experiment is then repeated 1e4 times to validate our results. The potential total available PV power for the generation due to irradiance in our setting is 1827 GW and 1828 GW in the normal distribution and uniform distribution experiments.

In our experiments, we assume that when an over-voltage occurs in a scenario at a node, the inverter connected to that node will be disconnected in that scenario. We then report how much real power is curtailed due to the inverter optimised responses (denoted by *Inv. Act.*), how much is curtailed due to the inveters being disconnected from the grid (denoted by *Inv. Trip.*) and the aggregate curtailment (denoted by *Inv. Agg.*). Also in our experiments, we consider the probability levels $\beta = 0.05$ and $\gamma = 0.01$, and assume two segments for each random variable, i.e., $L = 2$.

5.7.1 Simulations on a Two-Node System

To provide a clear example, we first conduct experiments using only two load nodes of the 37-node system. In this example, we only have 12 decision variables and 8 random variables (in the example in Section 5.5, we had only 2 decision variables and 2 random variables). Fig. 5.2 shows the simulation results. We can see that our approach, using both N^{T1} and N^{Cam}, can successfully handle the JCC problem and obtain the parameters of the piecewise affine functions. Also, we can see that similarly to Section 5.5, using N^{T1} samples can more accurately capture the JCC, meaning that the out-of-sample results are closer to the design parameter ($\gamma = 0.01$) and therefore less conserva-

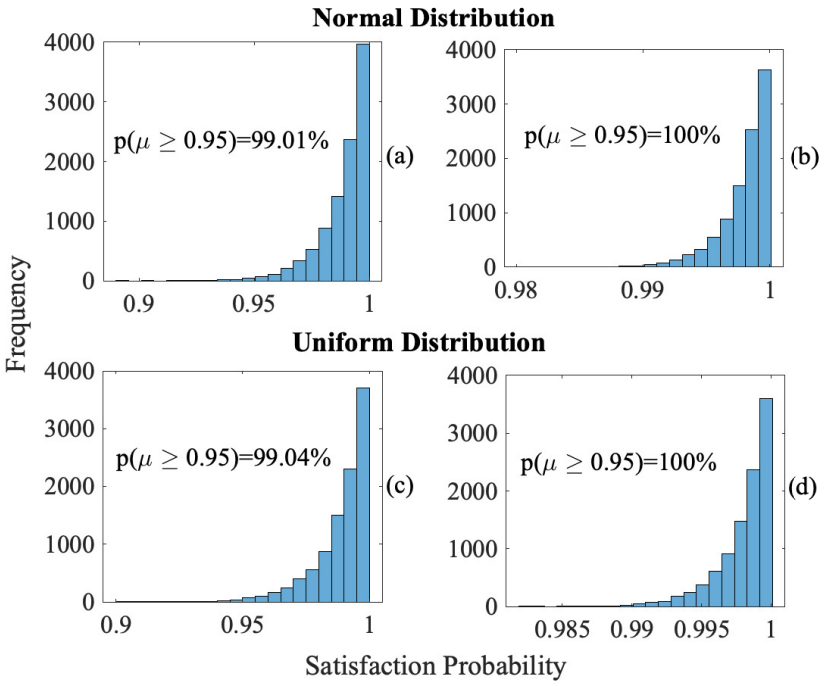

Figure 5.2: Histogram of satisfaction probability in the two-node experiment. The number of samples in (a) and (c) is $N^{T1} = 90$, while in (b) and (d) is $N^{Cam} = 425$.

tive. To find the impact of number of samples on out-of-sample results, we repeat the same experiment with the uniform distribution data for different number of samples and report the results in Fig. 5.3. For $N \geq 140$, we get a 100% JCC satisfaction, instead of the desired satisfaction 99% ($1 - \gamma = 0.99$). Also, since the number of samples should be an integer, in this problem $N^{T1} = 90$ is equal to the smallest number of samples required to be collected for the given probability levels β and γ.

5.7.2 Simulations on the IEEE 37-Node System

In this system, the number of decision variables is $n = 32 \times 6$. Given β and γ, using (5.9), we need 4497 samples. These many samples are often not available in practice, and even if they were, they would lead to a computationally hard problem. Alternatively, as introduced in Section 5.1, authors in [88] offer an approach that might reduce the number of required samples depending on certain structural properties of the constraints in a problem. The JCC in our problem, the voltage limit constraint (5.38), takes the separable structure of the form Lemma

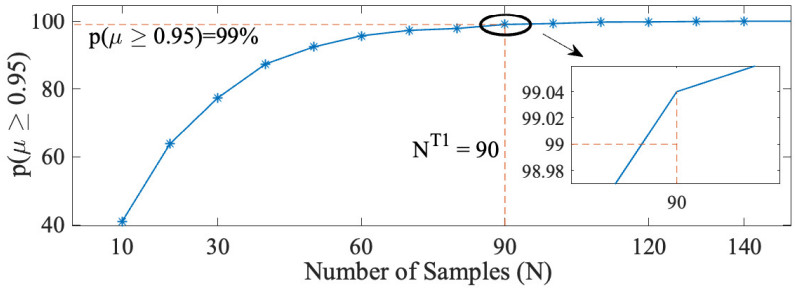

Figure 5.3: Sensitivity of constraint satisfaction to the number of samples in the two node experiment using the uniform distribution data.

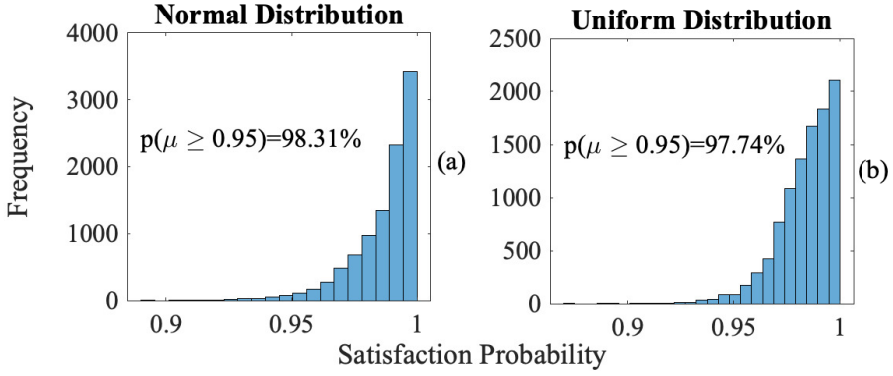

Figure 5.4: Histogram of satisfaction probability in the 37-bus experiment. The number of samples in (a) and (b) is $N^{T1}=90$.

1 in [88]. This Lemma states that in (5.9), n can be replaced with

$$n \rightarrow \min\left(n, l^c(m+1)\right), \tag{5.41}$$

where l^c denotes the number of constraints in JCC and m is the dimension of the random vector. However, since the number of the voltage constraints here is 32×2 and the dimension of the random vector is 32×4, the Lemma 1 does not decrease the number of required samples in our problem. Conversely, the number of samples required based on ***Theorem 1*** does not increase with the size of the problem, and hence, can still be used in this problem. ***Theorem 1*** states that given β and γ, here we need to take 90 samples. Fig. 5.4 shows the simulation results for the 37-bus system, using our approach with $N^{T1}=90$. We can see that our approach introduces less that 1.5% error while significantly reducing the number of required samples (from 4497 to 90).

Next, we compare our approach with the conventional scenario optimisation and adjustable robust approach, using the out-of-sample data. In the scenario optimisation approach, we use the JCC formulation for

Table 5.1: The average real power curtailment in MW for the IEEE 37-node test system

	Normal Distribution			Uniform Distribution		
	Inv. Act.	Inv. Trip.	Inv. Agg.	Inv. Act.	Inv. Trip.	Inv. Agg.
ASO	0.05	0.07	0.12	0.15	0.23	0.38
SO	0.92	1.38	2.30	1.31	1.97	3.28
AR	2.37	0	2.37	2.82	0	2.82

the voltage limit constraints but model all the control devices as slow-acting. Instead, in the adjustable robust approach, we treat all the constraints using the robust formulation while allowing the RPC to be a piecewise affine function of uncertainty. We summarise the simulation results in Table 5.1, where *ASO*, *SO* and *AR* refer to our approach, scenario optimisation approach and adjustable robust approach, respectively. We can see that our approach improves SO's performance by 88% as we empower SO with additional piecewise controllers that allow live adjustments according to the realisations of uncertain parameters. Also, we can see that our approach outperforms the AR approach by 86%, since it allows us to benefit from the probability information about the uncertain parameters.

5.7.3 Simulations on the IEEE 906-Node System

In this section, we extend our experiments to the IEEE 906-node European low voltage test feeder [35], modified by adding a 10 kVA PV system at each load node. Similarly to Section 5.7, we repeat our experiments where we assume the stochastic variations of PV generations and demands from their predicted values follow a normal distribution in the first experiment and follow a uniform distribution in the second one.

Fig. 5.5 shows the histogram of satisfaction probability in the 906-node network. As can be seen, our simulation results in this section agree with the results in the previous section, showing that our proposed approximation of the chance-constrained programs can closely provide the designed confidence level. Notice that in this example, the number of decision variables is 333 (55×6 variables for the PV systems and 3 variables modelling the OLTCs responses), and if we use (5.9) to obtain the number of samples, we will get $N^{cam} = 7516$. However, based on our approximation, since the probability guarantee has not changed ($\beta = 0.05$ and $\gamma = 0.01$), we only need 90 samples to run the optimisation.

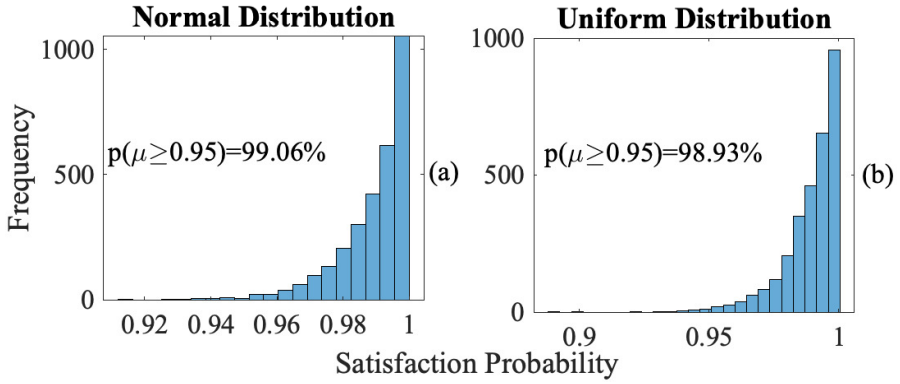

Figure 5.5: Histogram of satisfaction probability in the 906-node experiment. The number of samples in (a) and (b) is $N^{T1}=90$.

Table 5.2: The average real power curtailment in kW for the IEEE 906-node test system

	Normal Distribution			Uniform Distribution		
	Inv. Act.	Inv. Trip.	Inv. Agg.	Inv. Act.	Inv. Trip.	Inv. Agg.
ASO	40.06	2.21	42.27	51.8	2.27	54.07
SO	305.37	5.43	310.80	318.16	5.61	323.77
AR	254.63	0	254.63	274.46	0	274.46

Table 5.2 shows the RPC in our simulations, using different approaches. Again, similarly to the previous section, we can see that our ASO approach outperforms the alternative approaches by decreasing the RPC from 323.77 kW in the SO and 274.46 kW in the AR to kW in ASO (83% and 80% decrease, respectively).

To investigate the scalibility of our proposed scheme, we compare the solving time of our approach with alternative approaches, which are reported in Table. 5.3. Notice that the optimisation problem in our approach is solved periodically every 15 minutes (depending on the need of the system operator this can very form minutes to hours) using the most accurate forecast. We can see that our approach only took 8.68 seconds– well below the 15 minutes available– for our 906-node test system on a core i5 laptop computer.

5.8 Summary

We propose an adjustable scenario optimisation approach that empowers the conventional scenario optimisation approach with flexible

Table 5.3: Average computing time in the 906-node test system for different approaches.

	RO	SO	ASO
Time (s)	0.93	8.12	8.68

recourse decisions. We implement our approach on the voltage regulation problem in three-phase PV-rich distribution systems to coordinate slow- and fast-acting devices. Through numerical simulations in IEEE 37-node and 906-node test systems, we show that our approach improves the performance of traditional scenario optimisation that neglects the capability of fast-acting devices to take live recourse actions by more than 83%.

We show that using the number of samples in the scenario optimisation that provides an analytical guarantee, will require many samples that is often not available in practice. Instead, we propose an approach to approximate the number of required samples in the scenario optimisation to closely maintain the given probability guarantees. Using numerical simulations on different networks with different number of control variables, and on random variables from different probability distributions, we show that our approach closely approximates the number of samples required by the scenario optimisation to produce the probability guarantees. For example, in the case of the IEEE 906-node test system our approach reduces the number of scenarios from 7516 to only 90.

An extension to our work would be to explicitly account for non-i.i.d. historical data available in power systems within our modelling. This could ensure that our approach can handle the samples obtained from power system historical data that are often dependent on factors such as time of day, season and temperature.

Chapter 6

Conclusion

In this thesis, we explored solutions to our main question introduced in Chapter 1, i.e., *how to coordinate voltage control devices in PV-rich distribution systems to guarantee a safe and economical operation for both the network operators and consumers?* We studied different aspects of the problem and provided solutions to its key challenges in chapters 2– 5.

Our first step towards finding a solution to this problem was to establish whether the DSOs can rely on existing communication-less control schemes in distribution systems, or if there is an urgent need to invest in building communication infrastructure for the safe operation of the PV-rich distribution systems. Our studies in Chapter 2 on various available standards and innovative control schemes proposed in recent literature confirm the inadequacy of existing communication-less schemes, and the necessity of investing in communication infrastructure.

Therefore, in Chapters 3–5, we consider that a communication system exists in distribution systems. However, as discussed in these chapters, even in the presence of a communication system, the following main challenges need to be addressed before a solution to our main research question can be provided:

- The problem at hand is a very large-scale problem. Here we seek an algorithm capable of coordinating many residential and commercial inverters and other installed voltage control devices. This is especially problematic as the control algorithm needs to respond promptly (usually in the order of a couple of seconds) to frequent fluctuations in PV generation and demand. Hence, any proposed design must be scalable to such a large-scale problem and can produce a solution in a limited time.

- The response time of voltage control devices ranges from a couple

of minutes, e.g. capacitor banks, to less than a second in residential inverters. Hence, any applicable proposed design should factor in the time-scale difference in these devices and simultaneously coordinate their actions. Another challenge of slow-acting voltage control devices is that they work in discrete steps rather than continuous intervals. Therefore, if the optimisation solution is to be used in a real-world setting, this needs to be accurately modelled, or there should be a mechanism to map the optimisation solution to each device requirement.

- The uncertain and volatile nature of the PV generation and demand behaviour increases the difficulty of decision-making by control devices. Under such a highly volatile setting, the deterministic approaches that neglect the uncertain nature of the problem often fail to provide reliable control signals.

In Chapters 3–5, we gradually built a solution to address the above challenges.

6.1 Summary and Key Learnings

The solutions presented through chapters 3-5 each had their own key learnings that we summarise in the following:

- Chapter 3 summary: This chapter presents two novel two-stage Volt/Var control schemes based on the affinely adjustable robust counterpart (AARC) methodology, to mitigate the over-voltage issues caused by integration of photovoltaic panels into distribution systems. To cope with different grid code requirements, the first approach formulates the unused capacity of residential inverters to provide reactive power support based on the real power deviation, while the second approach formulates them based on voltage magnitude deviation. In the first stage of both schemes, we make central measurements throughout the network to determine a linear function, mapping the operating point deviations to the reactive power of inverters. In the second stage, the local controllers use the provided linear functions to determine the required reactive power to keep the voltages within the safe limits. Unlike similar approaches, voltage limit constraints are directly incorporated into the AARC problem, preventing the second stage controllers from unnecessarily use of reactive powers. We compare the performance of our schemes using a Monte-Carlo simulation with four other existing techniques on a real-world 27-bus and

the IEEE 906-bus LV feeders. Our simulations show that our approaches decrease the real power loss, reactive power usage, and line congestion compared to the other volt/var control schemes.

Key learnings: The reactive power of inverters, if coordinated, can reduce the negative impact of DER integration on the operation of distribution systems. However, the control approaches that only use reactive power fail to guarantee safe operation under all scenarios. This is because of limited available reactive power resources in distribution systems. Another learning from this chapter is that the AARC methodology has the potential to provide a systematic and scalable way to coordinate many inverters.

- Chapter 4 summary: This chapter builds upon our approach in Chapter 3 by extending its modelling in three main ways. Firstly, it extends the modelling to three-phase unbalanced distribution systems. Secondly, it allows to fully control both real and reactive power output of the PV inverters. Finally, it incorporates the probability distribution function of uncertain parameters to improve the performance of our approach in scenarios away from the worst-case realisation of the uncertainty. We formulate our approach as a linear program that minimises the real power curtailment (RPC) and reactive power usage of PV inverters while maintaining network voltages in an acceptable range. The optimisation model outputs the inverter controller parameters. In live operation, the controllers use the real-time local measurements to generate real and reactive power set-points of the corresponding inverters. The performance of the proposed approach is validated using Monte-Carlo simulations on IEEE 37-bus and 906-bus networks. The simulations show that the proposed approach improves the performance of AARC by 30% to 60% over a variety of experiments.

  Key learnings: Simultaneously coordinating real and reactive power of inverters connected to three-phase distribution systems can be achieved using the AARC methodology to mitigate voltage rise problems. Moreover, extending the AARC methodology to consider the probability distribution of random variables can significantly improve its performance.

- Chapter 5 summary: This chapter builds upon our approach in Chapter 4 by extending the modelling to incorporate soft constraints. To add the soft constraints into our modelling approach, we propose an adjustable scenario optimisation approach that

empowers the conventional scenario optimisation approach with flexible recourse decisions. We also propose an approach to approximate the number of required samples in the scenario optimisation. Using numerical simulations, we show that our approach, *i)* closely approximates the required number of samples to maintain the given probability guarantees in the scenario optimisation approach, *ii)* outperforms the conventional adjustable robust and scenario optimisation approaches, respectively, by 88% and 86% in our experiments.

Key learnings: Allowing a small probability of constraint violation can change the problem solution significantly. This will result in an outstanding improvement in the controllers' response, in terms of reducing the real power curtailment, for those instances that remain feasible.

6.2 Future Research

We have identified the following open research questions to improve the work done in this thesis.

- Throughout this thesis, we made several assumptions / simplification when modelling power systems. For example, we assumed that the demand and PV generation could be closely approximated using a constant power model, and that they have a single-phase connection to the grid. However, more representative models, such as ZIP demand model, and different connection types of customers, e.g. delta and star connections, have been developed in the literature to better capture the real-world behaviour of the devices connected to the grid. Hence, an important next step is explore how to incorporate these more complex models into the control algorithms developed in this thesis without losing the scalability of the algorithms.

- Our algorithms assume that the DSOs have access to the inverter controller of all the customers, and hence, can solve a central optimisation to coordinate the voltage control devices in the grid. However, due to privacy concerns and the fact that DOSs do not own these devices, the DSOs might not be able to directly control these devices. Hence, alternative approaches should be investigated to extend our algorithms to maintain consumers' privacy while still keeping the network secure.

- In Chapter 5 we showed that using chance constraint programs can bring significant benefits to operating distribution systems. However, we faced a trade-off between scalability and probability guarantees when using scenario optimisation in our analysis. Thus, an open question to research here is to see how the scalability of scenario optimisation can be improved without jeopardising the probability guarantees in chance constraint programs.

- In Chapters 4 and 5, when calculating the energy loss, we assumed that if an over-voltage occurs at a node, the inverter connected to that node will get disconnected from the grid, which results in a loss of energy that it could have produced and sent to the grid. We calculate this loss of energy after the fact, using scenarios in real-time. A natural extension of our work is to extend the modelling to account for the loss of energy due to disconnection in the optimisation model. This is potentially a challenging task as it requires dealing with binary random variables that depend on uncertain parameters.

- When performing numerical experiments in Chapters 4 and 5, we consider that if an overvoltage occurs, the inverters should get disconnected from the grid. Although the Australian standard [20] suggest that grid-connected inverters should get disconnected in sustained over-voltage scenarios, it suggests a response time depending on the severity of the over-voltage. It also suggests a reconnection mechanism for solar PV inverters. Although when performing the numerical experiments in Chapters 4 and 5, we inverter disconnection due to overvoltages, we did not model the required response time nor consider the inverter's reconnection. An extension to the modelling to consider the inverters' disconnection response time and reconnection, along with a comprehensive time-series analysis, can prepare the developed voltage control approaches for a more straightforward integration implementation in the grid.

- The convex OPF model (2.11) and linear OPF model (3.9) assume a central entity, like the DSO, has access to the inverter controller of all the customers and can solve a central optimisation problem to coordinate the voltage control devices in the grid. Such assumptions can become problematic when implementing these techniques in practice. Recent studies have shown that these OPFs can generally be solved by decomposition using Lagrangian techniques that require just the interchange of information among neighbouring buses [111]. Thus, a next step in our

current work is to extend the developed voltage approaches using a decomposition technique.

Appendix A

Simulation of the Local Voltage Control Approaches

Throughout this thesis, we repeatedly compare the performance of our proposed approaches with volt/var and volt/watt local voltage control approaches. These approaches can be viewed as a closed-loop feedback voltage controller algorithms, where they continuously measure the voltage at their connection point to the grid, and adjust real and reactive power of the inverters accordingly. In this appendix, we present how to simulate such control algorithm in distribution systems. We also discuss the instability of such control approach, and alternative implementation of volt/var and volt/watt controllers suggested in [37, 42, 44, 45] to improve their dynamical behaviour.

A.1 Real-time Feedback Control Model

A residential PV system usually consists of a sampling and measurement, maximum power point tracking algorithm and controller's logic, which together provide references for inner layer controllers of the inverter [62]. A detailed mathematical model of the components consists of nonlinear differential equations. Solving the detailed model in a time-continuous domain for a large distribution system over a long horizon is impractical. Instead, the authors in [41, 44, 45, 112, 113] suggest that the real time Volt/Var feedback problem can be modeled, approximately, as a discrete problem on a quasi-dynamical system.

Let $\mathcal{V} = \{0, ..., n\}$ denotes a set of nodes with cardinality $|\mathcal{V}| = n+1$ and $\mathcal{B} \subseteq \mathcal{V} \times \mathcal{V}$ denotes a set of branches and (i, k) or $i \to k$ represents a branch from node i to node k. For every node $i \in \mathcal{V}$, let $v_i = V_i^2$ denote the squared voltage magnitude, p_i be the real power injected to the grid at node i, and q_i be the reactive power injected to the grid at

node i. Also, let vector $\boldsymbol{V} \in \mathbb{R}^n$ denote the voltage magnitude of all the nodes, and vectors $\boldsymbol{p} \in \mathbb{R}^n$ and $\boldsymbol{q} \in \mathbb{R}^n$ collect the real and reactive power injection of all the nodes, respectively. For every branch $(i,k) \in \mathcal{B}$, let $z_{ik} = r_{ik} + jx_{ik}$ denote the complex impedance of the line, and l_{ik} denotes the squared current magnitude between node i and node k. Also, let P_{ij} and Q_{ij} denote the real and reactive powers sending from node i to node j. It is also assumed that the substation voltage set-point v_0 is given. Then, the *DistFlow* equations, which denote the relation between the injected real and reactive powers and the squared voltage magnitudes, is written as follows:

$$p_j = \sum_{k:j\to k} P_{jk} - (P_{ij} - r_{ij} l_{ij}) \qquad \forall j \in \mathcal{V} \tag{A.1a}$$

$$q_j = \sum_{k:j\to k} Q_{jk} - (Q_{ij} - x_{ij} l_{ij}) \qquad \forall j \in \mathcal{V} \tag{A.1b}$$

$$v_j = v_i - 2(r_{ij}P_{ij} + x_{ij}Q_{ij}) + (r_{ij}^2 + x_{ij}^2) l_{ij} \qquad \forall (i,j) \in \mathcal{B} \tag{A.1c}$$

$$v_i l_{ij} = P_{ij}^2 + Q_{ij}^2 \qquad \forall (i,j) \in \mathcal{B}. \tag{A.1d}$$

Let us represent (A.1) at time instance t into the following compact form:

$$\boldsymbol{V}_t = f(\boldsymbol{p}_t, \boldsymbol{q}_t) \tag{A.2}$$

The quasi-dynamical system can now be shown as the following:

$$\boldsymbol{V}_t = f(\boldsymbol{p}_t, \boldsymbol{q}_t) \tag{A.3a}$$

$$q_{i,t+1} = g_i(V_{i,t}, q_{i,t}), \tag{A.3b}$$

where function $g_i()$ denotes the controller logic at node i. In (A.3), $V_{i,t}$ and $q_{i,t}$ are current state variables (at time t), while $q_{i,t+1}$ is the state variable at the next time step. A controller based on the current state variables determines the new reactive power set-point $q_{i,t+1}$ based on (A.3b), which would result in a new voltage profile according to (A.3a). This iterative process will continue till it convergence to a solution. In what follows, we investigate performances of three different approaches in solving (A.3).

The first approach (we will refer to this approach as Iterative) that we investigate in dealing with (A.3) is the volt/var suggested by the IEEE standard 1547 [21]. We have introduced this approach in Section 2.2.1, and shown its schematic in Fig. 2.6. In this approach, the

reactive power of each inverter is calculated as follows:

$$q_{i,t+1} = \begin{cases} \big[-\alpha_{i,t}(V_{i,t} - (V^{nom} - \delta))\big]_{q_i^{min}}^{q_i^{max}} & V_{i,t} < V^{nom} - \delta \\ 0 & V^{nom} - \delta \leq V_{i,t} \leq V^{nom} + \delta \\ \big[-\alpha_{i,t}(V_{i,t} - (V^{nom} + \delta))\big]_{q_i^{min}}^{q_i^{max}} & V_{i,t} > V^{nom} + \delta, \end{cases} \tag{A.4}$$

where V^{nom} is the nominal voltage value, usually considered equal to one per unit. 2δ is the dead-band size, and $\alpha_{i,t} = \dfrac{q_{i,t}^{max}}{V_4 - V_3}$ is the droop slope at node i and time t, where V_3 and V_4 are fixed parameters. Operator $[.]_{.\,min}^{max}$ enforces the inverter reactive power capacity limit. Authors in [41] show that if replace (A.4) with (A.3b) in the problem (A.3), under certain conditions (in the next section, we will review these conditions), the quasi-dynamical system would not converge to a solution, which leads to oscillatory behaviour.

Authors in [42] have suggested an alternative approach (the second approach we will investigate) based on the gradient projection algorithm to implement the volt/var approach, which we will refer to it as smooth iterative approach, where the reactive power of each inverter is calculated as follows:

$$q_{i,t+1} = \begin{cases} \Big[q_{i,t} + d_i\big(V_{i,t} - (V^{nom} - \delta)\big) - \dfrac{1}{\alpha} q_{i,t}\Big)\Big]_{q_i^{min}}^{q_i^{max}} & V_{i,t} < V^{nom} - \delta \\ 0 & V^{nom} - \delta \leq V_{i,t} \leq V^{nom} + \delta \\ \Big[q_{i,t} + d_i\big(V_{i,t} - (V^{nom} + \delta)\big) - \dfrac{1}{\alpha} q_{i,t}\Big)\Big]_{q_i^{min}}^{q_i^{max}} & V_{i,t} > V^{nom} + \delta, \end{cases} \tag{A.5}$$

where $d_i > 0$ is the step size.

The third approach is to model the piecewise linear function (A.4) together with the power flow equation (A.2) as a mixed integer nonlinear programming (MINLP) problem, and solve it through commercial solvers. MINLP problems are generally NP-hard, but since the size of the problem here is relatively small, it can be solved by solvers such as *Bonmin*. What follows is the MINLP model used to solve (A.3):

$$\text{Power flow equations (A.1)} \tag{A.6a}$$

$$q_i = \sum_{l=0}^{h} \lambda_{i,l} \times \Gamma(u_l^q), \qquad v_i = \sum_{l=0}^{h} \lambda_{i,l} \times u_l^q \tag{A.6b}$$

$$0 \leq \lambda_{i,0} \leq w_{i,0}, \qquad 0 \leq \lambda_{i,k} \leq w_{i,h} \tag{A.6c}$$

$$0 \leq \lambda_{i,k} \leq w_{i,h} + w_{i,h-1} \quad l = 1, ..., h-1 \tag{A.6d}$$

Table A.1: piecewise linear volt/var curve fixed points

$\boldsymbol{u_l^q}$	0.95	0.98	1.02	1.05
$\boldsymbol{\Gamma(u_l^q)}$	$q_{i,t}^{max}$	0	0	$-q_{i,t}^{max}$

$$\sum_{l=0}^{h} \lambda_{i,l} = 1, \qquad \sum_{l=0}^{h-1} w_{i,l} = 1, \tag{A.6e}$$

where constraints (A.6b)-(A.6e) are used to model the piecewise linear volt /var curve. In (A.6), $w_{i,j,l} \in \{0,1\}$ is an auxiliary binary variable and $\lambda_{i,j,l} \in (0,1)$ is an auxiliary continuous variable. $\Gamma(u_l^q)$ and u_l^q are parameters, defining the piecewise linear volt/var curve based on predefined voltage and reactive power values, shown in Table A.1.

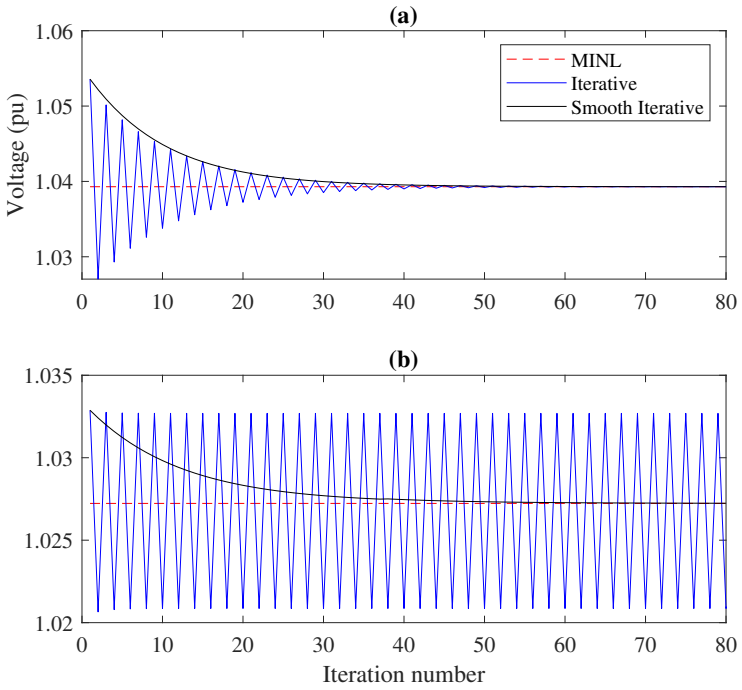

Figure A.1: Convergence comparison for MINLP, iterative and smooth iterative approaches. (a): Scenario 1,(b): Scenario 2.

A.2 Simulation Results

We consider a real 30-bus modern underground LV feeder with $R/X \approx 2$ located in Hobart, Australia. We carried out two experiments for two different scenarios, where we paired each node with a 5kVA PV system. In the first scenario, most of the inverter capacity (90%) is used for real power conversion, and the remaining unused capacity of the inverter is available for reactive power support. In the second scenario, 70% of the inverter capacity is used for real power conversion, and in turn, more capacity is available for reactive power support. The results of the first scenario are presented in Fig. A.1.a. It can be seen that all three approaches obtain the same solution. Authors in [41] provide sufficient conditions under which model (A.4) would not converge to a solution as follows:

$$max(\alpha_{i,t}) < \frac{1}{\lambda_{max}(X)} \tag{A.7a}$$

$$X = M^{-T} D_x M^{-1}, \tag{A.7b}$$

where operator $\lambda_{max}(.)$ denotes the maximum eigenvalue of a matrix and D_x is an $(N \times N)$ diagonal matrix with the i-th entry equal to the reactance x_{ij}. M is an $(N \times N)$ matrix which can be obtained from the $\big((N+1) \times N\big)$ incidence matrix $M^{\circ} = [m_{\circ} M^T]^T$. $m_{\circ}^T$ denotes the first row of M_0, which corresponds to bus 1, whose voltage is considered to be constant. Applying (A.7) on the under-sturdy distribution feeder, we obtain that the maximum value for $\alpha_{i,t}$ should be smaller than 129.09. In the second scenario, the higher available capacity for reactive power support would lead to a higher value of $\alpha_{i,t}$, which would lead to divergence in model (A.4), shown in Fig. A.1.b. It can be seen that models (A.5) and (A.6) still reach a same solution, while model (A.4) does not converge. This shows that models (A.5) and (A.6) can cover a wider range of volt/var problems. It should be stressed that the approximate time required to solve (A.6) is around 100 times more than the time required to solve (A.5). Therefore, throughout this thesis, we use model (A.5) for simulation of the real-time volt/var feedback control. Similarly, the volt/watt voltage control approach can be simulated using the gradient projection algorithm, which we did not include here to avoid repetition. Please, note that we use the optimisation model only to show that the other two iterative approaches will converge to the same value as the optimisation solution. However, we do not use the optimisation model throughout the thesis to simulate volt/var and volt/watt voltage control approaches. Also, other simulation environments, such as OpenDSS [51], could be used to simulate volt/var and

volt/watt voltage control approaches. However, since these environments are commonly restrictive and do not allow the implementation of novel control algorithms, which is the focus of our work in this thesis, we decided to implement all the control techniques in one platform using Python scripts. In doing so, we ensured that different approaches were compared in a similar condition.

Appendix B

Linear Programming

Throughout this thesis, we repeatedly formulate control and operation problems as linear programming optimisation models. We also use the Duality Theorem to obtain the robust counterpart of an uncertain linear program. Hence, to make easier for the readers to follow this thesis, we provide an overview of this topics. Although the provided materials should suffice for the readers to better understand the algorithms throughout the thesis, we strongly encourage the readers to refer to textbooks, e.g. [114] for more details on linear programming and duality theory.

B.1 Duality Theorem

Let $x \in \mathbb{R}^n$ be the decision variable of a linear optimisation problem, $c \in \mathbb{R}^n$, $A \in \mathbb{R}^{m \times n}$, and $b \in \mathbb{R}^m$ are parameters of the optimisation. Then, a general linear program (LP) can be formally stated as follows:

$$\max_x \; c^\intercal x \tag{B.1a}$$

$$Ax \leq b \tag{B.1b}$$

$$x \geq 0, \tag{B.1c}$$

which is also commonly referred to as the primal problem. Based on the duality principles, the dual of a given LP is another LP that is derived from the original (the primal) LP where: each variable in the primal LP becomes a constraint in the dual LP; each constraint in the primal LP becomes a variable in the dual LP, and the objective direction is inverted, i.e., maximum in the primal becomes minimum in the dual and vice versa [115]. The duality principles can be stated formally in

general terms as follows:

$$\min_{y} \; b^{\intercal} y \tag{B.2a}$$

$$A^{\intercal} y \geq c \tag{B.2b}$$

$$y \geq 0, \tag{B.2c}$$

where $y \in \mathbb{R}^m$ is the decision variable of the dual problem.

In Chapters 3–5, we use the duality principle to replace maximisation problems with their equivalent minimisation dual problems. Indeed, we use the Strong Duality theory which states that:

Strong Duality*: The dual has an optimal solution if and only if the primal does. If x^* and y^* are optimal solutions to the primal and dual, then $c^{\intercal} x^* = b^{\intercal} y^*$.*

Bibliography

[1] I. R. E. Agency, "Future of solar photovoltaic: deployment, investment, technology, grid integration and socio-economic aspects," *A Global Energy Transformation*, 2019.

[2] IEA, "Solar PV power generation in the sustainable development scenario, 2000-2030," *Online: https://www.iea.org/data-and-statistics/charts/solar-pv-power-generation-in-the-sustainable-development-scenario-2000-2030*, accessed on 1 Nov. 2021.

[3] M. Jaganmohan, "Global rooftop share in solar PV capacity additions 2015-2022," *Online: https://www.statista.com/statistics/1172031/rooftop-share-in-solar-pv-deployment/statisticContainer*, Jan 27, 2021.

[4] W. H. Kersting, *Distribution system modeling and analysis*. CRC press, 2006.

[5] C. Abbey, A. Baitch, B. Bak-Jensen, C. Carter, G. Celli, K. El Bakari, M. Fan, P. Georgilakis, T. Hearne, L. N. Ochoa *et al.*, *Planning and optimization methods for active distribution systems*. CIGRE (International Council on Large Electric Systems), 2014.

[6] S. Hashemi and J. Østergaard, "Efficient control of energy storage for increasing the PV hosting capacity of LV grids," *IEEE Trans. Smart Grid*, vol. 9, no. 3, pp. 2295–2303, 2016.

[7] A. Rodriguez-Calvo, R. Cossent, and P. Frías, "Integration of pv and EVs in unbalanced residential LV networks and implications for the smart grid and advanced metering infrastructure deployment," *International Journal of Electrical Power & Energy Systems*, vol. 91, pp. 121–134, 2017.

[8] M. Mahmoodi and L. Blackhall, "DER hosting capacity envelope in unbalanced distribution systems," in *2021 IEEE PES Innova-*

tive Smart Grid Technologies Europe (ISGT Europe). IEEE, 2021, pp. 1–6.

[9] M. A. Akbari, J. Aghaei, M. Barani, M. Savaghebi, M. Shafie-Khah, J. M. Guerrero, and J. P. Catalao, "New metrics for evaluating technical benefits and risks of DGs increasing penetration," *IEEE Trans. Smart Grid*, vol. 8, no. 6, pp. 2890–2902, 2017.

[10] N. K. Roy and H. R. Pota, "Current status and issues of concern for the integration of distributed generation into electricity networks," *IEEE Systems journal*, vol. 9, no. 3, pp. 933–944, 2014.

[11] S. R. Abadi, M. Mahmoodi, A. Fereidunian, G. Jahandoust, and H. Leasni, "Formal verification of fault location, isolation and service restoration in distribution automation using UPPAAL," in *2017 Conference on Electrical Power Distribution Networks Conference (EPDC)*. IEEE, 2017, pp. 96–100.

[12] S. M. N. R. Abadi, M. Davarpanah, M. Mahmoodi, S. Nasiri, and R. Bekhradian, "Multiobjective optimal DERs placement and sizing considering generator shaft fatigue," *IEEE Transactions on Power Systems*, vol. 33, no. 6, pp. 6787–6794, 2018.

[13] R. Tonkoski, L. A. Lopes, and T. H. El-Fouly, "Coordinated active power curtailment of grid connected PV inverters for overvoltage prevention," *IEEE Trans. Sustain. Energy*, vol. 2, no. 2, pp. 139–147, 2010.

[14] M. Zeraati, M. E. H. Golshan, and J. M. Guerrero, "Distributed control of battery energy storage systems for voltage regulation in distribution networks with high PV penetration," *IEEE Trans. Smart Grid*, vol. 9, no. 4, pp. 3582–3593, 2016.

[15] F. Olivier, P. Aristidou, D. Ernst, and T. Van Cutsem, "Active management of low-voltage networks for mitigating overvoltages due to photovoltaic units," *IEEE Trans. Smart Grid*, vol. 7, no. 2, pp. 926–936, 2015.

[16] J. Von Appen, T. Stetz, M. Braun, and A. Schmiegel, "Local voltage control strategies for PV storage systems in distribution grids," *IEEE Trans. Smart Grid*, vol. 5, no. 2, pp. 1002–1009, 2014.

[17] Y. Wang, K. Tan, X. Y. Peng, and P. L. So, "Coordinated control of distributed energy-storage systems for voltage regulation in distribution networks," *IEEE Trans. Power Del.*, vol. 31, no. 3, pp. 1132–1141, 2015.

[18] P. H. Divshali and L. Söder, "Improving hosting capacity of rooftop PVs by quadratic control of an LV-central BSS," *IEEE Trans. Smart Grid*, vol. 10, no. 1, pp. 919–927, 2017.

[19] K. E. Antoniadou-Plytaria, I. N. Kouveliotis-Lysikatos, P. S. Georgilakis, and N. D. Hatziargyriou, "Distributed and decentralized voltage control of smart distribution networks: Models, methods, and future research," *IEEE Trans. Smart Grid*, vol. 8, no. 6, pp. 2999–3008, 2017.

[20] "Australian/New Zealand standard: Grid connection of energy systems via inverters, inverter requirements, AS/NZS 4777.2," 2020.

[21] T. S. Basso and R. DeBlasio, "IEEE 1547 series of standards: interconnection issues," *IEEE Trans. Power Electron*, vol. 19, no. 5, pp. 1159–1162, 2004.

[22] E. Troester, "New German grid codes for connecting PV systems to the medium voltage power grid," in *2nd International workshop on concentrating photovoltaic power plants: optical design, production, grid connection*, 2009, pp. 1–4.

[23] M. Mahmoodi, S. M. N. RA, A. Attarha, L. Blackhall, and J. Hendriks, "Impact assessment of active network management schemes on DG capacity of distribution systems," in *2022 IEEE International Conference on Power Systems Technology (POWERCON)*. IEEE, 2022, pp. 1–7.

[24] H. J. Liu, W. Shi, and H. Zhu, "Decentralized dynamic optimization for power network voltage control," *IEEE Trans. Signal Inf. Process. Netw.*, vol. 3, no. 3, pp. 568–579, 2016.

[25] A. Abessi, V. Vahidinasab, and M. S. Ghazizadeh, "Centralized support distributed voltage control by using end-users as reactive power support," *IEEE Trans. Smart Grid*, vol. 7, no. 1, pp. 178–188, 2015.

[26] B. A. Robbins, C. N. Hadjicostis, and A. D. Domínguez-García, "A two-stage distributed architecture for voltage control in power distribution systems," *IEEE Trans. Power Syst.*, vol. 28, no. 2, pp. 1470–1482, 2012.

[27] R. A. Jabr, "Robust volt/var control with photovoltaics," *IEEE Trans. Power Syst.*, vol. 34, no. 3, pp. 2401–2408, 2019.

[28] H. S. Bidgoli and T. Van Cutsem, "Combined local and centralized voltage control in active distribution networks," *IEEE Trans. Power Syst.*, vol. 33, no. 2, pp. 1374–1384, 2017.

[29] Y. Xu, Z. Y. Dong, R. Zhang, and D. J. Hill, "Multi-timescale coordinated voltage/var control of high renewable-penetrated distribution systems," *IEEE Trans. Power Syst.*, vol. 32, no. 6, pp. 4398–4408, 2017.

[30] R. A. Jabr, "Linear decision rules for control of reactive power by distributed photovoltaic generators," *IEEE Trans. Power Syst.*, vol. 33, no. 2, pp. 2165–2174, 2017.

[31] S. M. N. R. Abadi, P. Scott, and S. Thiébaux, "A combined central-local volt/var approach in distribution systems with high PV uptake," in *2020 International Conference on Smart Grids and Energy Systems (SGES).* IEEE, 2020, pp. 606–611.

[32] S. Abadi, M. Mahmoodi, P. Scott, L. Blackhall, and S. Thiebaux, "Active management of LV residential networks under high PV penetration," in *2019 IEEE Milan PowerTech.* IEEE, 2019, pp. 1–6.

[33] M. Mahmoodi, M. Shaw, and L. Blackhall, "Voltage behaviour and distribution network performance with community energy storage systems and high PV uptake," in *Proceedings of the Eleventh ACM International Conference on Future Energy Systems*, 2020, pp. 388–390.

[34] E. McKenna and M. Thomson, "High-resolution stochastic integrated thermal–electrical domestic demand model," *Applied Energy*, vol. 165, pp. 445–461, 2016.

[35] IEEE European low voltage test feeder. [Online]. Available: https://site.ieee.org/pes-testfeeders/resources.

[36] D. Peharda, I. Ivanković, and N. Jaman, "Using data from scada for centralized transformer monitoring applications," *Procedia Engineering*, vol. 202, pp. 65–75, 2017.

[37] B. K. Perera, "Modelling of inverter interfaced renewable energy resources to investigate grid interactions," 2015.

[38] T. Sansawatt, L. F. Ochoa, and G. P. Harrison, "Smart decentralized control of DG for voltage and thermal constraint management," *IEEE Trans. Power Syst.*, vol. 27, no. 3, pp. 1637–1645, 2012.

[39] Z. Zhang, L. F. Ochoa, and G. Valverde, "A novel voltage sensitivity approach for the decentralized control of DG plants," *IEEE Trans. Power Syst.*, vol. 33, no. 2, pp. 1566–1576, 2017.

[40] A. Samadi, R. Eriksson, L. Söder, B. G. Rawn, and J. C. Boemer, "Coordinated active power-dependent voltage regulation in distribution grids with PV systems," *IEEE Trans. Power Del.*, vol. 29, no. 3, pp. 1454–1464, 2014.

[41] M. Farivar, X. Zho, and L. Che, "Local voltage control in distribution systems: An incremental control algorithm," in *2015 IEEE International Conference on Smart Grid Communications (SmartGridComm)*. IEEE, 2015, pp. 732–737.

[42] H. Zhu and H. J. Liu, "Fast local voltage control under limited reactive power: Optimality and stability analysis," *IEEE Trans. Power Syst.*, vol. 31, no. 5, pp. 3794–3803, 2015.

[43] M. G. Kashani, M. Mobarrez, and S. Bhattacharya, "Smart inverter volt-watt control design in high PV-penetrated distribution systems," *IEEE Trans. Ind Appl.*, vol. 55, no. 2, pp. 1147–1156, 2018.

[44] X. Zhou, M. Farivar, Z. Liu, L. Chen, and S. H. Low, "Reverse and forward engineering of local voltage control in distribution networks," *IEEE Trans. Autom. Control*, vol. 66, no. 3, pp. 1116–1128, 2020.

[45] N. Li, G. Qu, and M. Dahleh, "Real-time decentralized voltage control in distribution networks," in *2014 52nd Annual Allerton Conference on Communication, Control, and Computing (Allerton)*. IEEE, 2014, pp. 582–588.

[46] S. M. N. R. Abadi, A. Attarha, P. Scott, and S. Thiébaux, "Affinely adjustable robust volt/var control for distribution systems with high pv penetration," *IEEE Trans. Power Syst.*, vol. 36, no. 4, pp. 3238–3247, 2021.

[47] M. Farivar and S. H. Low, "Branch flow model: Relaxations and convexification—part i," *IEEE Trans. Power Syst.*, vol. 28, no. 3, pp. 2554–2564, 2013.

[48] Solar report. Australian Energy Counsil, [Online]. Available: https://www.energycouncil.com.au/media/5wkkaxts/australian-energy-council-solar-report_-jan-2022.pdf, January 2021.

[49] W. E. Hart, J.-P. Watson, and D. L. Woodruff, "Pyomo: modeling and solving mathematical programs in python," *Mathematical Programming Computation*, vol. 3, no. 3, pp. 219–260, 2011.

[50] J. M. Rupa and S. Ganesh, "Power flow analysis for radial distribution system using backward/forward sweep method," *International Journal of Electrical, Computer, Electronics and Communication Engineering*, vol. 8, no. 10, pp. 1540–1544, 2014.

[51] D. Montenegro, M. Hernandez, and G. Ramos, "Real time opendss framework for distribution systems simulation and analysis," in *2012 Sixth IEEE/PES Transmission and Distribution: Latin America Conference and Exposition (T&D-LA)*. IEEE, 2012, pp. 1–5.

[52] M. Jafari, T. O. Olowu, A. I. Sarwat, and M. A. Rahman, "Study of smart grid protection challenges with high photovoltaic penetration," in *2019 North American Power Symposium (NAPS)*. IEEE, 2019, pp. 1–6.

[53] D. K. Molzahn, F. Dörfler, H. Sandberg, S. H. Low, S. Chakrabarti, R. Baldick, and J. Lavaei, "A survey of distributed optimization and control algorithms for electric power systems," *IEEE Trans. Smart Grid*, vol. 8, no. 6, pp. 2941–2962, 2017.

[54] A. Ben-Tal, A. Goryashko, E. Guslitzer, and A. Nemirovski, "Adjustable robust solutions of uncertain linear programs," *Mathematical programming*, vol. 99, no. 2, pp. 351–376, 2004.

[55] A. Attarha, P. Scott, and S. Thiébaux, "Affinely adjustable robust ADMM for residential DER coordination in distribution networks," *IEEE Trans. Smart Grid*, 2019.

[56] S. Uebermasser, C. Groiss, A. Einfalt, N. Thie, M. Vasconcelos, J. Helguero, H. Laaksonen, and P. Hovila, "Requirements for coordinated ancillary services covering different voltage levels," *CIRED-Open Access Proceedings Journal*, vol. 2017, no. 1, pp. 1421–1424, 2017.

[57] A. Miller, R. Strahan, S. Mcnab, T. Crownshaw, S. Pandey, N. Watson, S. Lemon, and A. Wood, "Guideline for the connection of small-scale inverter based distributed generation: An introduction and summary," 2016.

[58] L. Gurobi Optimization, "Gurobi optimizer reference manual," 2020. [Online]. Available: http://www.gurobi.com

[59] V. C. Gungor, D. Sahin, T. Kocak, S. Ergut, C. Buccella, C. Cecati, and G. P. Hancke, "Smart grid technologies: Communication technologies and standards," *IEEE Trans. Ind. Informat.*, vol. 7, no. 4, pp. 529–539, 2011.

[60] G. P. McCormick, "Computability of global solutions to factorable nonconvex programs: Part I—convex underestimating problems," *Mathematical programming*, vol. 10, no. 1, pp. 147–175, 1976.

[61] P. M. Castro, "Tightening piecewise Mccormick relaxations for bilinear problems," *Computers & Chemical Engineering*, vol. 72, pp. 300–311, 2015.

[62] B. Perera, P. Ciufo, and S. Perera, "Advanced point of common coupling voltage controllers for grid-connected solar photovoltaic (PV) systems," *Renewable energy*, vol. 86, pp. 1037–1044, 2016.

[63] A. Attarha, S. M. N. RA, P. Scott, and S. Thiébaux, "Network-secure envelopes enabling reliable DER bidding in energy and reserve markets," *IEEE Transactions on Smart Grid*, vol. 13, no. 3, pp. 2050–2062, 2021.

[64] Y. Guo, H. Gao, Q. Wu, J. Østergaard, D. Yu, and M. Shahidehpour, "Distributed coordinated active and reactive power control of wind farms based on model predictive control," *International Journal of Electrical Power & Energy Systems*, vol. 104, pp. 78–88, 2019.

[65] "Grid connection of energy systems via inverters inverter requirements," AS/NZS 4777.2, Standards Australia, Oct. 2015.

[66] P. Li, M. Yang, and Q. Wu, "Confidence interval based distributionally robust real-time economic dispatch approach considering wind power accommodation risk," *IEEE Trans. Sustain. Energy*, vol. 12, no. 1, pp. 58–69, 2020.

[67] W. Wei, F. Liu, and S. Mei, "Distributionally robust co-optimization of energy and reserve dispatch," *IEEE Trans. Sustain. Energy*, vol. 7, no. 1, pp. 289–300, 2015.

[68] R. A. Jabr, "Distributionally robust CVaR constraints for power flow optimization," *IEEE Trans. Power Syst.*, vol. 35, no. 5, pp. 3764–3773, 2020.

[69] B. K. Poolla, A. R. Hota, S. Bolognani, D. S. Callaway, and A. Cherukuri, "Wasserstein distributionally robust look-ahead economic dispatch," *IEEE Trans. Power Syst.*, vol. 36, no. 3, pp. 2010–2022, 2020.

[70] Z. Li, W. Wu, B. Zhang, and B. Wang, "Adjustable robust real-time power dispatch with large-scale wind power integration," *IEEE Trans. Sustain. Energy*, vol. 6, no. 2, pp. 357–368, 2015.

[71] S. Cai, Y. Xie, Q. Wu, Z. Xiang, X. Jin, and M. Zhang, "Robust coordination of multiple power sources for sequential service restoration of distribution systems," *International Journal of Electrical Power & Energy Systems*, vol. 131, p. 107068, 2021.

[72] M. Mahmoodi, A. Attarha, S. M. N. RA, P. Scott, and L. Blackhall, "Adjustable robust approach to increase DG hosting capacity in active distribution systems," *Electric Power Systems Research*, vol. 211, p. 108347, 2022.

[73] H. Gao, J. Liu, and L. Wang, "Robust coordinated optimization of active and reactive power in active distribution systems," *IEEE Transactions on Smart Grid*, vol. 9, no. 5, pp. 4436–4447, 2017.

[74] X. Zeng, H. Wu, M. Ding, R. Bi, B. Xu, and J. Ding, "Two-stage robust optimization for practical reactive power in distribution network based on multiple constraint convex approximation," *International Journal of Electrical Power & Energy Systems*, vol. 134, p. 107414, 2022.

[75] S. M. N. RA, P. Scott, M. Mahmoodi, and A. Attarha, "Data-driven adjustable robust solution to voltage-regulation problem in pv-rich distribution systems," *International Journal of Electrical Power & Energy Systems*, vol. 141, p. 108118, 2022.

[76] L. Gan and S. H. Low, "Convex relaxations and linear approximation for optimal power flow in multiphase radial networks," in *2014 Power Systems Computation Conference*. IEEE, 2014, pp. 1–9.

[77] M. Vanin, H. Ergun, R. D'hulst, and D. Van Hertem, "Comparison of linear and conic power flow formulations for unbalanced low voltage network optimization," *Electric Power Systems Research*, vol. 189, p. 106699, 2020.

[78] B. L. Gorissen, İ. Yanıkoğlu, and D. den Hertog, "A practical guide to robust optimization," *Omega*, vol. 53, pp. 124–137, 2015.

[79] W. Zheng, W. Huang, D. J. Hill, and Y. Hou, "An adaptive distributionally robust model for three-phase distribution network reconfiguration," *IEEE Trans. Smart Grid*, 2020.

[80] M. S. S. Abad and J. Ma, "Photovoltaic hosting capacity sensitivity to active distribution network management," *IEEE Trans. Power Syst.*, 2020.

[81] M. Z. Liu, A. T. Procopiou, K. Petrou, L. F. Ochoa, T. Langstaff, J. Harding, and J. Theunissen, "On the fairness of PV curtailment schemes in residential distribution networks," *IEEE Trans. Smart Grid*, vol. 11, no. 5, pp. 4502–4512, 2020.

[82] A. Ben-Tal, L. El Ghaoui, and A. Nemirovski, *Robust optimization*. Princeton university press, 2009.

[83] S. Boyd and L. Vandenberghe, *Convex optimization*. Cambridge university press, 2004, pp. 215–273.

[84] E. Dusabimana and S.-G. Yoon, "A survey on the micro-phasor measurement unit in distribution networks," *Electronics*, vol. 9, no. 2, p. 305, 2020.

[85] A. Pena-Ordieres, D. K. Molzahn, L. A. Roald, and A. Wächter, "DC optimal power flow with joint chance constraints," *IEEE Trans. Power Syst.*, vol. 36, no. 1, pp. 147–158, 2020.

[86] G. Calafiore and M. C. Campi, "Uncertain convex programs: randomized solutions and confidence levels," *Mathematical Programming*, vol. 102, no. 1, pp. 25–46, 2005.

[87] M. C. Campi and S. Garatti, "The exact feasibility of randomized solutions of uncertain convex programs," *SIAM Journal on Optimization*, vol. 19, no. 3, pp. 1211–1230, 2008.

[88] X. Zhang, S. Grammatico, G. Schildbach, P. Goulart, and J. Lygeros, "On the sample size of random convex programs with structured dependence on the uncertainty," *Automatica*, vol. 60, pp. 182–188, 2015.

[89] M. S. Modarresi, L. Xie, M. C. Campi, S. Garatti, A. Care, A. A. Thatte, and P. Kumar, "Scenario-based economic dispatch with tunable risk levels in high-renewable power systems," *IEEE Trans. Power Syst.*, vol. 34, no. 6, pp. 5103–5114, 2018.

[90] S. M. N. RA, M. Burgess, M. Mahmoodi, A. Attarha, and P. Scott, "An adjustable scenario optimisation approach in operating PV-rich distribution systems," *IEEE Transactions on Power Systems*, 2022.

[91] A. Nemirovski and A. Shapiro, "Convex approximations of chance constrained programs," *SIAM Journal on Optimization*, vol. 17, no. 4, pp. 969–996, 2007.

[92] W. Chen, M. Sim, J. Sun, and C.-P. Teo, "From CVaR to uncertainty set: Implications in joint chance-constrained optimization," *Operations research*, vol. 58, no. 2, pp. 470–485, 2010.

[93] S. Zymler, D. Kuhn, and B. Rustem, "Distributionally robust joint chance constraints with second-order moment information," *Mathematical Programming*, vol. 137, no. 1, pp. 167–198, 2013.

[94] E. Delage and Y. Ye, "Distributionally robust optimization under moment uncertainty with application to data-driven problems," *Operations research*, vol. 58, no. 3, pp. 595–612, 2010.

[95] A. Zhou, M. Yang, M. Wang, and Y. Zhang, "A linear programming approximation of distributionally robust chance-constrained dispatch with Wasserstein distance," *IEEE Trans. Power Syst.*, vol. 35, no. 5, pp. 3366–3377, 2020.

[96] P. M. Esfahani and D. Kuhn, "Data-driven distributionally robust optimization using the Wasserstein metric: Performance guarantees and tractable reformulations," *Mathematical Programming*, vol. 171, no. 1, pp. 115–166, 2018.

[97] M. C. Campi and S. Garatti, "Wait-and-judge scenario optimization," *Mathematical Programming*, vol. 167, no. 1, pp. 155–189, 2018.

[98] M. Bucciarelli, S. Paoletti, and A. Vicino, "Optimal sizing of energy storage systems under uncertain demand and generation," *Applied Energy*, vol. 225, pp. 611–621, 2018.

[99] L. Roald and G. Andersson, "Chance-constrained AC optimal power flow: Reformulations and efficient algorithms," *IEEE Trans. Power Syst.*, vol. 33, no. 3, pp. 2906–2918, 2017.

[100] X. Geng and L. Xie, "Data-driven decision making in power systems with probabilistic guarantees: Theory and applications of chance-constrained optimization," *Annual reviews in control*, vol. 47, pp. 341–363, 2019.

[101] M. Doostizadeh, F. Aminifar, H. Ghasemi, and H. Lesani, "Energy and reserve scheduling under wind power uncertainty: An adjustable interval approach," *IEEE Trans. Smart Grid*, vol. 7, no. 6, pp. 2943–2952, 2016.

[102] L. Wu, M. Shahidehpour, and T. Li, "Stochastic security-constrained unit commitment," *IEEE Trans. Power Syst.*, vol. 22, no. 2, pp. 800–811, 2007.

[103] J. Qiu, Z. Y. Dong, J. Zhao, Y. Xu, F. Luo, and J. Yang, "A risk-based approach to multi-stage probabilistic transmission network planning," *IEEE Trans. Power Syst.*, vol. 31, no. 6, pp. 4867–4876, 2016.

[104] M. Vrakopoulou, K. Margellos, J. Lygeros, and G. Andersson, "A probabilistic framework for reserve scheduling and N-1 security assessment of systems with high wind power penetration," *IEEE Transactions on Power Systems*, vol. 28, no. 4, pp. 3885–3896, 2013.

[105] A. J. Kleywegt, A. Shapiro, and T. Homem-de Mello, "The sample average approximation method for stochastic discrete optimization," *SIAM Journal on Optimization*, vol. 12, no. 2, pp. 479–502, 2002.

[106] W. Hoeffding, "Probability for sums of bounded random variables," *J. Am. Stat. Assoc*, vol. 58, 1963.

[107] B. S. Everitt and A. Skrondal, "The cambridge dictionary of statistics," 2010.

[108] F. Capitanescu, "Tso–dso interaction: Active distribution network power chart for tso ancillary services provision," *Electric Power Systems Research*, vol. 163, pp. 226–230, 2018.

[109] W. Wu, Z. Tian, and B. Zhang, "An exact linearization method for oltc of transformer in branch flow model," *IEEE Transactions on Power Systems*, vol. 32, no. 3, pp. 2475–2476, 2016.

[110] "IEEE European low voltage test feeder." *[Online]. Available: https://site.ieee.org/pes-testfeeders/resources/,*.

[111] A. J. Conejo, F. J. Nogales, and F. J. Prieto, "A decomposition procedure based on approximate newton directions," *Mathematical programming*, vol. 93, no. 3, pp. 495–515, 2002.

[112] G. Qu and N. Li, "Optimal distributed feedback voltage control under limited reactive power," *IEEE Trans. Power Syst.*, vol. 35, no. 1, pp. 315–331, 2019.

[113] G. Cavraro and R. Carli, "Local and distributed voltage control algorithms in distribution networks," *IEEE Trans. Power Syst.*, vol. 33, no. 2, pp. 1420–1430, 2017.

[114] D. Bertsimas and J. N. Tsitsiklis, *Introduction to linear optimization*. Athena Scientific Belmont, MA, 1997, vol. 6.

[115] Dual linear program. [Online]. Available: https://en.wikipedia.org /wiki/Dual_linear_program.